Feasibility Assessment of a Waveguide-based Eye-Tracker

BY

BEATRICE PAZZUCCONI
Laurea, Politecnico di Milano, Milan, Italy, 2016

THESIS

Submitted as partial fulfillment of the requirements
for the degree of Master of Science in Bioengineering
in the Graduate College of the
University of Illinois at Chicago, 2019

Chicago, Illinois

Defense Committee:

Xincheng Yao, Chair and Advisor
James Lee
Andrea Aliverti, Politecnico di Milano

ACKNOWLEDGMENTS

Firstly, I thank my UIC advisor Xincheng Yao for offering me this wonderful opportunity and motivating me every time he thought I was not doing my best. Thanks to all my senior colleagues at LIERI Lab, that advised and shared their vital space with me and did their very best to put up with my non-negligible initial lack of expertise: Yiming Lu, Vittoria Maneo, Taeyoon Son, Minhaj Nur Alam, Taehoon Kim. Special thanks to Changgeng Liu and Devrim Toslak for always helping me when I asked. Also, many thanks to Dr. Lei Liu of UAB for the precious remote advising.

Huge thanks to Lynn Ann Thomas that kept us all together though application, enrolling and all the most unpleasant processes that had to be endured on the way here.

Thank you mamma e papà and not-so-little little brother Giammarco, and to all my family that made all of this possible, even if you knew how you'd miss me. Special thanks to Francesco, who I know did not want me to go but still supported me anyway.

Thanks to my coinquilini at Chicago: Ele, Marti, Vicky, Leo and Greta, Marco, Tommy e Giuli, that did not live with us but spent equally the days at our place. Thank to all friends of UIC, from Italy and not, to Buckingham nights, cibo gratis and Birra e Scrocco.

Thanks to all my friends that stayed in Italy and resigned not to get word from me for weeks at a time (you know how I am when I am busy, but still sorry!).

BP

TABLE OF CONTENTS

TABLE OF CONTENTS (continued)

CHAPTER **PAGE**

LIST OF TABLES

LIST OF FIGURES

LIST OF FIGURES (continued)

FIGURE **PAGE**

LIST OF ABBREVIATIONS

ALS	Amyotrophic Lateral Sclerosis
ANN	Artificial Neural Network
AR	Augmented Reality
ASD	Autistic Spectrum Disorder
CR	Corneal Reflex
CP	Cerebral Palsy
EOG	Electro-Oculo-Graphy
EM	Eye Movement
e.g.	*exempli gratia*, for example
FOV	Field Of View
GUI	Graphic User Interface
HCI	Human-Computer Interface
HWG	Holographic Wave-Guide
i.e.	*id est*, that is
IR	Infrared
LED	Light Emitting Diode
LS	Least Square

LIST OF ABBREVIATIONS (continued)

NIR	Near Infrared
OCT	Optical Coherence Tomography
OD	Oculomotor Disorders
OSS	Open Source Software
PCA	Principal Component Analysis
PCC	Pearson Correlation Coefficient
POG	Point Of Gaze
RANSAC	RANdom SAmple Consensus
RMS	Root Mean Square
RMSE	Root Means Square Error
SD	Standard Deviation
SPR	Surface Plasmon Resonance
SSE	Sum of Square Errors
SVM	Support Vector Machine
TIR	Total Internal Reflection
VR	Virtual Reality
WD	Working Distance
WG	Waveguide

SUMMARY

Eye-tracking has emerged in recent years as a potentially powerful tool in the the biomedical panorama. The rich amount of information it conveys about the subject's physiological, neurological and physiological state makes it an attractive investigative resource. The immediacy of eye movements for human beings can be successfully exploited to build intuitive communication interfaces for the disabled and rehabilitative devices.

These characteristics make the application of eye-tracking techniques particularly suitable for ophthalmic clinical assessment. More specifically, it could prove crucial in the diagnosis and treatment of oculomotor disorders. This group of pathologies is at the same time very common and dangerously underestimated – particularly in children – although it is possible to successfully treat them (both surgically and with eye rehabilitation procedures).

The difficulty in the diagnosis, gravity evaluation and follow-up of oculomotor disorders arises from a plethora of causes: the assessment is either completely subjective to the physician or based on clinical evaluation scales that often prove difficult to use or inconsistent; the procedure itself is time-consuming, difficult for the subject to comply with (especially for children), and often it is difficult to obtain reliable measures.

To make up for the bulkiness and high cost of most wearable eye-tracking setups, the recent trend towards miniaturization and integration can be exploited. In particular, one can take advantage of the availability of cheap, light waveguides. The performances of these components in terms of image quality and efficiency are constantly being improved, and represent now a competing alternative to the traditional image and light transmission methods.

SUMMARY (continued)

The purpose of this dissertation is to illustrate how a novel design for a new eye-tracking methodology has been tested for technical feasibility.

More in detail, the ability of an holographic waveguide to convey sufficiently good images for eye-tracking was investigated. The images were processed off-line with a custom developed program based on the Starburst algorithm, to extrapolate the parameters relevant to the pupil and corneal reflex centers, in a semi-automatic procedure. The relation of the components of the vector connecting the above-mentioned points relative to eye rotation was analyzed.

Various setups have been experimented on, to try to increase the level of likeliness to reality.

Successive steps will be focused on improving the shortcomings found in this preliminary results and to include also a part for measuring eye accommodation. The ultimate goal is the development of a wearable, low-weight, low-cost oculometer, that will reduce time of testing, increase objectivity and reliability of standard assessment for oculomotor diseases.

The dissertation is divided as follows:

1. in Chapter 1, it is given an overview on eye-tracking applications, advantages and disadvantages, and classification, with specific regards to the pupil-corneal reflection method. Following, a brief description of holographic waveguides and their applications. Then the reader will be introduced on the clinical relevance and prominence of oculomotor diseases, and why the current state-of-art methods for assessing such maladies are unsatisfactory. Finally, a short discussion on the improvements that a waveguide-based oculometer could introduce is given.
2. in Chapter 2 the components used for the experiment are illustrated, and the procedure for the experiments is described.

3. in Chapter 3 are listed the results of the experiments described in he previous chapter, along with a brief description of the data processing.

4. in Chapter 4 a discussion on the previously obtained results is given. Finally further improvements are proposed.

CHAPTER 1

BACKGROUND

1.1 Eye-Tracking

The first studies of eye movements (EMs) are indeed quite old and date back to the 19th century [14] (according to Duchowski [15], the first objective method appeared es early as 1901). Nevertheless, it is only from the beginning of 1990s that first successful devices for eye and gaze tracking start to appear [52].

Both the hardware and software related to eye-tracking have been going under a massive development in recent years, and there is a growing interest in the possible applications of this technique.

As it can be easily imagined, being able to understand where a person is looking at is tremendously useful under multiple points of view. It can give information about where the attention of the subject is directed [4, 14, 23], and if the movements are supposed to follow certain patterns, it can tell us about the health state of the person. Being a one of the first and most frequent gesture carried out by human beings, EMs relate to health state, psychological condition, environment and insights about our behaviour in different situations [4, 23, 52].

As a consequence, eye-tracking devices have a huge number of applications, that can be divided roughly in two categories [14, 15, 52]:

Clinical and scientific analysis of the EMs allows for a deeper comprehension of motor controls, feedback sensory loops and, in general, of the functioning of the human body. But the possibilities do not end here: eye-tracking is employed also in psychiatry, cognitive and behavioural

studies, as EMs present patterns that are indicative of particular conditions [4,23]. From the clinical point of view, being controlled by cranial nerves rather than spinal nerves, EMs are least affected by spinal injuries or conditions like CP (cerebral palsy), and are usually the last to resent from neurodegenerative diseases such as amyotrophic lateral sclerosis (ALS). This makes them a powerful resources for assistive technologies [4,15,51]. On the other hand, the ability to correctly focus the gaze on the target can be influenced by a variety of conditions (e.g. trauma) other than strictly optical impairments. Therefore, being able to precisely analyze EMs can prove an interesting diagnostic and rehabilitative tool.

Re-creative and commercial the ever-growing availability of miniaturized, wearable, wireless devices allows for eye-tracking to be incorporated in VR (virtual reality) or AR (augmented reality) applications, as well as being employed to create intuitive human-computer interfaces (HCI) [4, 23]. Smartphone and video-games applications are a good example. Commercial applications include marketing investigation for costumer preferences and similar [14]. Another interesting use of eye-tracking technology is the one of the so called e-Learning, i.e. to help designing new methods to improve outcome and increase wellness in the learning environment [4].

1.1.1 Advantages and Disadvantages of Eye-tracking Systems

Being one of the most natural and fast movements carried out by human beings, eye-tracking based devices benefit from being intuitive and quick-responding [4]. Nevertheless, some complicated tasks such as word synthesis can prove difficult to be translated in EM patterns, so that some applications are only mastered after practising. Another major drawback of eye-tracking based

communication is that is very hard to confirm the gaze intentionality, i.e. any input from the user can be interpreted as command (this has been named "Mida's touch"' defect [52]). Another problem is that these systems require careful calibration [14,15] and often need restricted conditions (e.g. on the subject position and lighting conditions) to properly work [15,19,63]. Another critical point, up to some years ago, was the one of the weight and invasiveness of the head-mounted devices [14,23,52], but has been partially relaxed thanks to new advancements in technologies (see in the next section 1.2) and the development of new recognition algorithms for remote gaze-trackers. The technological development is also tackling another issue often linked to eye-tracking devices that is the high cost [4,14,63].

1.1.2 Difference Between Eye-tracking and Gaze-tracking

It is appropriate to point out a subtle difference running between the two terms *eye-tracking* and *gaze-tracking* [15,52].

Eye-tracking refers to the measure of the movement of the eye ball in the socket with respect to the head.

With *gaze-tracking*, one refers to a successive mapping of such eye position with respect to the environment (the so-called "Point Of Gaze" (POG) [15,52]). The POG is the point in the scenario that is imagined on the *fovea* [1] [23]. This information can be obtained only integrating proper eye-tracking data with measures of head position or with data of the surrounding environment [15,52,63]. Moreover, not all types of eye-trackers can also be used for gaze-tracking. The ones that are best fit for this purpose are video-based techniques.

---

[1] The portion of the retina corresponding to highest visual acuity

In literature and advertisement the two terms are increasingly used as interchangeable, due to the fact that gaze-tracking is much more frequently used for practical applications.

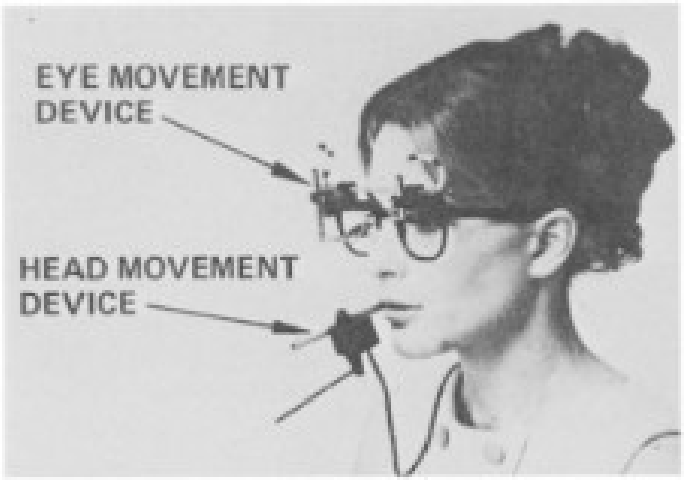

Figure 1: Integration of head and eye movement, reprinted with permission [63].

1.1.3 Taxonomy

Multiple authors have provided a classification of eye-tracking techniques [4]. Despite the great variety of methods (and new ones are constantly developed), a quite consistent division can be proposed.

1.1.3.1 Wearable vs. Remote Tracker

The first classification is purely based on the placement of the device: we distinguish *remote* trackers from *head-mounted* (or wearable) ones [14, 15, 23]. Wearable eye-trackers encompass a support (whether resembling spectacles or with a helmet-like harness) to hold the equipment close

to the subject's eye. Possibly they also have instruments to measure head position and/or the surrounding environment, to give gaze information. They are best suited for study of moving subjects but not for continuous monitoring [14, 23]. Remote devices are made up of one or multiple cameras that record the subject and the scene and usually calculate the gaze with image-processing techniques [14, 23].

1.1.3.2 Eye Movement Estimation Method

The most interesting classification is on the method used to calculate the EMs.

Sensor-based trackers rely on electrodes (EOG, Electro-Oculo-Graphy) or corneal contact lenses.

EOG was the first method to be invented to monitor EMs, and – although outdated – is still used today. As one can see in Figure 2, the method is quite invasive and only relative motion of the eye respect to the head can be recorded. EOG relies on the difference in electric potential recorded from the retina to the cornea, that is measured as a bipolar vector by the electrodes. [4, 15, 52, 63] The orientation of the vector is indicative of eye ball orientation.

Its applications are in ophtalmic physiology and study of the EMs during sleep [52].

Contacts covering the *cornea*[1] (and actually the most of the front part of the *sclera*[2] [63]), on the other hand, can exploit some different mechanisms (reflective surfaces or conductive wires for example) to measure EMs [15].

---

[1]The central frontal part of the outermost layer of the eyeball that covers the iris and pupil and admits light to the interior being transparent. It has a slight different curvature than the rest of the surface and so it can be felt and observed even with closed eyelids as a small bulge.

[2]commonly known as "white of the eye", it is the protective outermost layer that wraps the eye ball. It originates the *cornea* frontally and connects with the optic nerve sheath on the posterior side.

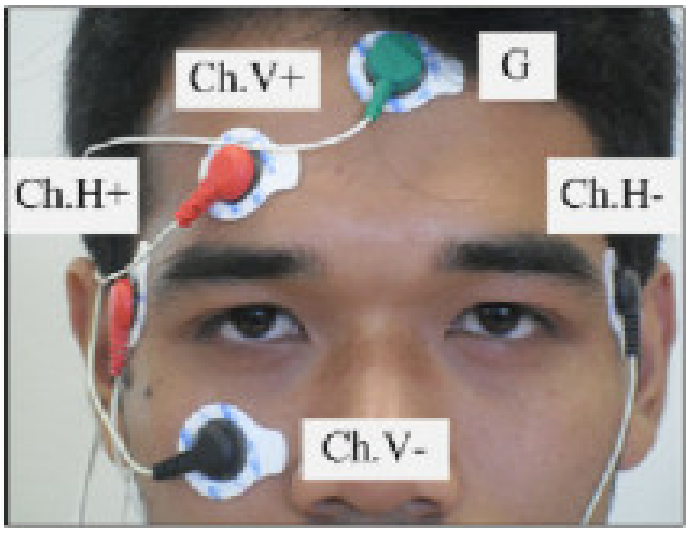

Figure 2: Electro-Oculo-Graphy setup, reprinted with permission [46].

The placement of such device is shown in Figure 3. Although the most precise and sensitive approach [15, 63], it has lost popularity today, mainly due to the discomfort it brings to the subject. Also, it only gives information about eye orientation respect to the head.

Figure 3: Scleral contact lens for eye-tracking, reprinted with permission [15].

Image processing-based trackers rely on pictures (and, increasingly, videos) of the eye under specified illumination setting. They can also give POG information (if combined with other measures [15, 63]) and are generally less invasive but also less precise [15]. They represent today the most popular alternative for eye-tracking [15]. They are based either on *image recognition techniques* – that use the appearance of the eye and or/face – or on *prominent features recognition* (such as pupil, *limbus*[1], or corneal reflex (CR)) [4, 15, 63].

A further classification can be made on the type of light these device employ. If the light is shone to the eye co-axially respect to the camera, the reflection from the back of the eye is recorded and so the pupil appears brighter than the iris ("bright pupil" approach). If, on the other hand, the light source and camera are not aligned respect to the eye, the pupil will appear dark ("dark pupil" approach) [4, 27, 52, 63].

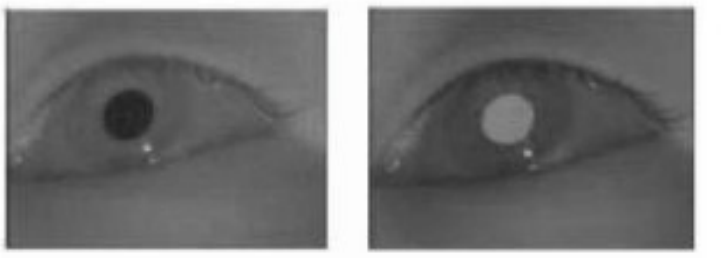

Figure 4: Difference between dark and bright pupil, reprinted with permission [4], ©[2013] IEEE.

[1]the junction where the *sclera* forms the *cornea* and the two curvatures meet forming a small groove

Depending on the different contrast between pupil and iris, a dark pupil vs. a bright pupil approach may be preferred. If, as in Asian and African subjects, the iris is very dark and meddles with the pupil, a bright pupil strategy will be best suited for pupil isolation [37]. The light can be in the visible or IR range, but the latter is more commonly used since the human eye is insensitive to it. This prevents the illumination source to cause the pupil to constrict and make the measure hard, and avoids distracting the subject.

Appearance based-trackers may rely on complex processing algorithms (such as PCA, ANN, SVM, classifiers...) [4] and are mostly used in remote eye-trackers [14]. A comparison of some other works on this topic is reported in Table I by Al-Rahayfeh and Faezipour [4].

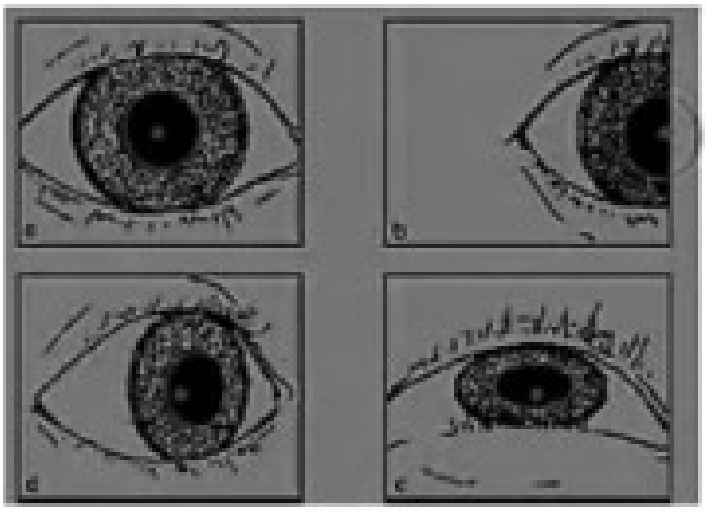

Figure 5: How the apparent pupil size varies with eye orientation, reprinted with permission [15].

TABLE I: TABLE COMPARING SOME IMAGE-BASED EYE-TRACKING TECHNIQUES, REPRINTED WITH PERMISSION [4], ©[2013] IEEE.

Method	Detection Accuracy (%)	Angle Accuracy (degree)	CPU time (ms)
Eye tracking using Pattern Recognition			
Raudonis *et al.* [4]	100%	N/A	N/A
Kuo *et al.* [6]	90%	N/A	N/A
Yuan and Kebin [9]	N/A	1	N/A
Lui and Lui [7]	94.1%	N/A	N/A
Khairosfaizal and Nor'aini [17]	86%	N/A	N/A
Hotrakool *et al.* [8]	100%	N/A	12.92
Shape-based eye tracking			
Yang *et al.* [13]	N/A	0.5	N/A
Yang *et al.* [14]	N/A	Horizontal: 0.327 Vertical: 0.3	N/A
Mehrubeoglu *et al.* [11]	90%	N/A	49.7
Eye tracking using eye models			
Zhu and Ji [23] (First scheme)	N/A	Horizontal: 1.14 Vertical: 1.58	N/A
Zhu and Ji [23] (Second scheme)	N/A	Horizontal: 0.68 Vertical: 0.83	N/A
Eye tracking using hybrid techniques			
Li and Wee [12]	N/A	0.5	N/A
Huang *et al.* [24]	95.63%	N/A	N/A
Coetzer and Hancke [25]	98.1%	N/A	N/A

Figure 5 shows the drawing of an eye, taken at different orientation respect to the camera. The apparent change in size and orientation of the pupil ellipsoid can be exploited by image processing algorithms to infer eye-orientation respect to the camera. Knowing the position of the camera, it is possible to estimate the POG.

The second type of trackers consist mostly in *limbus* (see Figure 6), pupil, and pupil-CR trackers, that have been growing in popularity in the recent years [15,23,63]. A more detailed description of such method is given in the following section.

As one can easily imagine, the methods relying on prominent features of the eye are most reliable when considering multiple hints at a time [15]. For example, an eye-tracker relying only on CR without having the reference of the pupil, would register eye rotation even simply shifting the illuminator respect to the subject's face, without the need for changing gaze direction [63].

Sensor-based eye-trackers are only of wearable type, while image-based ones can be either.

1.1.4 Pupil-Corneal Reflection Trackers

This class of eye-trackers has become increasingly popular in the recent years, being now one of the most used video-based methods, because of the relative superior precision and robustness of the method respect to other image processing-based trackers. POG information can be obtained by combining the information from the eye images with the one of the surrounding scene [15, 23, 63].

Purkinje images (a.k.a. Purkinje reflexes, Purkinje-Sanson images) are reflections from various eye structures that can be observed from outside as "glints" on the eye ball surface. Usually at least 4 are observed. They are named P1, P2 ... and so on. The first reflection, also known as CR,

Figure 6: A wearable limbus eye-tracker, reprinted with permission [15].

results from the interface of the *cornea* and air and it is the strongest one. The others derive from the inner *cornea* discontinuity, outer and inner surface of the crystalline lens respectively [15,23,55].

The pupil is the aperture in the frontal part of the eye that allows light to enter and strike the retina. It is delimited by an annular muscular structure (the iris), that regulates pupil diameter by reducing and increasing its thickness.

The relative pupil center-CR distance remains almost constant if eye and head move consistently, but change if the eye rotates in the socket instead. This holds for a very large range of rotation, until the illumination falls off the *cornea* and lands beyond the *limbus* [15, 27, 63]. It is also to be noted that the natural range of eye rotations is not as wide as the possible eye-tracking range:

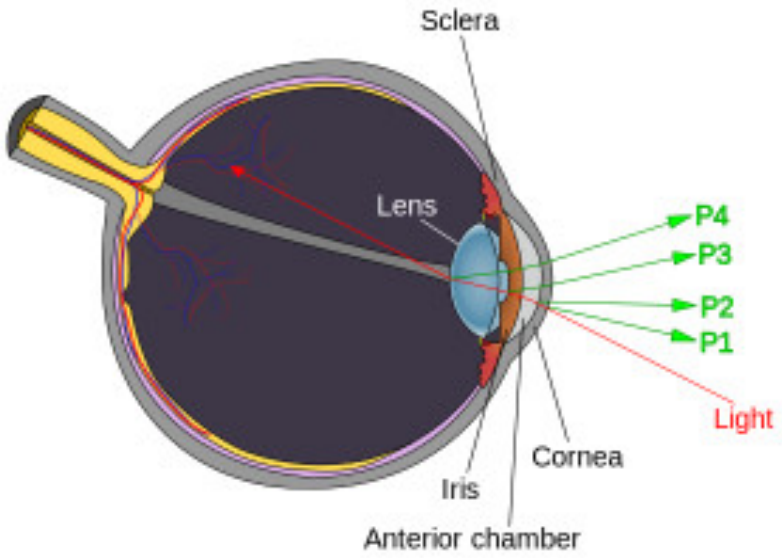

Figure 7: Schematic of the Purkinje images origin, image from [55].

according to Bahill et al. [7], human saccades[1] hardly ever exceed 15° of rotation, and also Young and Sheena [63] hold that if a rotation greater than 30° is needed, head rotation is involved.

Pupil-CR tracking can be performed both with white and IR light, and both with dark and bright pupil approach in principle. In reality, it is restricted to IR lighting, because it needs clear images of the pupil that can be obtained only with wearable eye-trackers, and in this case, a visible light illumination would be disturbing for the subject [37].

---

[1]A quick, small and simultaneous movement of both eyes that is interspersed with fixation phases. It is one of the fastest movements of the eye and is critical in increasing perceived images resolution.

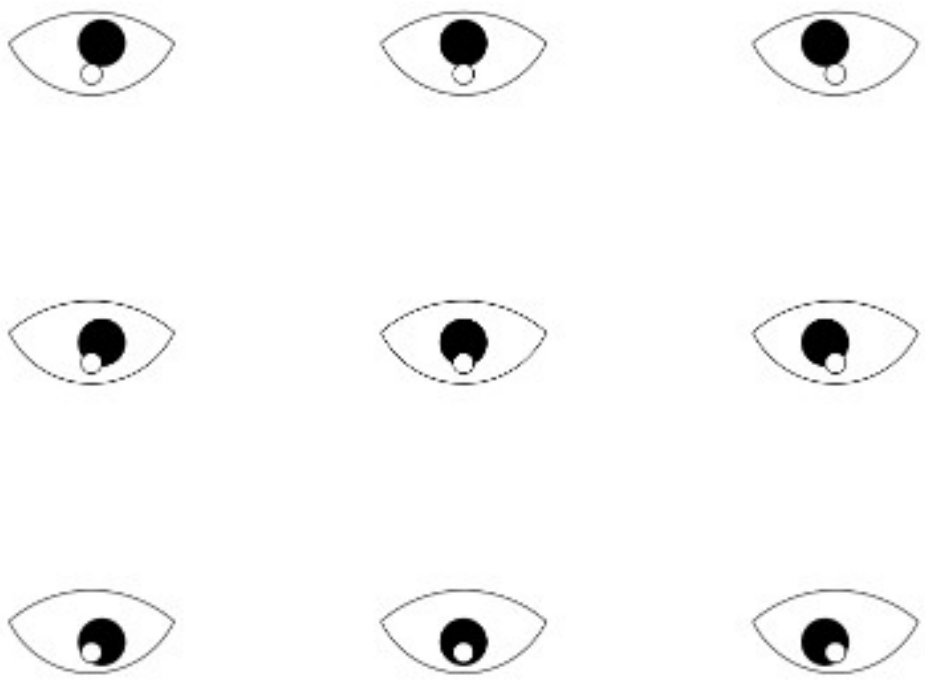

Figure 8: How the relative distance between CR and pupil varies with eye orientation, reprinted with permission [15].

There is also evidence that using the first and fourth Purkinje images one can track EMs. Anyway, since the fourth reflection is pretty weak and can be observed only with optimal lighting conditions, and head stabilization may be needed, these "dual Purkinje images" trackers only remained as proof-of-concept [15, 63].

1.1.5 Eye-tracking Softwares

Automated procedure for calculation of the POG are most easily applied to image-based trackers, mainly through image processing techniques. This is in general true for image-based trackers, but most of all for pupil-CR ones, since they have proven by far the preferred strategy in the current panorama.

The most consistent part of the eye-tracker's software is – rather obviously – the parameter extraction part. The procedure should be reliable, robust, quick enough to ensure real-time performances, and not too computationally heavy. If the software is to be used in association with a GUI, it should be intuitive and user-friendly. Of course, the ensemble of requirements is very demanding and no perfect solution exists. Proof of this is the appalling number of new parameter extraction-procedures that pop up in literature.

A complete revision of such procedures would go well beyond the scope of this dissertation and will not be treated here, especially considering the complexity and extension of these solutions, and the underlying non-trivial statistics and data processing concepts. The specific implementation of the software used for this feasibility assessment will be discussed more in detail in 2.7 and in the appendixes.

After the procedure for parameter extraction is validated, the mapping and calibration procedures are performed. These will be discussed more in detail in successive paragraphs because they will not be implemented in the algorithm.

There are literally a multitude of softwares taking care of parameter extraction, calibration and mapping, as well as some other functions, depending on the specific case. The most refined ones are provided by the tracker producer (as for examples, Tobii™) and are designed for the specific application, but also a great number, open-source solutions are constantly being issued.

The well-known Starburst algorithm is an example, as are these other two Matlab® toolboxes evaluated by Berger et al. [8] and Andreu et al. [5]. Fuhl et al. [19] present a review of some other algorithms used mainly in the research environment.

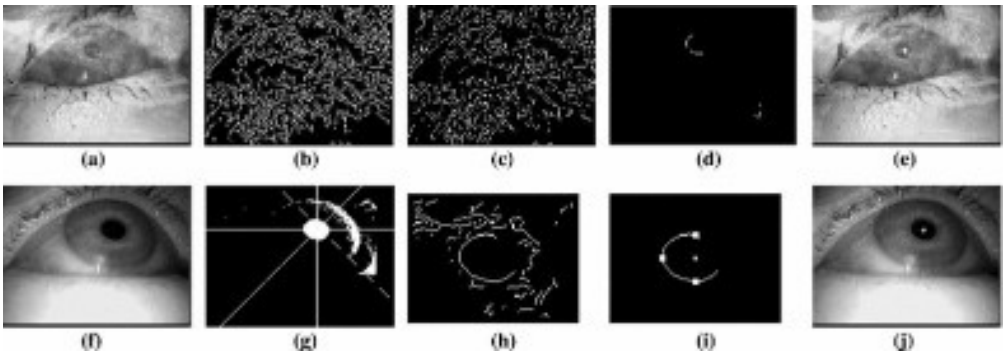

Figure 9: Visualization of the ExCuSe feature extraction algorithm, reprinted with permission [19].

1.1.5.1 Mapping

The eye-tracker software must be able to translate the information from the image (in the case of pupil-CR tracker, the two components x and y of the vector connecting the centers of the two regions) into the reference system of the specific program [15]. In the case of graphical applications, the vector information must be translated in coordinates relative to the surrounding scenario (usually recorded with a camera close to eye of the subject). If the eye-tracker is monocular, only a mapping on a 2D plane will be possible, while if the two eyes are tracked, a 3D mapping is possible (see Figure 10).

When working in 2D (the most common case), the mapping of the eye-tracker coordinate x, ranging $[x_0, x_1]$ to a new screen coordinate, X, ranging $[X_0, X_1]$ is simply given by the linear transform equation [15]:

$$X = \frac{(x - x_0)(X_1 - X_0)}{(x_1 - x_0)} + X_0 \tag{1.1}$$

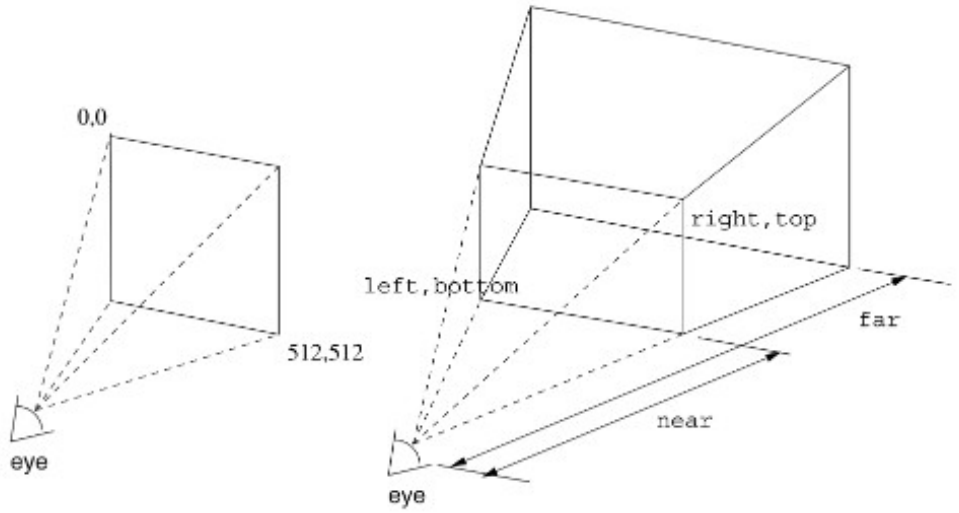

Figure 10: Mapping on monocular vs. binocular eye-tracker, reprinted with permission [15].

and same goes for the other coordinate.

Mapping 3D coordinates is indeed a bit more complex, but not impossible to handle with, for reference, see Duchowski [15].

More complex mapping procedures are the one relative to remote eye-trackers. For an introduction on this topic, see Guestrin [23] and again Duchowski [15].

1.1.5.2 Calibration

Almost all eye-tracking setups require calibration to properly work for quantitative measurement [15, 22].

In general, calibration is a procedure by which some data with known correspondence to the desired output is given to the system. The system used calibration data and the corresponding output to refine some internal parameters and establish a input-output relationship. When new

data is presented, the previously established relationship is used to guess the new corresponding outputs. Generally, some previous knowledge about the input-output relationship is required. These calibration points should span the whole expected dynamic range of the measure to be able to capture the full picture. They also should be enough to capture intermediate dynamics variations, but not too many in order to to make the procedure too time-consuming and computationally heavy.

For the specific case of gaze-trackers, calibration is performed by feeding the system a series of inputs (eye images with components calculated by the procedure) that corresponds to known points in the scenario. This is achieved by having the subject facing a screen with some markers, and asking to gaze at each marker in turn. Usually 3, 5 or 9 points in square grids are used, at the extreme gaze angles [15, 22].

The calibration procedure has also the function to define the image characteristics for the specific experiment (brightness, contrast of the frames) [15], as these parameters are crucial to perform reliable image processing to obtain results. Also, this renders the specific experiment tailored to subject's individual characteristics [22] and so reduces unreliability caused by inter-individual variability. For example, if the pupil is to be firstly identified by filtering the image for dark spots, the threshold of such filter must be appropriately chosen. Of course, there are a number of factors that can change the optimal threshold: lighting conditions, presence of spectacles, make-up, droopy eyelids or very dark irises...

1.2 Holographic Waveguides

1.2.1 General Introduction

In general, an optical WG (Waveguide) is a device that is able to transmit light between two points, i.e confining the propagation of the wave-fronts [2]. Optical WGs are commonly fabricated

with dielectric material (mostly glass, plastics and semiconductors). The principle underlying light confinement is most often TIR (Total Internal reflection) deriving from a refractive index in-homogeneity but also other mechanisms (reflection, SPR) can be used [2].

Waveguides confining light propagation in a line are called *channel waveguides* (e.g. optical fiber), while the ones confining it in a plane are called *planar waveguides* [2, 61].

Depending on the fabrication material, different fabrication techniques can be exploited: photolithographic and micro-fabrication techniques can be used for integrated WGs with semiconductor substrates, laser writing on crystal, glass substrates, lamination and stratification processes [2].

Many different classifications exists. They are relative to: mode distribution, refractive index variation, geometry, etc. [2, 61]

Their ranges of applications is huge, but here only the one relative to see-through display will be discussed.

1.2.2 Waveguides Applied to Augmented and Virtual Reality

Optical planar WGs are currently the most favourable candidate for the development of see-through displays (fundamental for AR and VR applications), out-competing mirror-based approaches. Waveguide-based solutions are lighter, smaller and allow for more appealing form factors than mirror-based ones. Mirror displays require mechanic and electronic compensation of distortion and narrow FOV in front of the user, resulting in a higher relative cost and bulk, while all other components can be conveniently placed on the side on the case of WGs [13, 39]. The form of these components is usually flat, and can be fabricated in various ways. The central body of the WGs transmits light, while the in- and out-couplers gather light from the source and re-combine it in front of the user respectively.

Figure 11: Vuxiz™ (top) and Hololens™ (bottom), image from [17].

There are different types of optical WGs used for displaying purposes, mainly classified considering the types of in- and out-couplers [21, 39]:

Diffractive a pattern of small groove is etched at the in- and out-coupler location (whether by additive or subtractive techniques) and acts as a diffraction grating. Also known as "surface relief" waveguides. The incoming light is decomposed in diffraction patterns at the entrance and re-combined at the output. Its drawbacks are high color aberration (dispersion or components) and reduced FOV.

The original design was patented by Nokia™ [17, 21, 60]. It is now licensed to Microsoft Hololens™ and Vuzix™ [17, 21, 39].

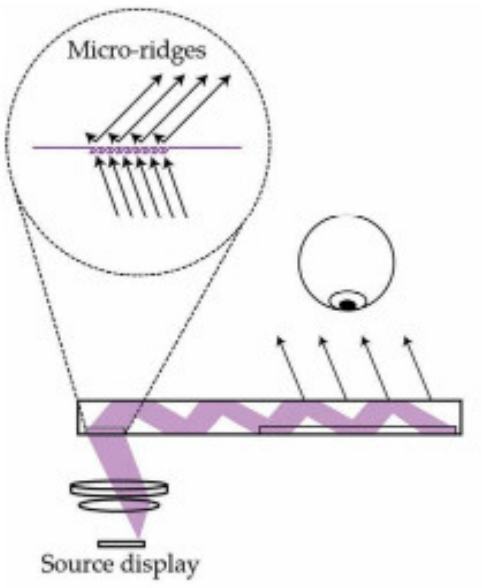

Figure 12: Schematics of a diffractive WG, image from [17].

Holographic a holographic pattern[1] is engraved in the thin-film photo-polymer in- and out-couples with laser scanning. Represents a major innovation respect to diffractive waveguides, since it is much more compact and efficient in terms of transmission and FOV [6, 17, 21, 53].

Since only one specific wavelength is efficiently transmitted (i.e. one color), current research efforts are in combining stratified WGs so that multiple wavelengths can be transmitted and a colored image can be obtained trying to minimize the color-crosstalk [26, 64, 65]. The other main research direction is in the increase of the efficiency [64, 65]. It used by Sony™ and

[1] A holographic pattern or hologram is a recording of the light interference field created by an image. Contrarily to a photograph, it is not recognizable as image if not properly lit. When it is illuminated in the right way, it creates an image that is virtually indiscernible from the original object it generates it, as it contains visual cues pertaining to 3D perception such as depth and parallax. Originally it could only be actuated by lasers, but now also special computer screens are capable of generating holographic images [58].

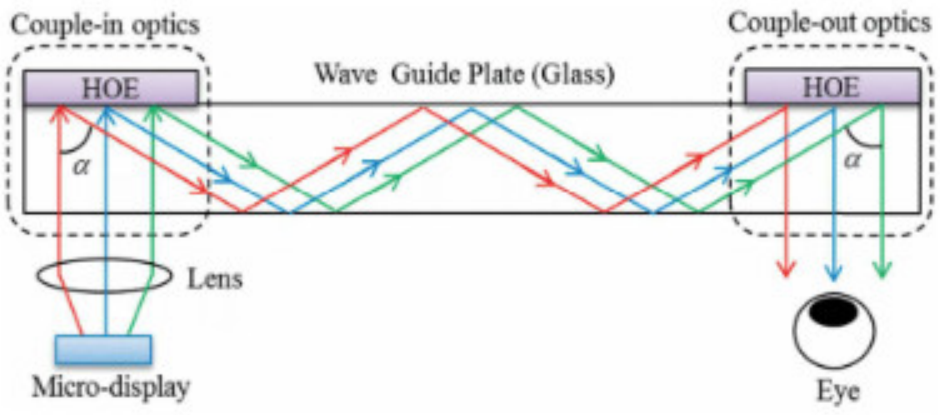

Figure 13: Propagation of light in a HWG, image from [17].

Konica Minolta™ [60]. Also, switching or active HWGs (holographic waveguides) have been produced [21, 53, 60].

Polarized exploits polarized reflectors and stratified plastic layers on glass. It is used by Lumus™ [60]. Has a large FOV but has a very low efficiency, its very complex to manufacture and expensive [39]. It still resents color dispersion problems.

Reflective rely on semi-reflective mirrors, that have the advantage of nullifying color dispersion. Also, it doesn't rely on extravagant fabrication techniques, so it should be easy to produce. The drawback is that the substrate needs to be very thick (1-2cm vs. few mm of other approaches) and therefore it is not suitable for AR applications [39]. It is used by Google™ and Epson™ [39, 60].

According to what emerges from the previous considerations [13, 17, 21, 53], HWGs make currently the most attractive alternative for see-through displays, and one can easily verify the amount

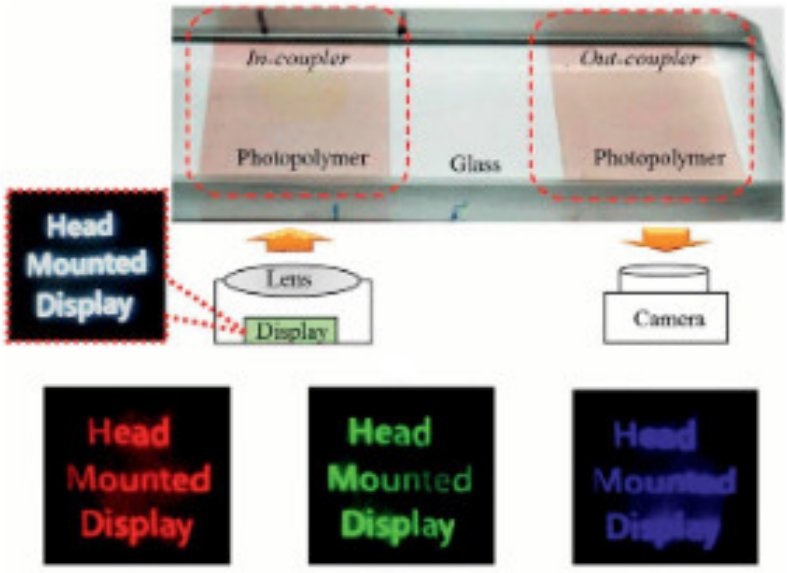

Figure 14: Pictures from a full color HWG, image from [17].

of efforts that is currently going into improving their performances [6, 26, 64, 65]. HWGs are for the moment an optimal compromise between cost, ease of fabrication, efficiency and size effectiveness [13, 17, 53] and there is hope that the advantage in using them will keep increasing as research progresses [65].

1.3 Oculomotor Disorders

Oculomotor Disorders (ODs) or Binocular Vision Disorders (BVDs) encompass a broad category of vision impairments that reduce the capability of the eye to move and focus the target on the *fovea* [45]. They are distinct from other vision disorders because are not related to the refractive properties of the eye component but to its mobility in a more general way.

ODs may affect [1, 3, 10–12, 16, 42, 44, 45, 48, 49]:

- accommodation: the ability of the crystalline lens to deform and change its focal length, so that the image of the target hits the retina even if the target itself changes position,
- vergence: dis-conjugate movement of the eyes that brings both of the eyes on the target,
- conjugated EMs such as saccades, pursuit movements, fixations,
- *stereopsis*, i.e. the ability to perceive the 3D features of a scenario,
- the synchronization between these components and between the eyes.

All these movements are of primary importance to be able to correctly visualize an object on the retina, a fundamental task to correctly develop, gain independence and live everyday life [1]. Proof of this is that often successful athletes are individuals with superior oculomotor capabilities [31]. This also applies to many other cases, and one can easily understand how ODs have huge impact on the patients' life quality, affecting they development, academic and athletic performance [1].

ODs have also been linked to learning and reading disabilities (such as disleyxa) [1, 12, 16, 42], adverse academic behaviour [10], prolonged use of video-displays [40], trauma [54].

1.3.1 Clinical Prevalence

Binocular Vision Disorders are an extremely diffused clinical diagnosis. Many studies have assessed that [49,54], and also have underlined the alarming percentages of prevalence respect to other vision diseases especially for what concerns paediatric practice [11, 42, 44, 48, 49]. It is even more worrying the fact that ODs are often under-detected [1, 32], due mainly to the severe limitations of the state-of-art diagnostic procedures. Lara et at. [32] report that as little as 1% of children are diagnosed with BVDs, against the higher prevalence found in other studies. According to Scheiman et al. [48], accomodation and binocular impairments are far more diffused than refractive defects in

children (from 8.5 to 9.7 times more frequent), and also underlies the lack of a data basis in order to properly diagnose these conditions. Rouse et al. [44] and Borsting et al. [11] highlight the high percentage of children in school age affected by BVDs, and the connection between accomodative and vergence disfunctions.

This percentage of wrong evaluations is disturbing because affects severely prevention and early diagnosis routines, that would reduce considerably the human and economic burden of ODs.

Furthermore, there is proof that treatments of BVDs can yield successful results [10, 49].

1.3.2 Why Current Clinical Assessments of ODs Are Not Satisfying

Routine tests for BVDs are prone to a substantial number of shortcomings:

- They are based on lengthy procedures (like the cover-uncover test[1] [57]), that rely massively on patients' compliance. Aside from the low cost-effectiveness of the approach, it appears evident that in the case of children, correctly understand the directions and maintaining the required attention to carry out the instructions for a long time may be troublesome;
- The results are based on the physician's subjective judgment (or even on non-expert one [24]) and are therefore prone to inter- and infra-observer variability[2], even if they're using a scale;
- The judgment scales employed may be complex to be used by non-experts or, even worse, may give inconsistent results [25]. Objective measures are hardly ever employed, as the scales are mostly semi-quantitative, see Figure 15;
- To allow for a comprehensive assessment of the impairment, all the oculomotor components should be assessed together, to ensure the same testing conditions and be able to evaluated also the interactions among them. Normally the accomodative, vergence, movement components are separately examined.

---

[1]The test consist in having the patient stare at a target and covering/uncovering one of the eyes with a screen, the modalities depend on the specific procedure. The deviation of the other eye when the first one is covered/uncovered is observed.

[2]Inter-observer variability refers to the fact that two different people may give different responses when examining the same result. Infra-observer variability refers to the fact that the same observer may give two different responses on the same results in different times or situations.

In the light of what said above, it is evident that a comprehensive assessment of binocular performances should be carried out in an efficient and objective manner to properly address ODs [10, 11, 42, 44].

1.4 Why a Waveguide-based Eye-tracker?

1.4.1 Eye-Tracking in Medical Applications

Boardman et al. [4] state:

> *A search of the term "eye-tracking" in PubMed returns 3060 results that report its use in a diverse range of applications including studies of typical development, intellectual disability, pain, autism spectrum disorder (ASD), neurodegenerative diseases and use as a teaching aid in emergency medicine.*

This is indicative of the great prominence eye-tracking is gaining today in the biomedical field. As pointed out in 1.1, eye-tracking not only it is proving a resource in the assistance of the motor-impaired [4, 9, 51, 52], but it has been exploited in very wide range of applications.

Eye-trackers have been used to:

- evaluate psychiatric disorders [20, 29],
- early diagnosis, screening and following up of cognitive disorders such as dyslexia [41] and atypical development of children, such as ASD [9, 18],
- gain insights about consequences of trauma [47],
- investigate cognitive processes in adults and infants [43],
- research learning strategies and improve training methodologies [43].

Please read this questionnaire and tick the appropriate boxes

	Never	Infrequently	Sometimes	Fairly often	Always
1. Do your eyes feel tired when reading or doing close work?					
2. Do your eyes feel uncomfortable when reading or doing close work?					
3. Do you have headaches (*that come on*) when reading or doing close work?					
4. Do you feel sleepy when reading or doing close work?					
If so, do you think that it is because you were tired at the time?	Yes / No				
5. Do you lose concentration when reading or doing close work?					
If so, do you think that it is because you were not engaged with the content?	Yes / No				
6. Do you have trouble remembering what you have read?					
If so, do you think that has anything to do with your eyes?	Yes / No				
7. Do you have double vision when reading or doing close work?					
8. Do you see the words move, jump, swim or appear to float on the page when reading or doing close work?					
9. Do you feel like you read slowly?					
If so, do you think that has anything to do with your eyes?	Yes / No				
10. Do your eyes ever hurt when reading or doing close work?					
11. Do your eyes ever feel sore when reading or doing close work?					
12. Do you feel a pulling feeling around your eyes when reading or doing close work?					
13. Do you notice the words blurring or coming in and out of focus when reading or doing close work?					
14. Do you lose your place while reading or doing close work?					
15. Do you have to re-read the same line of words when reading?					
If so, do you think it is because your eyes have made it necessary?	Yes / No				

Figure 15: Example of a survey for convergence insufficiency delivered by physicians, reprinted with permission [28].

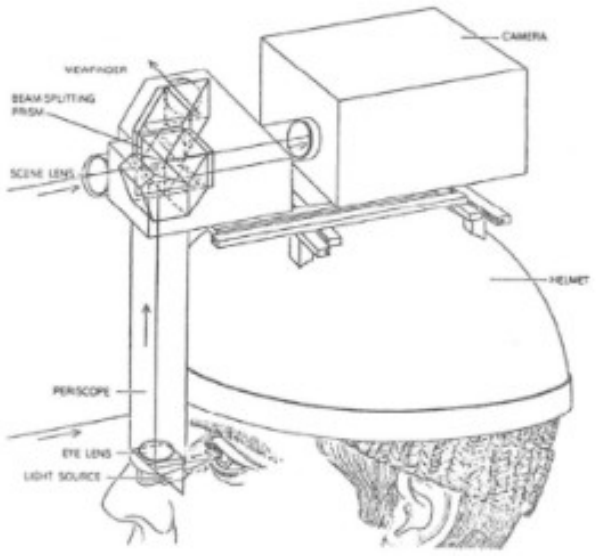

Figure 16: And old mirror and prism-based eye-tracker, reprinted with permission [63].

As also pointed out by Boardman at al [9], eye-trackers may prove a fundamental resource in evaluating children in preverbial phase (before talking), under multiple points of view (physical, cognitive, psychological). This need is particularly felt in the prospective of the efforts made in early diagnosis of a multitude of diseases [9, 22].

The recent developments in reducing bulk and weight of wearable eye-trackers as well as advancements made in remote trackers are promising for what regards uses with children [9, 14, 22], since is notorious that children do not put up well with being harnessed in bulky constraints to be looked in the eyes.

1.4.2 Advantages of a Holographic Waveguide-based Eye-tracker

The advantages associate with a wearable see-through HWG-based eye-tracker can be summarized as:

- compactness and lightness: increased ease for positioning lenses in front of the patients to test accommodation, and comfort in wearing (see Figure 16 and compare with Figure 11),
- reduction of the diagnostic exam length: ideally, only one repetition is needed, and the parameter extraction is left to an automated image processing procedure, which is much quicker than human evaluation,
- objectivity of the measurements: the EMs are evaluated in terms of rotations (degrees), velocity (degrees/seconds), latency (in seconds) etc. . . , that is much more objective than the semi-quantitative scales commonly used,
- possibility to test in daily life-situations, not only in lab environment.

Furthermore, HWG technology could be exploited to integrate a measurement of accommodation in the device, so that the relevant parameters to evaluate ODs can be simultaneously assessed. In Chapter 2 the reader will find some considerations on the accommodation part and why it was not possible test it in these preliminary experiments.

In the light of what discussed in sections 1.1, 1.2, 1.3 and in the above paragraph, it is evident now that exploiting current eye-tracking and HWGs technologies could solve the problems associated with the traditional evaluation of BVDs. The social and clinical impact of this improvement would be consistent, considering the high prevalence of these impairments and the importance of

prevention and early diagnosis. Moreover, the device could be exploited also by other clinicians working in the ophtalmology field and experts in visual rehabilitation and eLearning.

CHAPTER 2

MATERIALS AND METHODS

Here are listed the part of the optical apparatus that was used to assess the feasibility of the waveguide. Since various setups were tested, but not all of them were found suitable, only the components that were used thoroughly have a complete description.

2.1 Holographic Waveguide

The waveguide was fabricated in Dr. Juan Liu laboratory, that is collaborating with ours for the development of this prototype. It comprises a rectangular 20 x 60 mm glass substrate, 3 mm thick, with photopolymeric film holographic in and out-couplers. An additional Fresnel lens (focal length 40 mm) is built in front of the in-coupler to collimate the entering light.

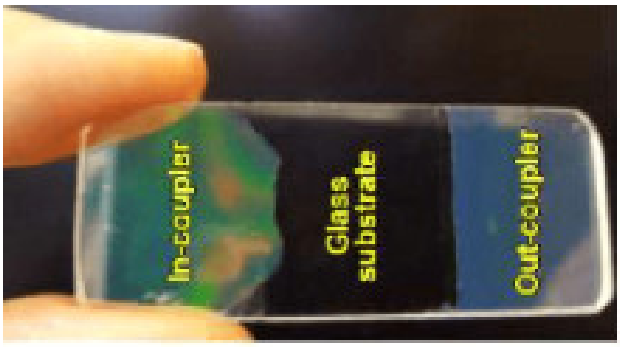

Figure 17: The holographic waveguide used in the experiment (without holder).

The maximum diffractive efficiency was estimated to be around 20% for green light (532 nm), that is why the chosen LED has a peak wavelength of 530 nm.

Unfortunately, this calls for the use of a very powerful illumination, and moreover in the visible range, that makes this prototype unsuitable for human experiments. In fact, in this design the WG is not used – as it is common – to transmit images from a display in front of the view, but the other way round, i.e. to transmit the reflect light from the illuminated eye to the camera. Since a high power illumination in the visible range is required to obtain decent images, it is not possible to try with a human subject at this point yet, as it would be extremely uncomfortable.

In principle, a *fundus* image[1] of the eye could be registered, to monitor accommodation. Unfortunately, as one can read in 2.4, it was not possible to find or build a suitable model for accommodation in short time, therefore that part was not evaluated.

In order to use the WG in the various setups, a holder was designed and 3D printed. The holder allows for moving the waveguide on the laboratory table and rotate it around its shorter side.

It is also worth pointing out that image quality depended greatly on the relative orientation of the WG respect to the camera (and, to a lesser extent, respect to the model eye). In 2.6 the reader can observe the difference between Table II and Table III, where the image quality consistently improved when the WG was slightly askew respect to the camera.

---

[1] A photograph of the back structures of the eye, i.e. retina, vessels...

Some other trials were performed to test some possible alternative setups. Since non of them proved satisfactory, they're only briefly discussed here without any mention in the following sections:

- Rotation about the longer WG axis was tested to try and improve image quality. Since the tabletop poser only allowed for tilting the WG around its shorter axis, the setup was re-arranged to have the WG with its longer side vertical respect to the poser. No significative improvement of the images was observed however. Moreover, it appears that the WG elongates images in the direction of its shorter axis. Consequently, the original setup with the WG longer axis placed horizontally was preferred. This way, we ensured that horizontal rotation of the eye model on the rotational stage was free of distortions. The vertical elongation is also one of the reasons why a simultaneous vertical and horizontal rotation experiment showed decreased accuracy and linearity.
- An attempt to use to WG at spectacle distance (12-14 mm) was made. The results did not prove satisfactory as indeed was expected, since the focal length of the Fresnel lens at the in-coupler is about 40 mm, the WG cannot correctly image objects so close without consistent distortion. Additionally, the high power needed by the LED and the high brightness of illumination already made clear that this prototype was not suited for a wearable setup.
- Finally, the transmission properties of the WG were tested by swapping positions of LED and camera. the pictures proved too dark to be of any usefulness for eye-tracking. Moreover, in this setup the camera is viewing the eye at an angle that would mar the symmetry of the tracking range.

2.2 LED and Camera

The camera used to acquire pictures is a commercially available webcam from Logitech™(C9020, Logitech™, Lausanne, CH). More information can be found online. A inexpensive (about 80$) model was chosen in order to be able to realize a cheap prototype. The focal length of the front lens was estimated in previous experiments to be 3.67 mm.

The light source is a table mounted green LED from Thorlabs™ (M530L3, Thorlabs™, Newton, NJ, US). Its peak emission wavelength is 530 nm, and consumes 350 mW power at its maximum (a very bright illumination), mounted in a 30.5 mm ⌀ housing.

.

Figure 18: Mounted LED, from `https://www.thorlabs.com`

In order to collimate the beam, a cage holding a lens was mounted in front of the LED. It consists of 2 matching frames and 4 rods, so that the cage holding the lens can slide with respect to the

one fixated on the LED, also from Thorlabs™. See 2.6 and Figure 19. The lens was an achromatic doublet with anti-reflective coating (AC254-060, Thorlabs™, Newton, NJ, US), mounted on a frame.

Figure 19: Example of a cage for mounting collimating lens, from `https://www.thorlabs.com`

2.3 Beamsplitter and Relay Lens System

The preliminary images indicated that a skewed illumination of the model eye caused great asymmetry in the CR, reducing the range of reliable tracking, as described in 2.6. Consequently, a pellicle beamsplitter (BP145B1, Thorlabs™, Newton, NJ, US) was added in order to have a frontal illumination.

A beamsplitter is an optical component that works in the following way: when hit by a beam of light on the splitting side, a certain amount of it (say 50%) is allowed to pass through, while the rest is bounced back, in a direction depending on the incidence angle according to the laws

of reflection. When the light hits the opposite side, the component acts as a beam composer, i.e. the other way round. Beamsplitter are commonly classified according to their shape (cube, plate, film...).

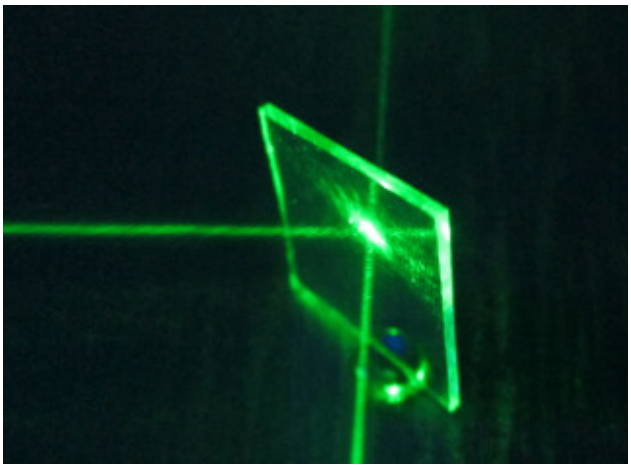

Figure 20: Example of a plate beamsplitter, from [56].

The beamsplitter was initially placed between the WG and the model eye, approximately turned 45° respect to the optical axis, with the LED illuminating at a 90° angle. The schematics of the arrangement is represented in Figure 35. The percentage of light the beamsplitter reflects on the model eye is 45%.

Additionally, a set of de-magnifying relay lenses was added between the beamsplitter and the WG in order to enlarge the FOV and to better accommodate the beamsplitter in front of the eye

Figure 21: Pellicle beamsplitter, from `https://www.thorlabs.com`

(in fact, the presence of the beamsplitter made had to position the WG exactly at 40 mm in front of model eye). For a more detailed treatise of the underlying optics, see Appendix B.

Firstly, a pair of mounted achromatic doublets with anti-reflective coating of 100mm (AC508 100) and 80mm (AC508 080) focal lengths was employed. Then the 80mm lens was replaced by a 30mm one (AC127 030) to obtain greater de-magnification: from 0.73 to 0.28.

The lenses were also from Thorlabs™. Note that since they're thick lenses, not the focal length but the working distance (WD) was considered in the calculations for magnification, see Figure 22.

By reducing the image size of the image, a better resolution could be attained, because the strong reflection from the ceramic was weakened, and consequently the image was less saturated. The range of tracking improved greatly, from $\pm 20^\circ$ to almost $\pm 50^\circ$ (see 2.6).

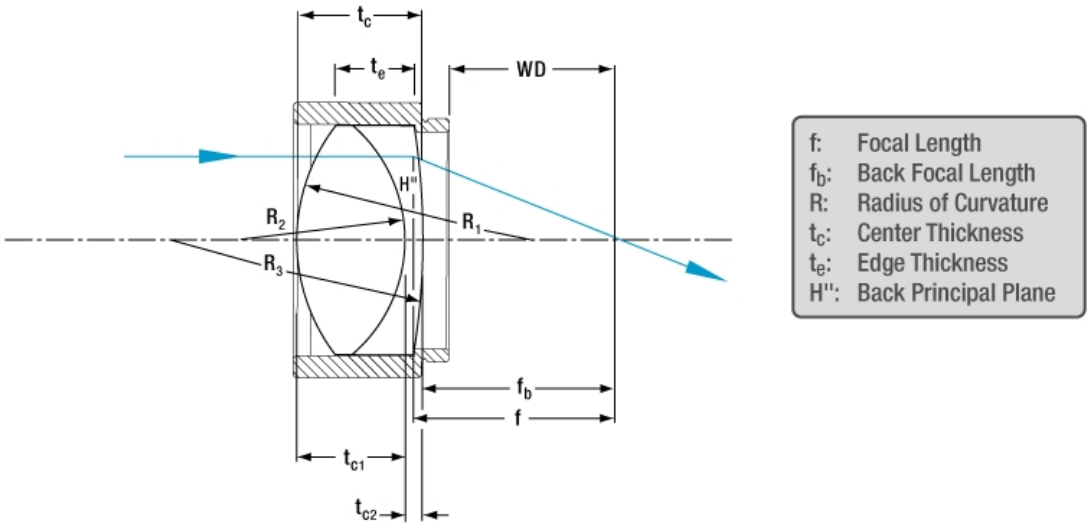

Figure 22: Achromatic doublet diagram, from `https://www.thorlabs.com`

2.4 Eye Model

The model eye for eye-tracking was chosen among porcelain prostheses having an acceptably sharp pupil vs. iris contrast and CR shape. The model eye was set onto a custom 3D printed mount connected to a laboratory translational-rotational stage from Thorlabs™(XYR1, Thorlabs™, Newton, NJ, US) to be able to quantify its rotations.

Careful adjustment of the poser into the stage is required to make sure the center of the latter coincides with the physiological center of rotation of the eye (13.5mm behind the corneal apex).

The model eye proved satisfactory for preliminary test, but presents a series of drawbacks that make it difficult to perform a more comprehensive assessment:

- it is only an aesthetic replacement, i.e. it is manufactured to look like an eye from outside, but lacks the internal part (no crystalline lens, no retina etc.). Consequently, no testing on the accommodation or *fundus* can be performed,
- for the same reason as above, the correct physiologic parameters are not guaranteed to be respected, i.e. even correctly placing the center of rotation behind the cornea may not ensure a completely realistic performance,
- the cornea curvature is not perfectly spherical, and it is slightly asymmetrical, being more elongated on the vertical axis. Consequently, the simultaneous vertical and horizontal rotation is not reliable for testing, as also discussed in 2.6,
- for the same reason as above, the CR shows progressively stronger astigmatism (becomes elongated instead of circular) as the eye rotates, and not a clear change in shape as is would on a real eye when the illumination falls off the *cornea*.

Luckily, it appears from the experiments that the proportions are accurate enough that, with a careful positioning, a realistic rotation can be simulated on the horizontal axis. As a consequence, to simulate a vertical rotation, it was finally decided to use the eye model in the same position and rotate the black rubber screen of the dummy eyelids.

As for the CR astigmatism, it is possible to partially compensate it with the image processing algorithm, that is set to recognize the CR region and compute its center. As long as the aberration is not excessive, we can assume the center of the CR ellipsoid approximates the one that would be

.

Figure 23: Stage for the eye model, from `https://www.thorlabs.com`

calculated for a circular CR. For the physiologic ranges of eye rotations [7, 63], the approximation can be considered valid.

2.4.1 Other Eye Models

Other eye models were tried in order to make up for the shortcomings of the prosthetic one, mainly for the lack of the possibility to measure accommodation. Because of various reasons, they proved not useful for accommodation measure and/or less suitable than the prosthetic one. Anyway, to be thorough, they are briefly described below.

First Custom Built Eye Model a lens mimicking the cornea was glued with refractive index matching Norland™ optical adhesive (NOA 61, Norland™, Crannbury, NJ, US) to the front of an adjustable circular iris diaphragm and tube (also from Thorlabs™, ID8). The idea was that the diaphragm would simulate the adjustable pupil aperture. On the back of the diaphragm,

a threaded ring with attached a printed image of a *fundus* was placed. By adjusting the ring position by screwing or unscrewing it on the diaphragm, we would simulate accommodation.

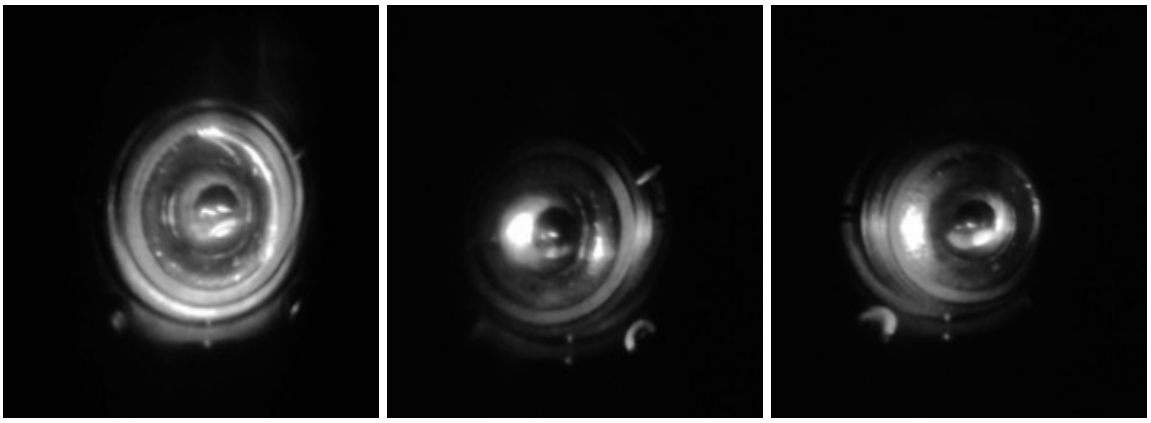

(a) (b) (c)

Figure 24: Pictures from the first alternative eye model.

Unfortunately, the model resulted unsatisfactory, as the low contrast and the strong reflection from the metal mount of the diaphragm and the back part of the lens and glue front makes it impossible to isolate pupil and CR. Moreover, the retinal pattern on the back was not visible, so the accommodation part cannot be tested, as one can see in Figure 24. This is probably due to the very small focal length of the lens (15 mm) that creates very large distortions in the patterns. Unfortunately, this could not be solved as no components of comparable lengths are available.

Commercially Available OCT Eye Model the image quality is quite good but there are again some strong reflections from the border and two corneal reflections probably originating from the double plastic surfaces. This model cannot handle the accommodation part (no adjustable components) but it may be decent for eye-tracking, although not as good as the prosthetic one.

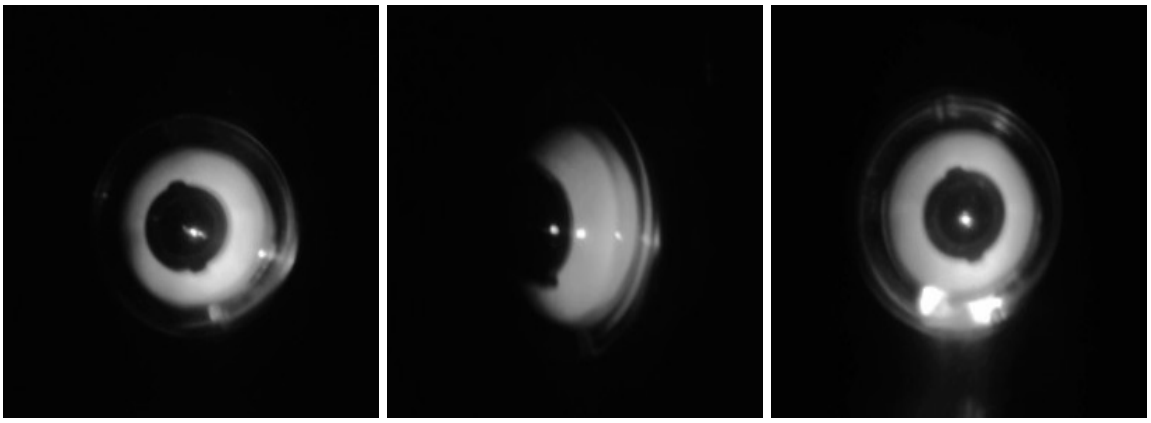

(a) (b) (c)

Figure 25: Pictures from the OCT eye model.

Second Custom Built Eye Model the pieces were designed with SolidWorks™ and 3D printed. The dimensions and placement of components was suggested by Dr. Lei Liu, collaborating with our lab for the creation of the prototype. The model comprises two shells mimicking the bulb (the rear one in principle should have been hollow in order to allow for placement of a laser pointer, to better trace eye movements on a screen. However, since the model that was

built in the allotted time did non prove worthy of further trials, the laser pointer part was neglected. The front part has a flat frontal section with a small hole (mimicking a pupil, with no possibility of replicating changing pupil size). A round lens (the same of the first model) was glued on the flat front part to simulate the cornea, while an absorbing filter with cut-on wavelength at 1000 nm (FGL1000, Thorlabs™ Newton, NJ, US) was glued to the inner part of the front flat section, to simulate pupil light absorption. As instructed, the shells were printer in dark matte plastic to avoid unwanted reflections. A 2-piece holder was also printed to ensure right rotation.

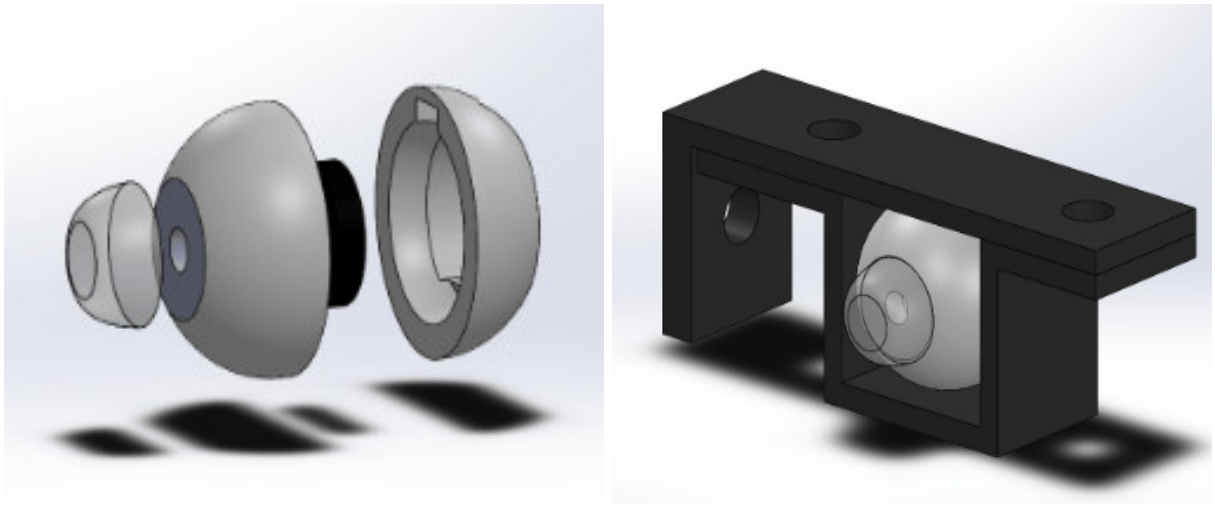

(a) Exploded view of eye model components (b) Eye model inside holder

Figure 26: Second custom built eye model and holder.

Unfortunately, also this eye model was not good enough for eye-tracking, as the contrast offered by the dark plastic respect to the background is not enough for image segmentation, given the quite low efficiency of the WG. In turn, the clear plastic of the 3D printer caused too much reflection, rendering CR identification impossible.

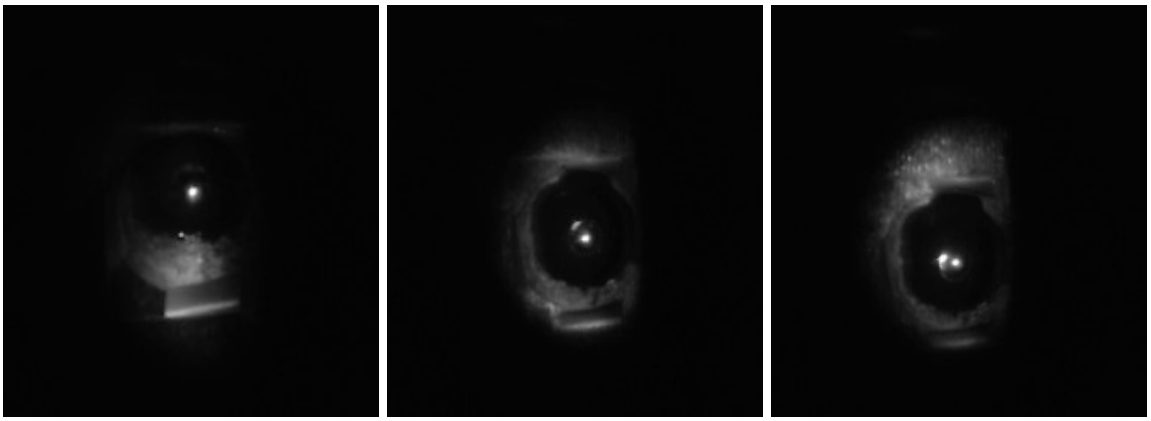

(a) (b) (c)

Figure 27: Pictures from the second alternative eye model.

It was concluded that for preliminary eye-tracking testing, the ceramic prosthetic eye could do in the lack of best alternatives with quick turn around time. For the accommodation part (which is out of the scope of this dissertation), it was suggested the purchase of a dedicated model for future experiments. In short, constructing a model eye capable of handling accommodation and EMs at once is extremely hard to do in laboratory facilities.

2.5 Eyelids

As the image-processing procedure proved satisfactory for a preliminary testing, it was suggested by Dr. Lei Liu that also eyelids should be simulated. In normal eye-tracking applications, the presence of the eyelids is usually an inconvenience for extreme rotations, as they hide part of the pupil, and that must be taken into account when trying an algorithm. Also, since much if the white part of the eye was covered by the eyelids, the overall brightness of the image decreases. On the other hand, stray reflections from the white ceramics can be avoided this way.

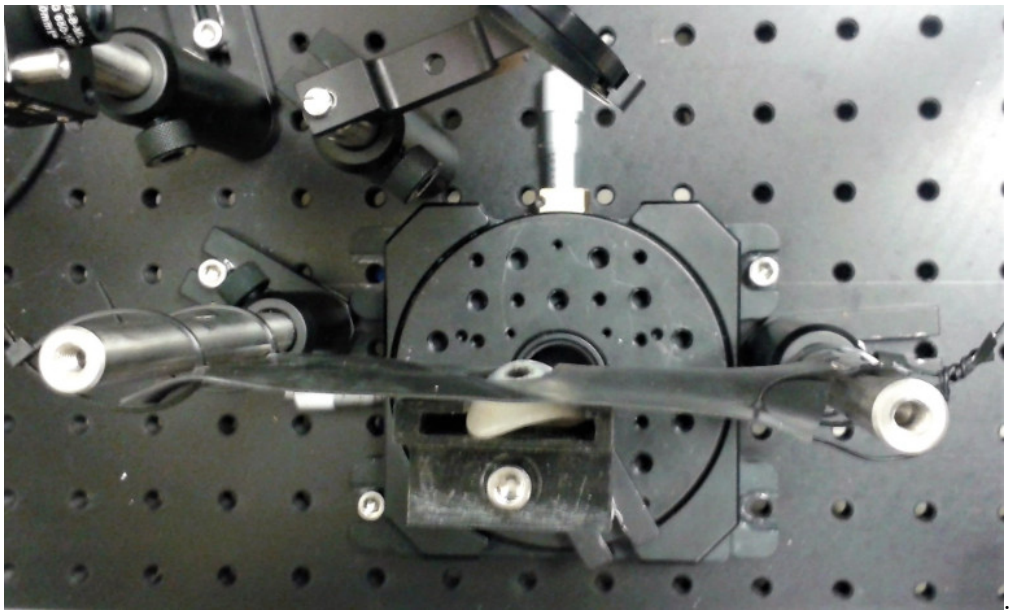

Figure 28: Dummy eyelids setup.

Since eyelids move when the eye rotates, a black rubber square screen with a cut-out opening was held by posers in front of the eye model, slightly covering it, so that the model eye was able to push them on the side when rotating. As explained in 2.4, since the vertical axis of the prosthetic model eye shows a larger curvature than the horizontal one, rendering the vertical rotation not reliable, it was simulated rotating the screen instead.

The results with and without dummy eyelids are similar, and therefore in Chapter 3 only the more accurate experiments with eyelids are reported, however, in some images it was necessary either to re-trim the area of interest (to cut out strong reflection from the rubber) or to change manually the threshold for image segmentation.

Additionally, a trial using a custom built 2D rotational stage was performed although it did not prove completely satisfactory (as discussed in 2.6), is still reported in the Results section for sake of completeness. In this case the eyelids could not be placed independently of the eye model and needed to be taped on the holder.

2.6 Setups

2.6.1 Preliminary Adjustments

The most basic setup comprised only LED, camera, WG and eye model. The LED is approximately at a 45° angle respect to the eye model, about 10 cm afar, at maximum intensity, see Figure 29, and Figure 30. The images are acquired and saved with National Instruments™ data acquisition software. With this configuration, it is possible to place the waveguide facing directly the model with at the correct 40mm focal length.

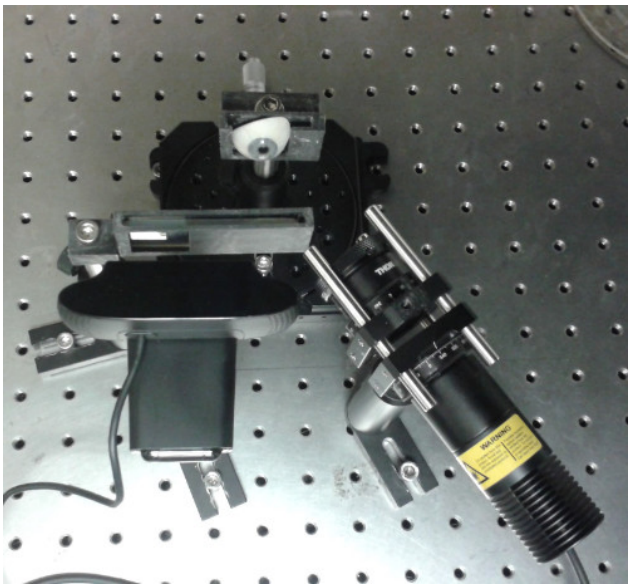

Figure 29: Preliminary setup picture.

Careful adjustment of the relative position of the components so that the camera could catch the strongest collimated image from the output coupler was required (as multiple orders of diffracted images are created at the out-coupler).

To investigate if changing the camera parameters could improve picture quality, six sets of pictures were taken, each one varying one parameter between Brightness, Contrast, Sharpness, Saturation and Backlight compensation respect to the first trial. The acquisition procedure is the following: 5° steps, ranging from 20° to the left facing the eye model (negative degrees) to 20° to the right (positive degrees).

These parameters do not seem to affect considerably picture quality, as it can be seen in Figure 32, so the default settings were used in all other trials. Minor adjustments of contrast and brightness, if needed, were performed by image processing tools in Matlab™ or ImageJ OSS.

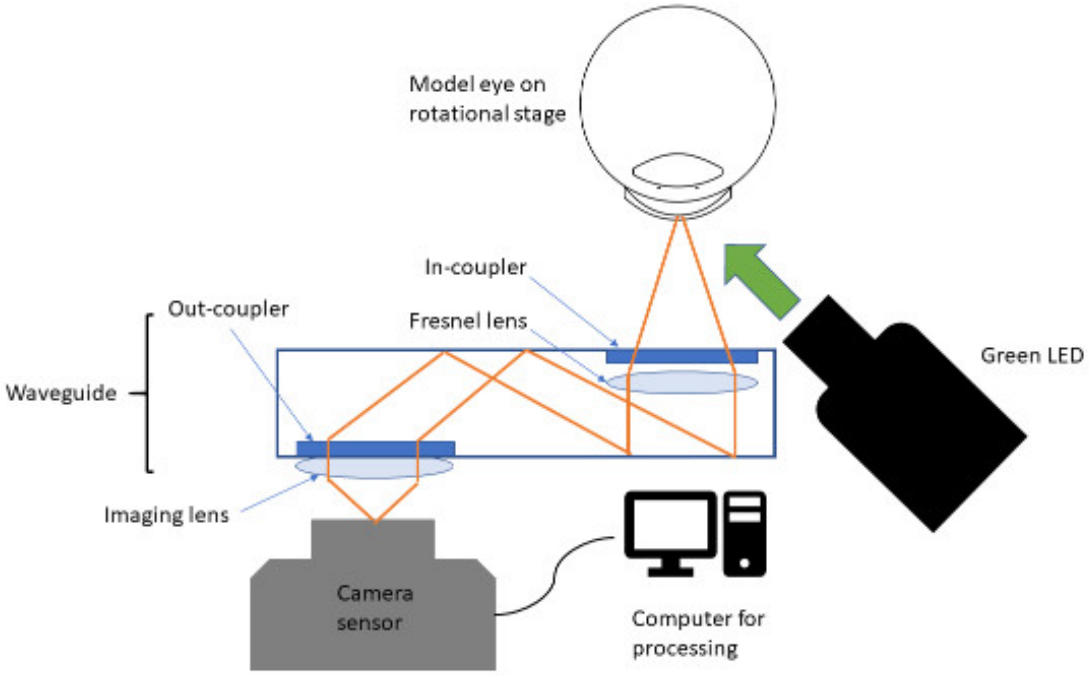

Figure 30: Preliminary setup scheme.

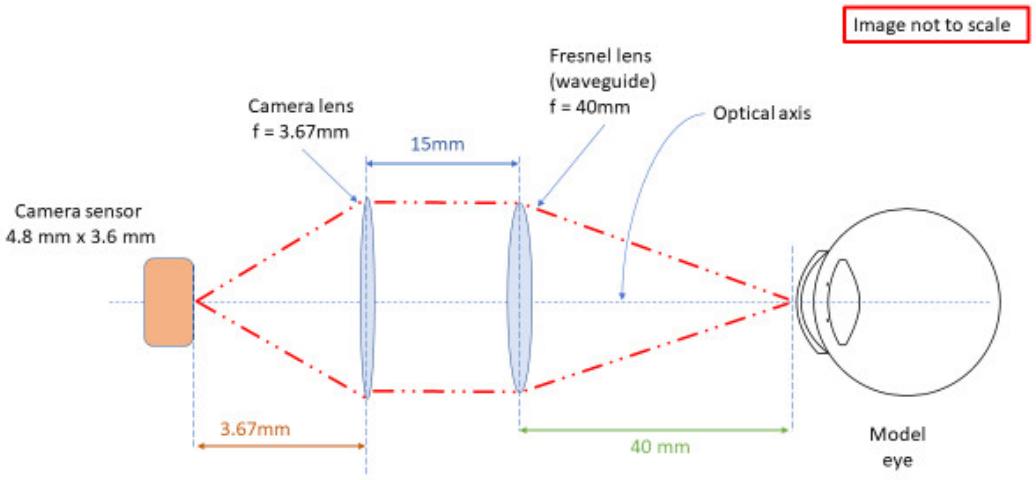

Figure 31: Preliminary setup optical model.

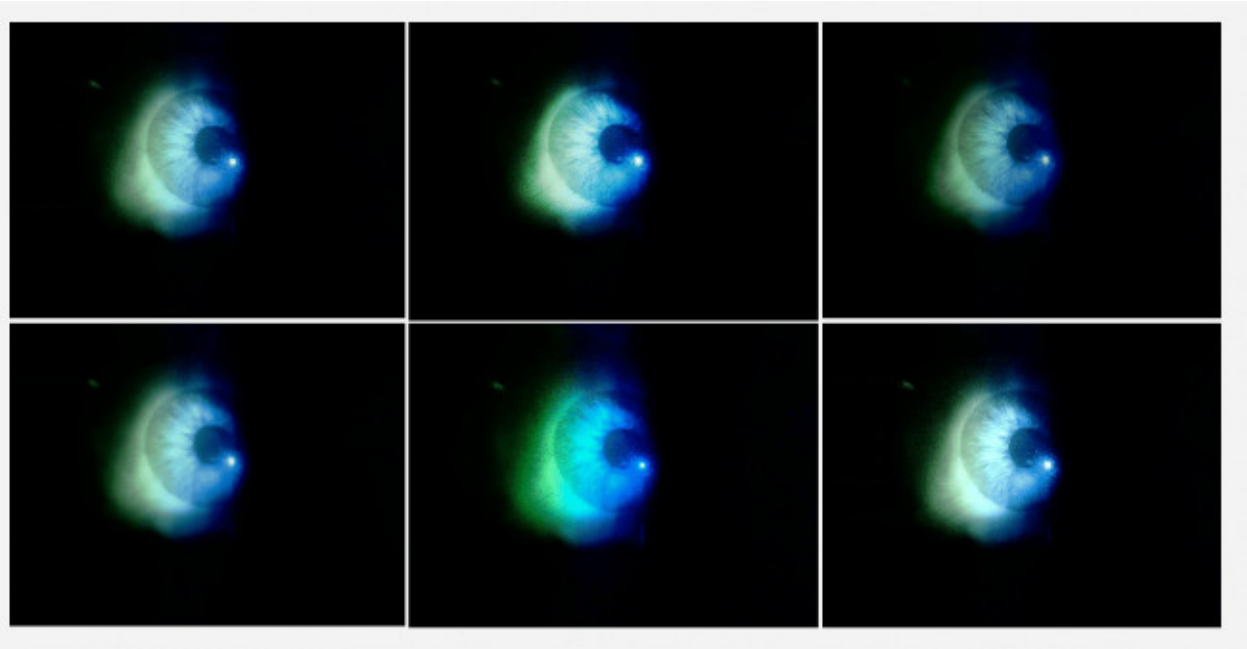

Figure 32: Influence of camera settings on image quality (all pictures are +10°).

Next it was tested the influence of LED settings: intensity, focus dimension and orientation. Images were acquired with the same previous procedure.

- Trial 1: reducing the intensity by 1/3, other parameters constant.
- Trial 2: light intensity at maximum, focus reduced so that it covers only iris and pupil part, other parameters constant.
- Trial 3: both intensity reduced by 1/3 and focus reduced to iris area. Orientation constant.
- Trial 4: intensity at maximum, focus at widest, orientation was more frontal (approximately 30°) as much as permitted by waveguide casing.
- Trial 5: as trial 4 but with light intensity reduced by 1/3.

- Trial 6: as trial 5 but with focus reduced to cover only iris and pupil area.
- Trial 7: as trial 4 but with focus reduced to iris area.

In the Figure 33, the reader can observe some comparative pictures of the various trials.

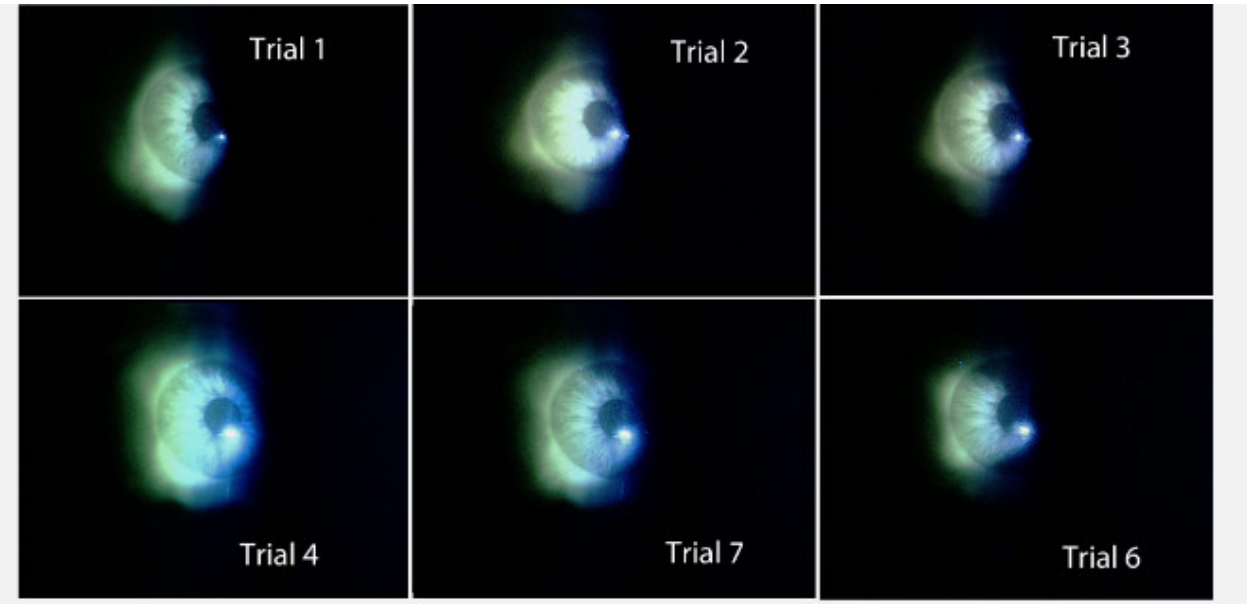

Figure 33: Influence of LED parameters on image quality (all pictures are +10°).

Some considerations can be drawn:

- images obtained with more frontal illumination look definitely better (trials 4, 5, 6, 7), despite a shadow from the waveguide covering partially the LED, as it can be expected with a more symmetrical setup;
- reducing the light intensity is good for avoiding saturation of image (trials 1, 3, 5, 6);

- reducing the focus size on the other hand does not seem to improve the results as much (trials 2, 3, 5, 7). Observing 1 vs. 2, 4 vs. 7 and 5 vs. 6, that the image looks slightly less blurred with a more focused light source, but that this implies that the pupil almost disappears for small rotations, for it goes out of illumination source.

Also, in all these trials, it is necessary to point out the strong astigmatism noticed for leftwise rotations, due to the fact that the light source hits the eye model on the right side. The CR is already weakly distinguishable for very small rotations (-10°), be it because of saturation of the image or because the light is too askew, while for rightwise (positive) rotations, it can be distinguished up to 20° in some trials, as it can be observed in Figure 34.

Furthermore, it can be observed that the clearly illuminated part of the image is restricted to the iris and a bit of the *sclera*, even keeping the light beam at maximum width. Such a narrow FOV is not enough for rotations greater than 20°.

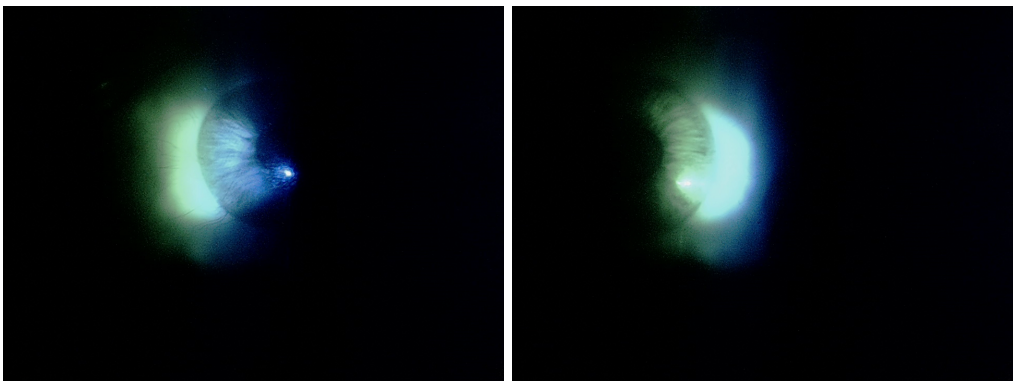

(a) 15° rightwise rotation (b) 15° leftwise rotation

Figure 34: Effect of the skewed illumination.

As a mean to fix these inconveniences, a beamsplitter was added in order to have frontal LED illumination and mend asymmetric range, while a de-magnifying lenses system was employed to enlarge FOV, reducing the saturation and enabling a wider range to be tracked.

2.6.2 Beamsplitter and Relay Lenses System

2.6.2.1 Beamsplitter

The arrangement of the system was already described in 2.3, and id depicted in Figure 35.

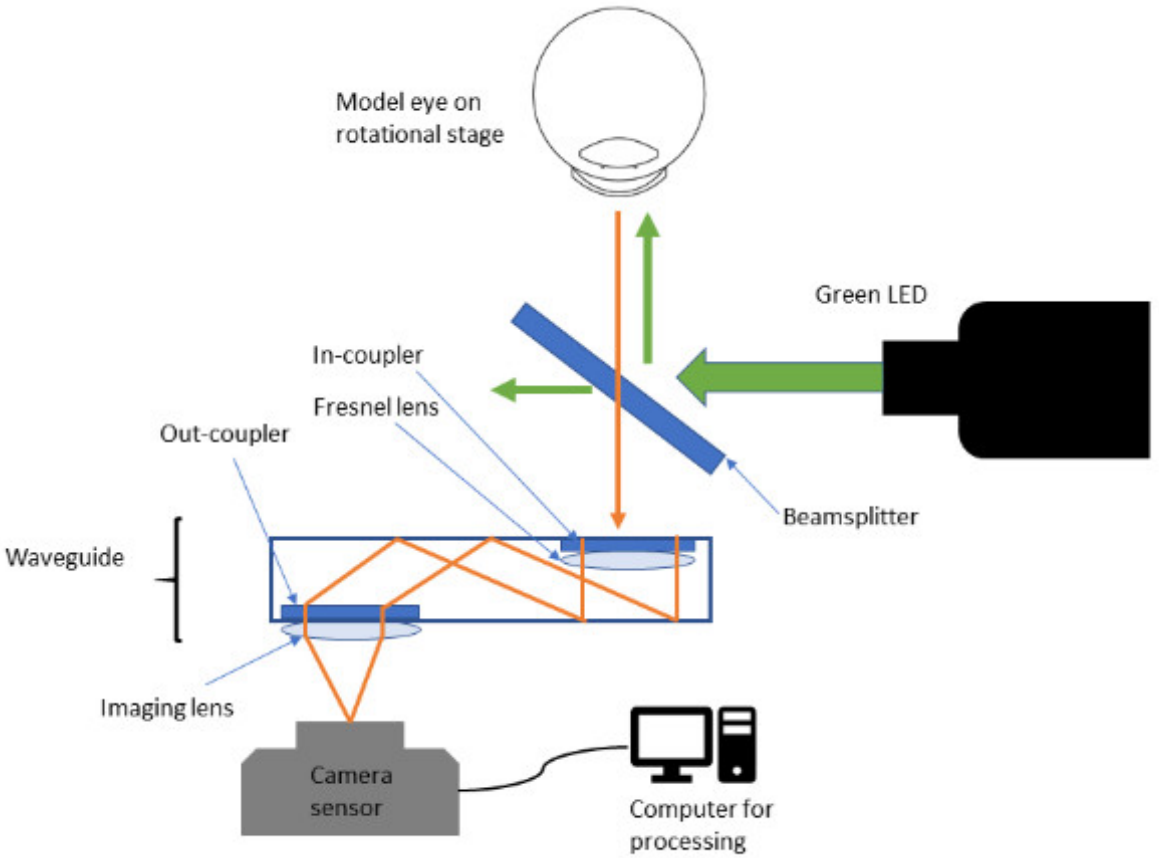

Figure 35: Scheme for the addition of the beamsplitter.

The addition of the beamsplitter alone granted the asymmetry of the pictures but only slightly improved the image quality, as the illuminated region stayed very narrow, as one can see in Figure 36. The loss of illumination due to the beamsplitter was acceptable, as it was previously observed a trade-off between reduction of contrast (lower illumination power) and image saturation (higher illumination power). To achieve a higher range of tracking positions, it was necessary to add relay lenses.

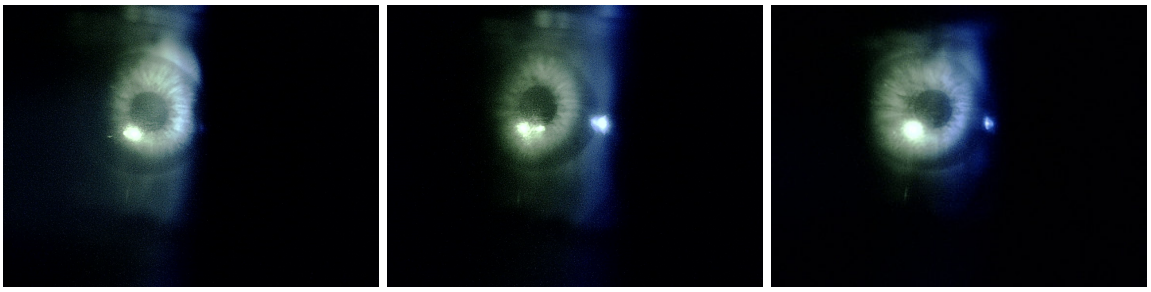

(a) (b) (c)

Figure 36: Improvement of image quality after addition of beamsplitter (all pictures are 0°).

2.6.2.2 First Set of Relay Lenses

In order to enlarge FOV, a de-magnifying lens system was added. Initially, the setup shown in Figure 38 and Figure 39 accomplished a magnification of 0.72 (i.e. a de-magnificcation of about 25%).

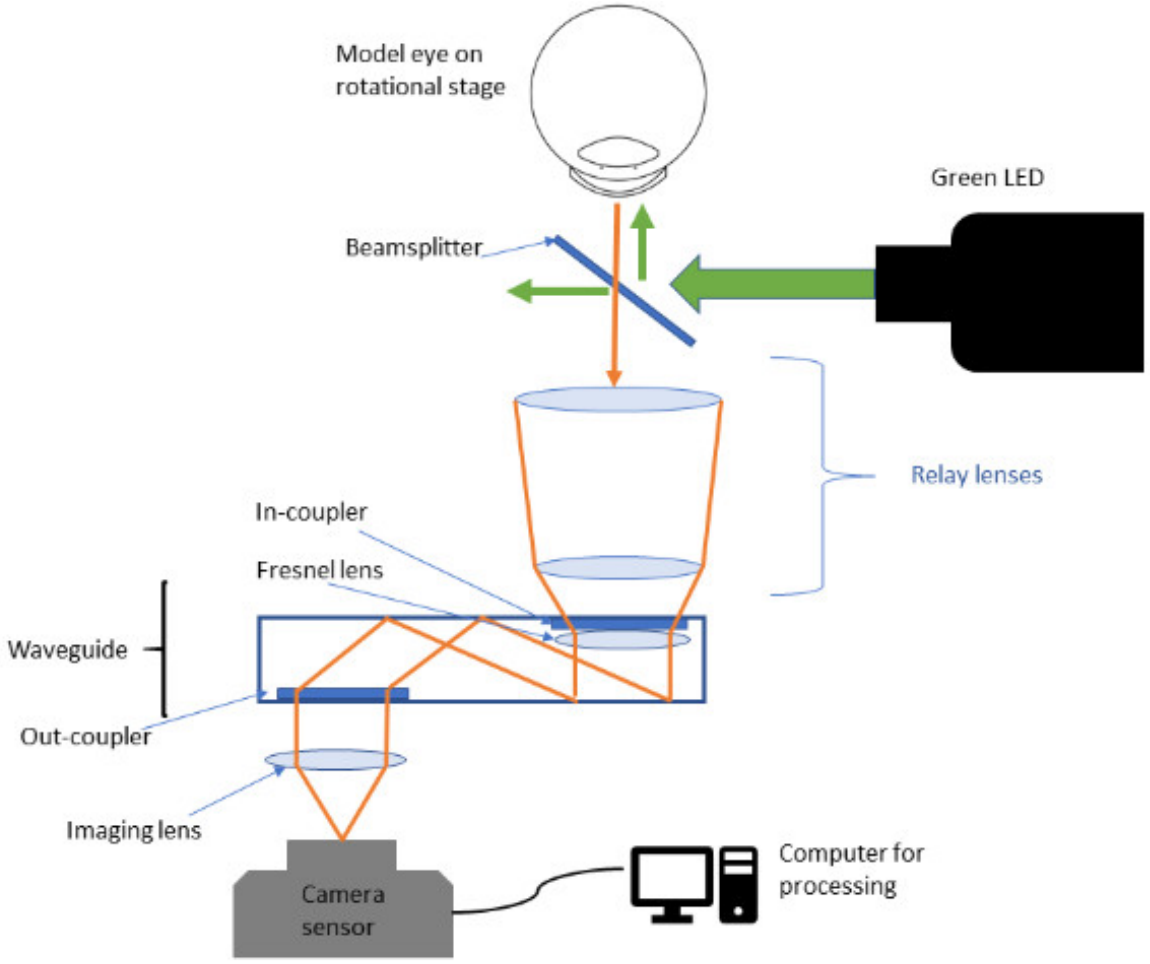

Figure 37: Scheme for the addition of relay lenses.

The improvement of the image quality was evident, as one can tell from Table II. However, the images acquired with the relay system are reversed. This is actually no problem as it can be easily fixed with image processing.

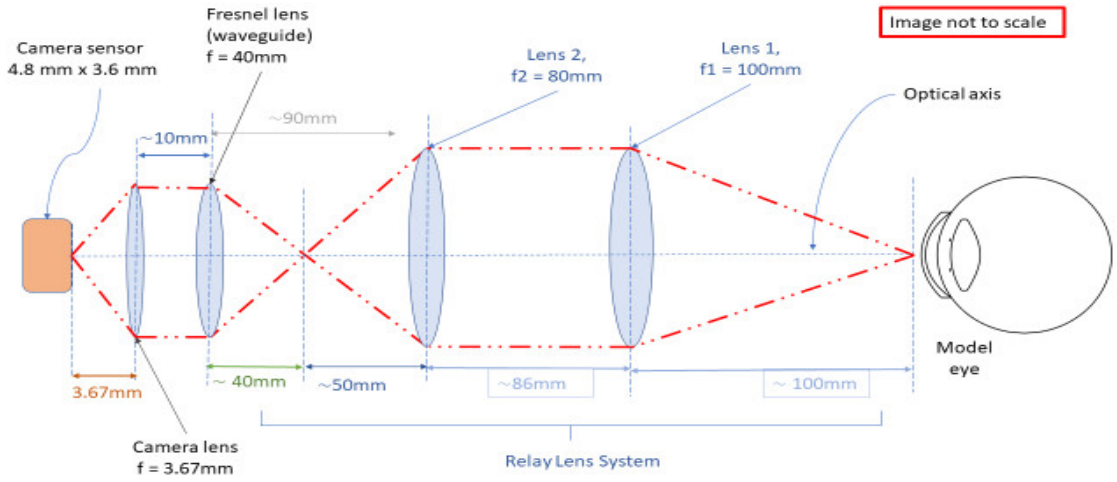

Figure 38: First set of relay lenses optical model.

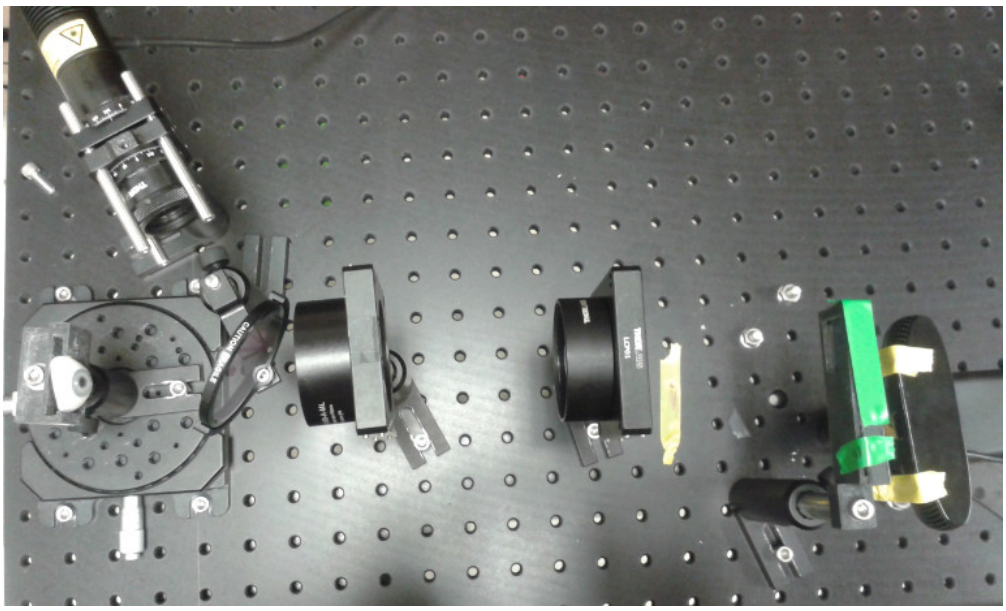

Figure 39: First set of relay lenses picture.

TABLE II: TABLE COMPARING BEAMSPLITTER AND RELAY LENS SYSTEM EFFECT ON IMAGE QUALITY.

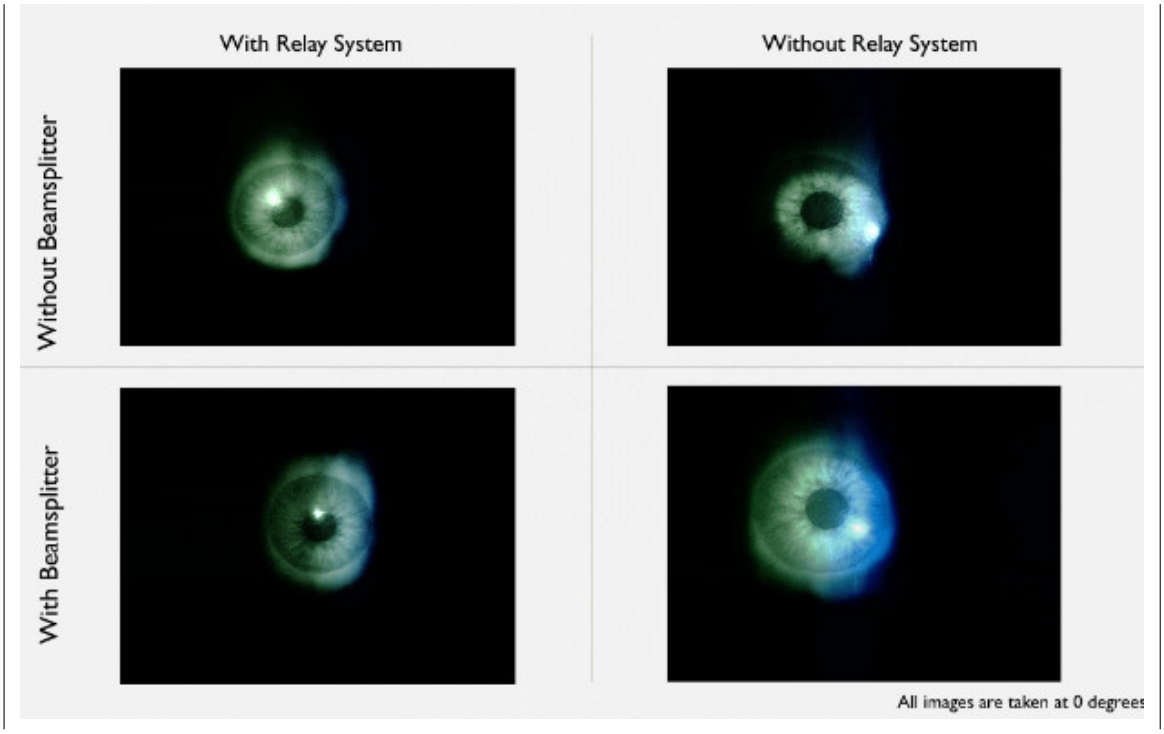

2.6.2.3 Second Set of Relay Lenses

A further de-magnification ($|M| = 0.28$, a 70% de-magnification) was tested with the second set of lenses depicted in Figure 41 and Figure 40.

The new setup allowed for recording images up to 45° of rotation in both directions, with a good enough resolution despite the de-magnification, as it can be observed in Table III. The Table compares the pictures taken with the two different setups at 0° an intermediate rotation and at the two extremes of rotation, that is 20° for the first setup and 45° for the second. Observe also

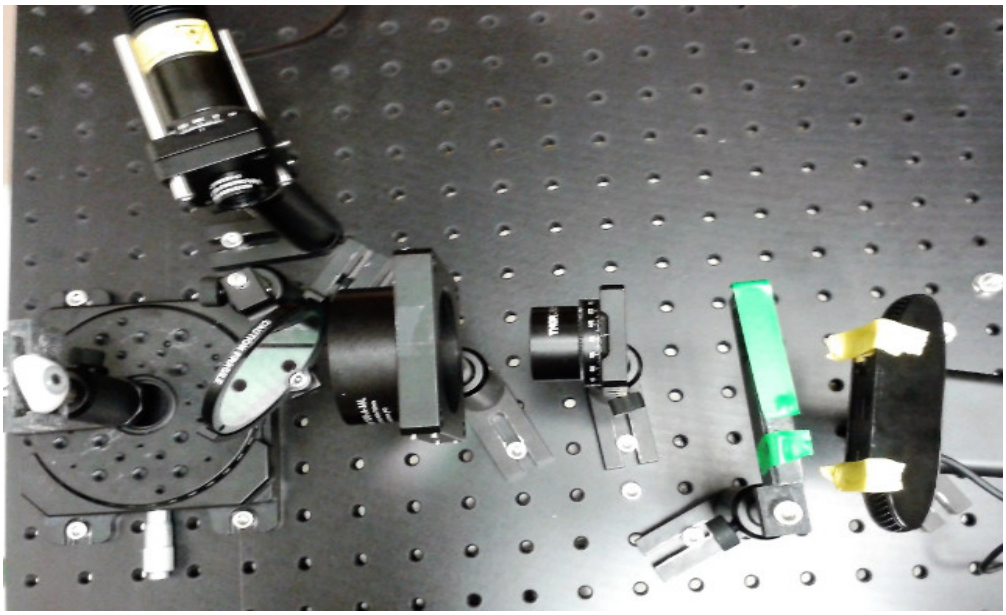

Figure 40: Second set of relay lenses picture.

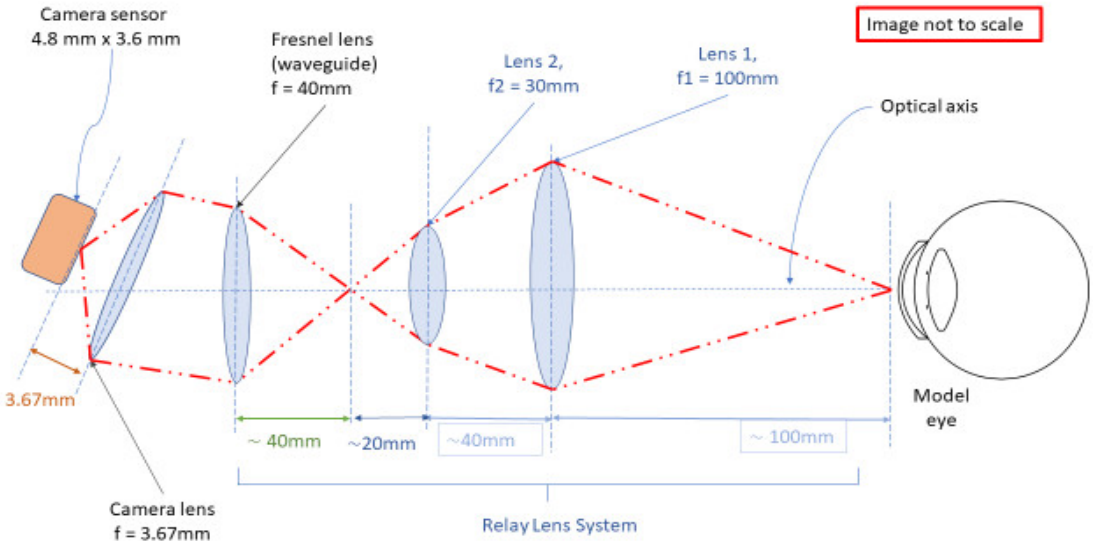

Figure 41: Second set of relay lenses optical model.

the different de-magnification entities. At this point the image quality was deemed appropriate to start the creating of an image processing procedure, described in section 2.7.

TABLE III: TABLE COMPARING THE TWO DIFFERENT RELAY SYSTEMS.

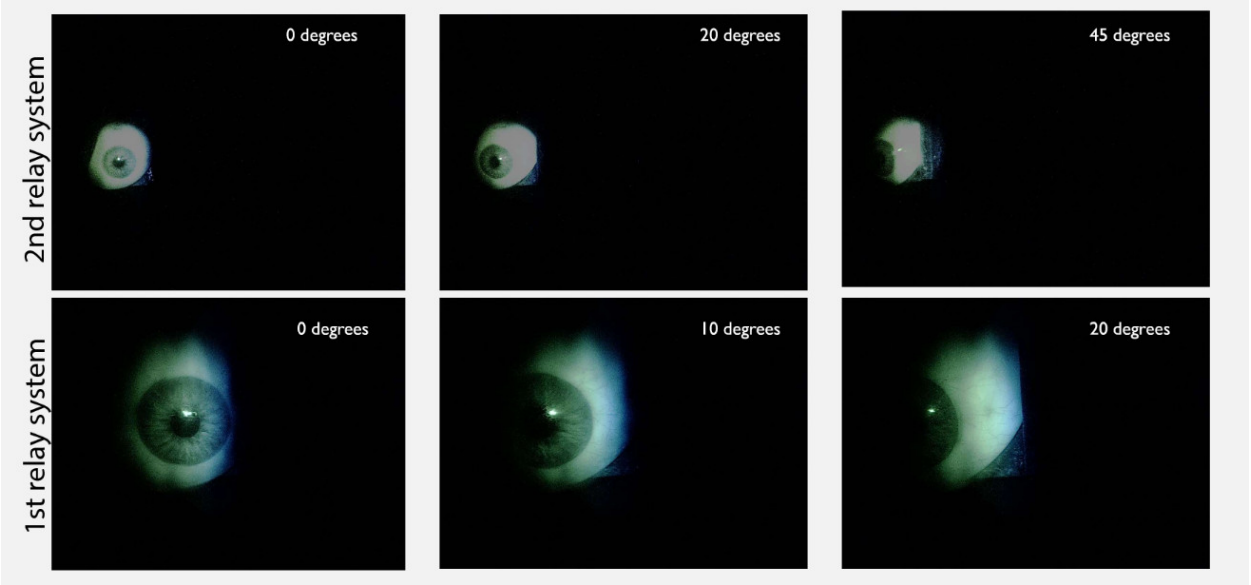

Another important observation was the one already mentioned in 1.2, that is that the image quality improves when the WG is put at an approximate 20° angle respect to the camera, as schematized in Figure 41, Figure 33 and Figure 42. This may be partially due to the non perfect alignment of the WG in the casing, and to the presence of and angle respect to the WG normal of the principal order of diffraction.

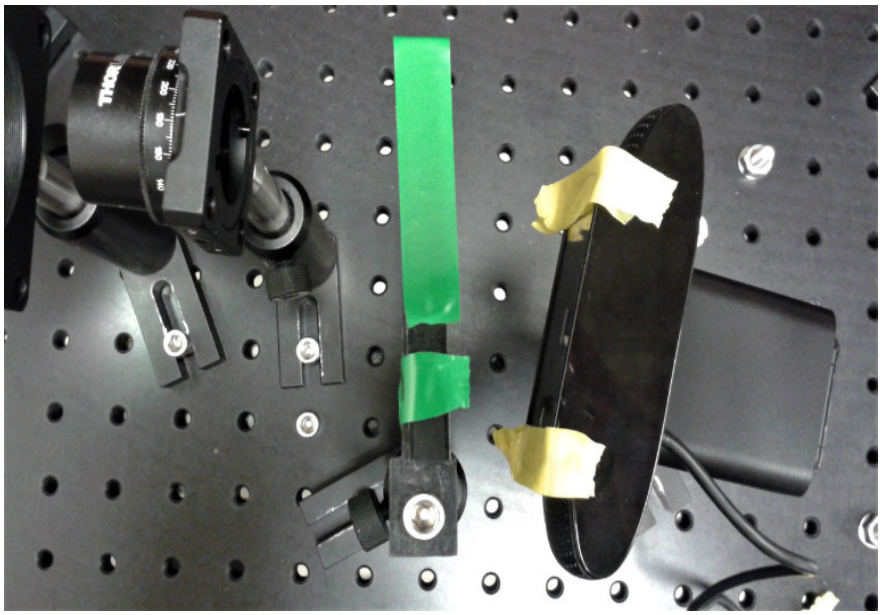

Figure 42: Detail of the angle between WG and camera.

An important note: in the perspective of creating a wearable setup, it is clear that the relay lens system cannot be included. In the compact version of the system, however, the light source will be almost frontal to the eye, there will be no need for the beamsplitter and the relay system (which is hampering because reverses the image and make the whole system bulky), as one can see in Figure 43. Also, by getting rid of the above said components, it will also be possible to better exploit all the input light intensity to avoid the pupil being confused with the dark background (due to losses through lenses and beamsplitter), as well as of other distortions that might be caused by the lenses. Therefore, compactness of the possible finished product should not be an issue. Additionally, a system that proves feasible with all the above said losses of light and distortions, it will be probably even better performing without them in the finished design.

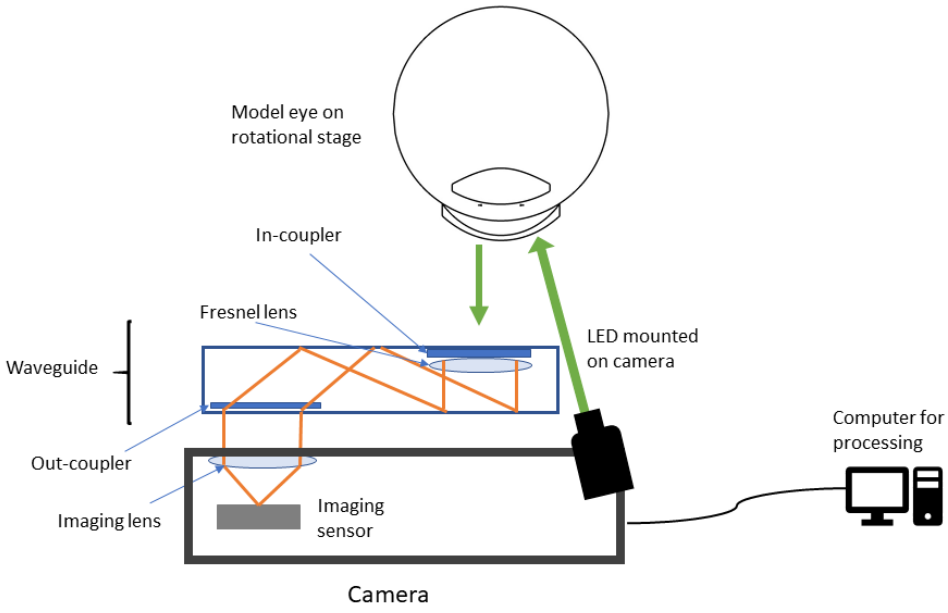

Figure 43: Wearable setup scheme.

2.6.3 2D Rotations

To perform a thorough evaluation, a poser combining two rotational stages was created by printing 3D custom mounts designed with SolidWorks™(as available 2D gimbals had a too narrow range of rotations to be of interest). The horizontal stage hold such a mount in which a smaller stage is held at a 90° angle, so to allow for simultaneous vertical and horizontal rotations. The second stage holds a mount in which to place the model eye. See also Figure 44.

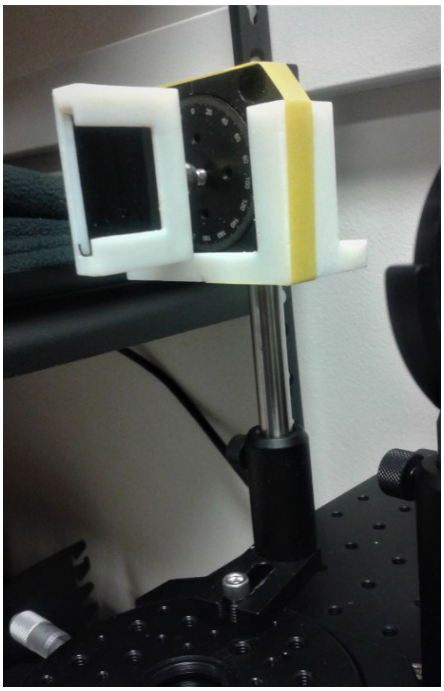

(a) 2D rotational stage picture.

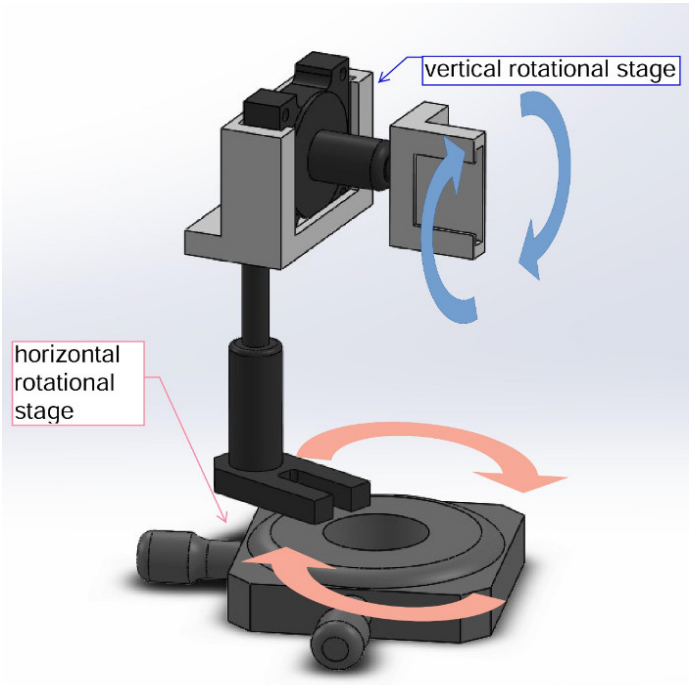

(b) 2D rotational stage CAD model.

Figure 44: 2D custom built rotational stage

Unfortunately, due to:

- the asymmetry of the model eye,
- the fact that with this setup, the rotation center of the eye model is harder to pinpoint and control and so it is not representative,
- the rotation of one of the two stages inevitably displaces the eye, so it exits the illuminated zone for extreme rotations (obviously, this cannot be made up for by moving the LED to illuminate again the eye model, as it would disrupt any linearity in the pupil center-CR vector vs. eye rotation).

The results of the image processing proved a worse performance than in the single rotation trials.

Additionally, the higher ranges of movement rendered it impossible to realize realistic dummy eye-lids. The only option was to wrap the model eye in some black matte rubber with a cut out opening, but is clearly not as faithful as the screen shown in 2.5.

Since this arrangement did not resemble faithfully physiological eye rotations, and eyelids movements, it is not considered in the final discussion for feasibility, although still presented in Chapter 3 for completeness.

To summarize: in the final setup, the rotation on the vertical axis was simulated simply by rotating the dummy eyelid screen so that the cut out opening had its longer dimension on the vertical axis rather than on the horizontal one.

2.7 Image Processing Algorithm

2.7.1 The Starburst Procedure

The algorithm was developed by Li and Parkhurst as an Opens Source program in 2005 [35]. For the reader's interest, the address of GitHub repository for original files is `https://github.com/thirtysixthspan/Starburst`. It is based on the pupil center-CR vector change to infer the gaze of the seer, and requires two videos, one of the eye of the user and one of the scene onto which to plot the gaze.

It was initially met with a good enthusiasm and used by Li et al. [33, 36], and later adapted by Li and Parkhusrt for *limbus* tracking [34]. Apparently the procedure has not aged well, as Fuhl et al. [19] show in their review of state-of-art eye-tracking algorithms. Despite this, the model idea is still valid as merges both feature-based detection (i.e. based on the analysis of the pixels of the image) and model-based techniques (i.e. seek the model of pupil that best fits the presented

image. Usually this is accomplished iterating a fitting procedure and changing some parameters of the mdoel with each cycle). Moreover, compared to other procedures, is still quite simple.

The procedure can be schematized as:

1. Image acquisition by extracting frames from eye video,
2. Gaussian filter to remove noise, the standard deviation of the smoothing can be decided by user.
3. Windowing and adaptive threshold filtering to find CR: the image is filtered with a threshold that is lowered with each repetition, increasing the number and area of bright spots. The optimal threshold is determined when the ratio of area of the largest bright spot (the CR) to the sum of the others starts decreasing (as in the beginning the CR will grow faster than false reflections, until the threshold grows too low). This ensures the CR is located in its full extension.
4. Removal of the CR by radial interpolation: the radius of the CR identified in the previous step is multiplied by a factor (by default 2.5 assuming Gaussian profile). The central pixel is set to the average of the intensities of the perimeter pixels and then each radius' pixels are swapped with the result of a linear interpolation between the central pixel and corresponding perimeter pixel intensities.
5. Estimation of pupil contour by extending a number of rays from the pupil center best guess with edge detection (threshold to be set by user). For each edge point candidate, a set of additional rays is created and new edge points are identified. This procedure is repeated until convergence (i.e. the new edge point at that iteration are below a certain threshold, also set

by user), using each time as a start point the average of positions of the candidates. Figure 45 and Figure 46 show these steps.

Figure 45: Pupil contour using Starburst procedure. (a) the first set of rays is driven outwards and finds pupil contour candidates, (b) and (c) compare the second set of rays emerging from a true edge point vs. a false one. Reprinted with permission [36], ©[2005] IEEE.

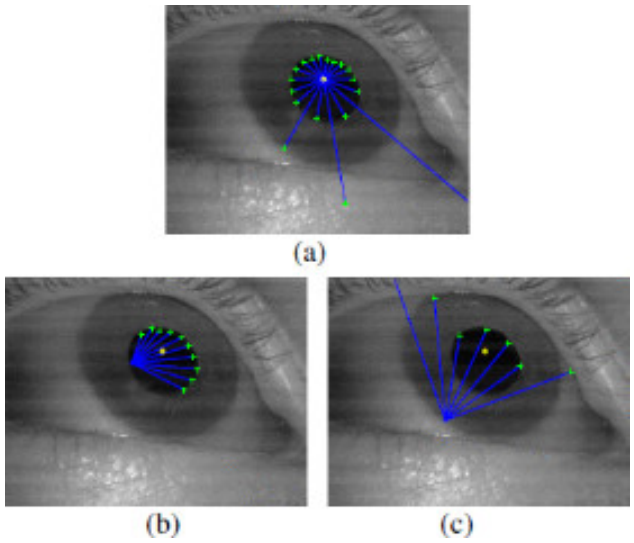

6. Fitting of and ellipse to the edge points through a RANSAC (RANdom SAmple Consensus) paradigm. This strategy is used when applying model fitting to a distribution containing outliers in order to decide which points are acceptable and which ones would only mislead the fitting. RANSAC is an iterative mechanisms that pics many sparse and random groups of point from the main data set, uses each to fit a model, and keeps the fitting that agrees

Figure 46: Iteration of the pupil edge detection. Reprinted with permission [36], ©[2005] IEEE.

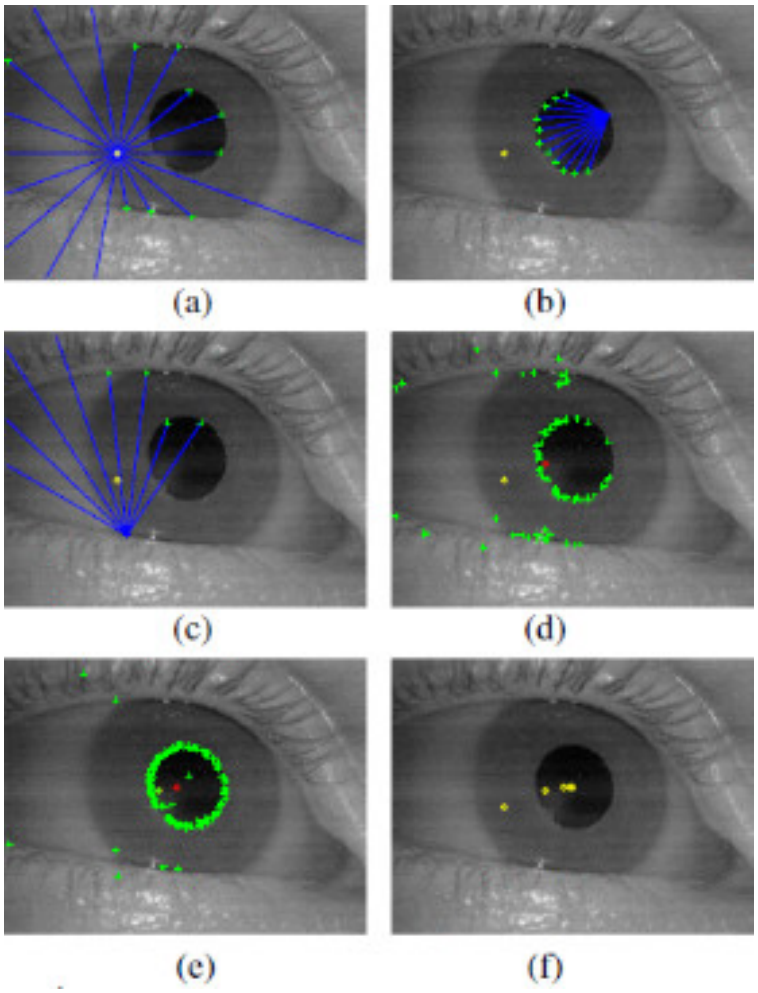

with the whole data set at best. The number of maximum iterations an also be set by the user.

7. Model-based optimization of the ellipse found at the preceding point using Nelder-Mead Simplex search for convergence.

8. Apply calibration to estimate gaze point in scene.

Figure 47 summarizes the procedure.

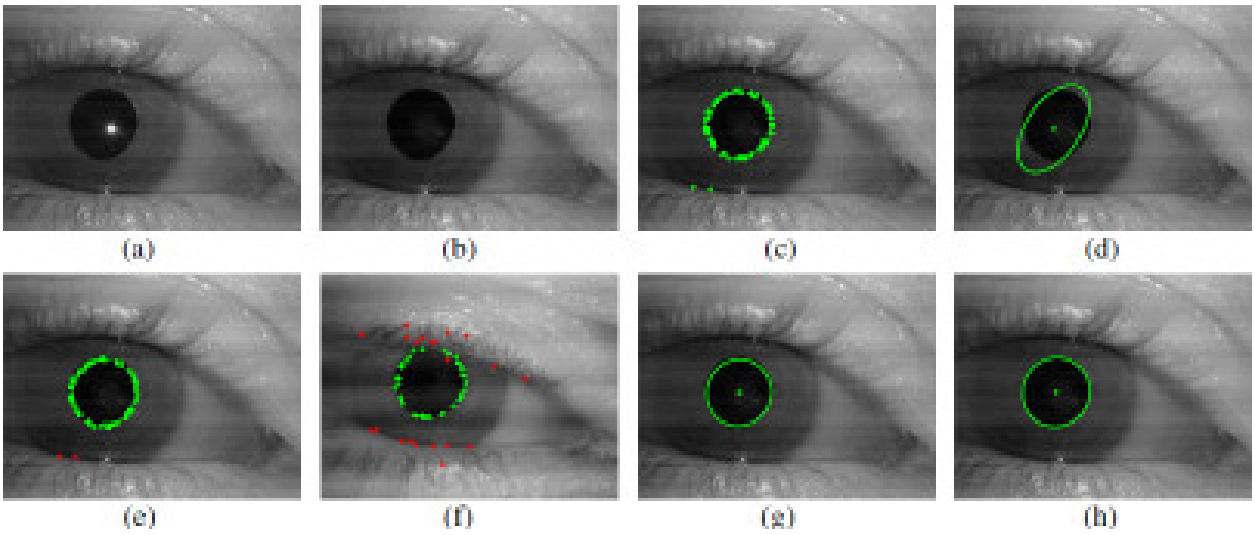

Figure 47: The Starburst procedure: (a) Gaussian filtering, (b) CR removal, (c) Pupil edge detection, (d) Normal least-square ellipse fitting (with outliers), (e,f) How RANSAC discriminates in-liers (green) and out-liers (red), (g) Best fitting ellipse, exploiting in-liers identification from RANSAC, (h) Model-based fitting. Reprinted with permission [36], ©[2005] IEEE.

Unfortunately, the original procedure proved very hard to employ for this specific application. First of all, the code is very poorly commented, that makes understanding of the procedure very hard. Secondly, it was written to be used on Linux OS, so that adapting to Windows™ platform was required for some functions. Finally, it has not been updated for at least 7 years, that means that many Matlab™ functions and also some shell commands do not work anymore or are deprecated and end up in errors, crashes and weird results.

Figure 48: Some images processed by updated Starburst.

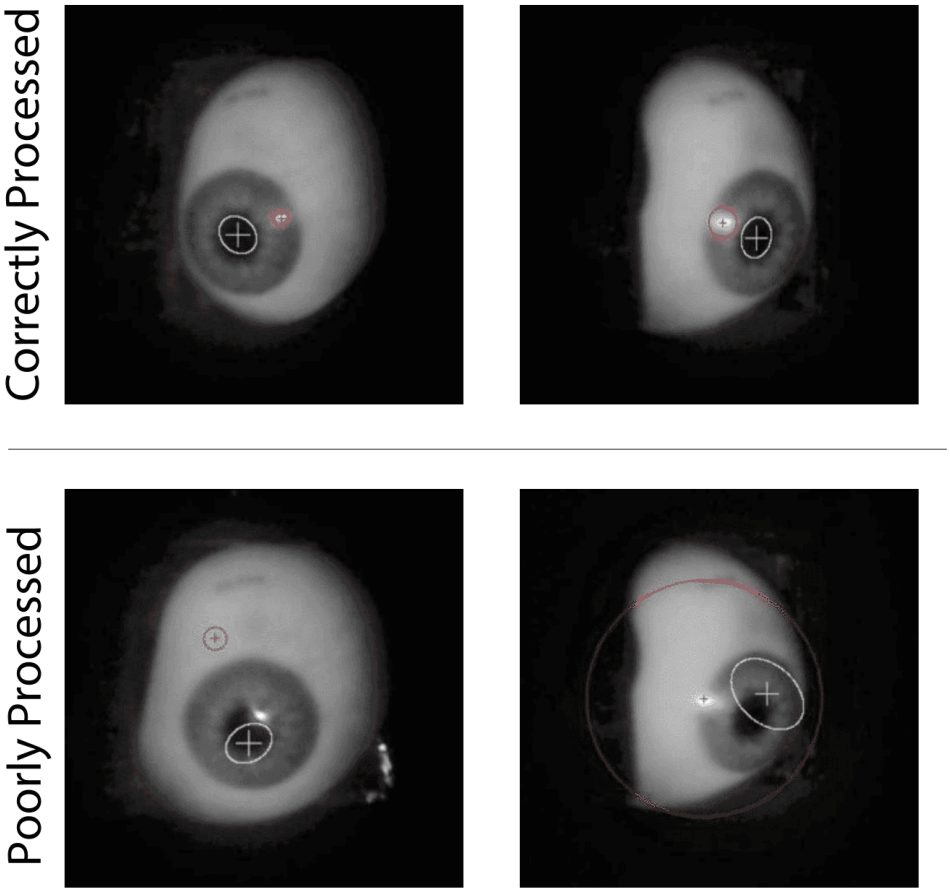

Despite trying to fix the original Starburst for more than two weeks, the rate of correctly processed images was still very low, despite having been able to correct the majority of errors (on an average 5 on 21 images, 24% of the total, was incorrectly segmented), as shown in Figure 48. This arises from the complexity of some parts of the procedure combined with the poor explanation and comment on the code, that made the source of error impossible to track. Most probably, the main source of errors at this point is the fact that the prosthetic model eye used for trying the Starburst is not perfectly accurate (in particular the iris-pupil border is much blurrier than in real

eye) and that it did not have dummy eyelids yet. Consequently, it was decide to create a new procedure, described in the next paragraph.

2.7.2 The New Procedure

See the shortcoming of the Starburst in this application, a semi-automated procedure was created relying on the Image Segmenter Tool from the Image Processing Toolbox in Matlab™. Only the `remove_corneal_reflection` procedure from the original Starburst was kept almost untouched respect to the original version. The other parts of the algorithm have been re-written, added comments, and adapted for using newer versions of Matlab™ on newer Windows™ platforms, to the point it can be considered a new procedure entirely, despite following the same general outline as Starburst. Almost certainly this algorithm would not perform as well as the Starburst in its best shape, but it easily customizeable and more handy for quick processing of laboratory data experiments.

Here is outlined the working principle. For further information on the functions that are not displayed here, see Appendix C.

2.7.2.1 Initialization, File Handling, Save

The first part of the code asks the user to select the working folder in which there are the images to be processed. There is also another function (`extract_images_from_video`) in C that allows to extract the pictures as frames from a video, as most eye-tracking applications are video-based rather than picture based, although this was not the instance.

In the case the user has a video input, the folder named `'Eye'` is created by the function and the frames are named `'Eye_00001.jpg'` and so on. the video should be in the same folder as the algorithm files. In the other case, it is up to the user to properly name the folder and images.

The procedure outputs:

- a `.mat` file storing the parameters extracted in the `CR_matrix`, `Ellipse_matrix`, `Diff_vector_matrix`, named `'Results.mat'`, gathering the respective vectors for each image index,
- a set of pictures named `'Eye_res_00001'` and so on, on which the algorithm traces the CR equivalent circle and the pupil ellipsoid.

These are placed in a folder called `Results`. The images are for the used to check if the algorithm has effectively worked or not, and possibly fix the problems or discards useless data. The folder and documents are created automatically by the procedure in this initialization part.

This part also contains some parameters the user can change, namely:

- `CR_smoothing`, that determines how many times the equivalent radius of the CR found in `regionprops` has to be multiplied before removal. This essentially depends on the image brightness and contrast and should be determined by the used trying the procedure on a sample image,
- `window_w`, that determines the size of a window that cuts the original image into a new one for processing (the original picture however is left untouched). This is showed in C.6 This has a double function: to lower the computational load on the processor by handling smaller sized pictures, and to cut out disturbing stray reflections that might lead to false recognition. This step assumes that the eye is in the center of the picture, and depends on the picture size, resolution, eye position in the scenario. For this it is essential that the eye doesn't move too much in the picture series.

As the black rubber simulating the eyelids sometimes caused very strong reflection to be misinterpreted for CR, and to fix that, it was necessary to re-trim the images separately. In the perspective of calculating the pupil center-CR vector it does not affect the reliability (as it is a difference vector it is immune to shifting of the image origin), but renders unreliable the positioning of CR vector and pupil ellipse vector for those instances.

However, this should not be a problem in real situations because first of all true eyelids do not cause such reflections, and, secondly, the physiological range of rotations is usually under 30°. In any case, should be the need, an automatic procedure for windowing can be carried out by preliminary recognition of the pupil with, for example:

- by asking the user to select a best guess position on some frames for the pupil and then use this information to window the frame,
- using Hough's transform, that seeks circles but can be also used for ellipses. This strategy could also be used to improve pupil and CR recognition.

The body of the procedure is enclosed in a `while frame_index <= last_frame` that loops through the identified frame ranges (from `first_frame` to `last_frame`). For each image the relevant parameters are extracted and stored in vectors. Then a copy of the original color image is created and the data of the CR centroid and pupil ellipsoid are used to plot the shapes in the image. Then the image is saved in the `Results` folder. The matrices storing the vectors are added the last entry and the counter for the image index is incremented for the new cycle.

Finally, when `frame_index=last_frame`, all the updated matrices are written in the `'Results.mat'` file and the procedure ends.

2.7.2.2 Parameter Extraction

The procedure is not *per se* complicated, but relies heavily on the accurate choice of thresholds, smoothing parameter and windowing. Of these parameters, the most critical ones for the automation are `CR_Smoothing`, as determines how the pupil will be well interpolated by the ellipse, and of course thresholds.

As the adaptive threshold mechanism and RANSAC procedure in the original algorithm did not prove reliable, in the new one they are not not implemented. Nevertheless, upon improving the procedure for complete automation, they are certainly additions that would be worth considering.

Finally, it may be worth pondering an alternative interpolation procedure for the removal of CR in the image, that may improve robustness of the subsequent pupil recognition.

The current procedure can be summarized as follows:

1. mask the image to extract the CR as the brightest spot,
2. remove the CR, storing it relevant parameters (x and y position of the centroid and equivalent radius),
3. invert the image so that now the pupil is the brightest spot,
4. mask the image again to extract the pupil,
5. store the pupil relevant parameters (x and y position of the ellipsoid, lengths of major and minor axis, orientation).

Figure 49 exemplifies these steps, while the corresponding code portion is illustrated in C.9.

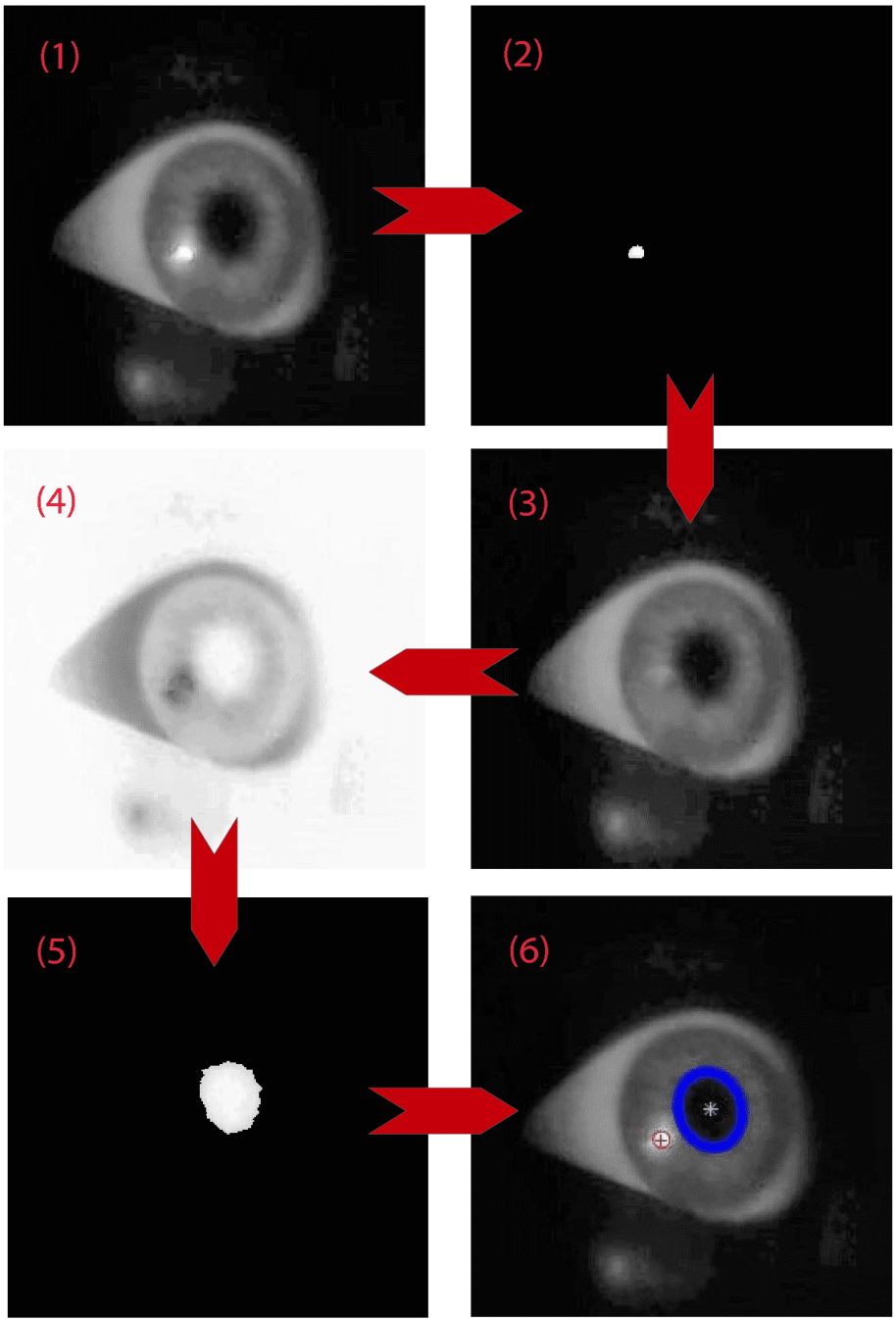

Figure 49: Parameter extraction procedure scheme (images at 30°).

2.7.2.3 Calibration

The Image Segmenter Tool allows for the user to define the threshold for filtering the image. The value of these thresholds is crucial for determining the correctness of classification. The user should try and load some images from the data set into the Image Segmenter GUI and select the best thresholds, running the algorithm body step by step. Then in the Image Segmenter is possible to save the mask created this way, generating a function that is to named appropriately and used in the automatic run of the procedure.

In listings C.7 and C.8 are represented two examples of this auto-generated functions.

Also, automatic brightness and contrast of the images are possible using Matlab™ functions, such as `imadjust`, if a satisfying compromise cannot be reached, and the code of the body of the function can be updated with those.

In the calibration procedure are included `CR_smoothing` and `window_w` as well, as already discussed in 2.7.2.1.

CHAPTER 3

RESULTS

Here are described in detail two experimental procedures and the results of the subsequent data processing. In Appendix A a summary of some statistical concepts used in this chapter is given. Some conventions are common to both experiments:

Rotations: positive horizontal rotations are intended for rightwise facing the stage (or upwards for vertical ones) and negative rotations are intended for leftwise (on downwards). The preliminary pictures were copied and re-named with their orientation, e.g. `'neg30deg.jpg'` etc. Because of the relay lenses, however, the images are reversed.

Pre-processing: ImageJ OSS was used to trim the pictures to a specified pixel size (400x400). The pictures are copied and re-named to be used by the algorithm. Maps of the `'Eye_00001.jpg'` to the original naming were filled.

Matlab™ processing: the image processing algorithm was calibrated in Matlab™ until all the pictures were properly corrected (if needed, some pictures were re-trimmed, and note was taken of the displacement respect to the others), then run on the data set.

Also note that, depending on the slight shift between the light source and model eye position, the location of the CR at neutral position (`0deg`) varies among different acquisitions, although this in theory has the only effect of shifting the intercept of the interpolation line.

3.1 Simultaneous 2D Rotation Experimental Procedure

An attempt of evaluating the two rotations in once was made with the aid of a custom-build 2D rotational stage, described in 2.6.

1. Acquisition of pictures: pictures spaced 10° in purely horizontal and vertical rotation, and in "diagonal" rotations (with the same rotation on the vertical and horizontal axis). The range was ±30°. Three separate folders of pictures, one for each session, were processed separately.
2. Trimming, re-naming and filling of the mapping tables, see Table IV.
3. Separate calibration and processing of the algorithm for the vertical and horizontal acquisition and for fixations.
4. Post-processing: for each session of acquisition, the `'Results.mat'` was loaded in Matlab™.

   Vertical and Horizontal Rotations: linear regression was calculated between the known rotations and the array of horizontal or vertical component of pupil center and CR (relevant to the rotation). Pearson correlation (R^2) coefficient was calculated, and a significance test to assess reliability of the linear hypothesis was performed. The values of the component of vector difference vs. orientation were plotted against the line defined by linear regression), see Figure 51, Figure 52. The interpolation error vector (actual value of rotation minus value predicted by the interpolating line) was calculated. The value of offsets, corresponding rotations, predicted value and errors were stored in a `.csv` table.

   Diagonal Rotation: linear regression was computed separately between the horizontal rotations and horizontal component values of pupil center-CR vector and the corresponding

vertical data. The rest of the analysis followed the same procedure as for pure vertical or horizontal rotations, see Figure 53.

For this specific case, one picture (relative to `30_30deg.jpg`, i.e. upward-right rotation of 30°) did not have CR and so was not used in the processing. It was also necessary for the image horizontal `'Eye_00006.jpg'`, or `'neg_20.jpg'` to be re-trimmed to get rid of the strong reflection from the dummy eyelids that was affecting the results.

TABLE IV: MAP OF EYE FRAME NUMBER TO ROTATION (SIMULTANEOUS 2D ROTATION EXPERIMENT).

		HORIZONTAL ROTATION						
		-30° (LEFT)	**-20°**	**-10°**	**0°**	**10°**	**20°**	**30°(RIGHT)**
VERTICAL ROTATION	**-30°(DOWN)**	neg30_neg30			neg30_0			
	-20°		neg20_neg20		neg20_0			
	-10°			neg10_neg10	neg10_0			
	0°	0_neg30	0_neg20	0_neg10	0_0	0_10	0_20	0_30
	10°				10_0	10_10		
	20°				20_0		20_20	
	30°(UP)				30_0			30_30

		HORIZONTAL ROTATION						
		-30° (LEFT)	**-20°**	**-10°**	**0°**	**10°**	**20°**	**30°(RIGHT)**
VERTICAL ROTATION	**-30°(DOWN)**	7			1			
	-20°		6		2			
	-10°			5	3			
	0°	7	6	5	4	3	2	1
	10°				4	3		
	20°				5		2	
	30°(UP)				6			1

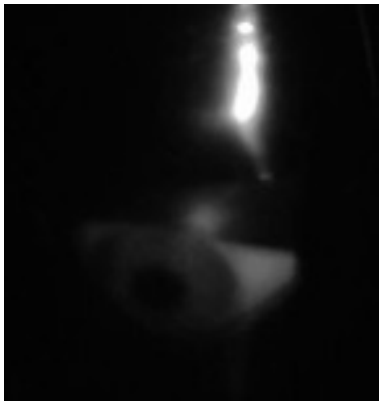

(a) Picture excluded from processing (30°, 30°).

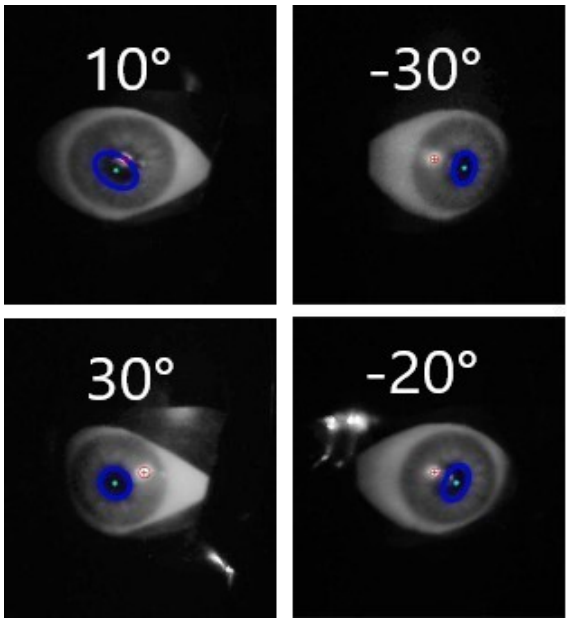

(b) Representative pictures from horizontal rotation experiment.

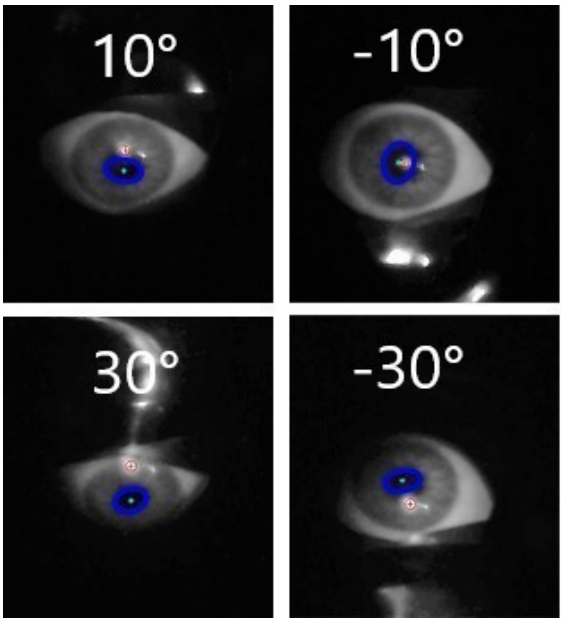

(c) Representative pictures from vertical rotation experiment.

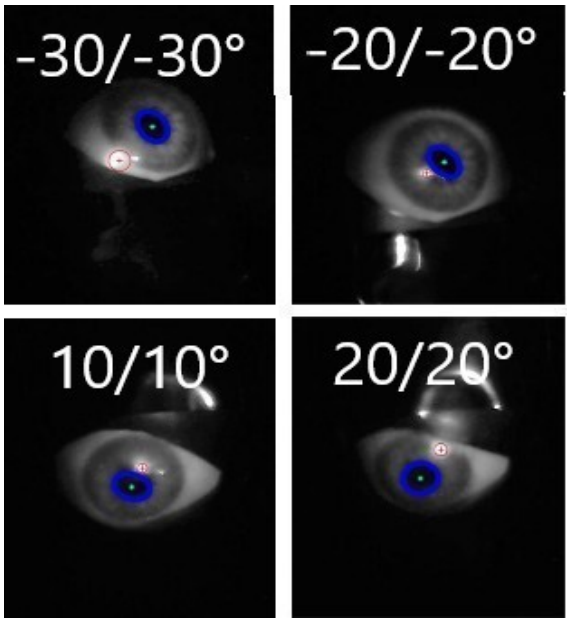

(d) Representative pictures from diagonal rotation experiment.

Figure 50: Representative pictures of the simultaneous 2D rotation experiments

Horizontal Rotation: the regression results were:

$$y = -0.7578x - 2.3536 \tag{3.1}$$

Where

y = horizontal rotation of the eye,

x = horizontal component of the pupil center-CR vector.

The R^2 test for linearity gave a result of $R = -98.64\%$, with p-value for significance $<< 0.05$.

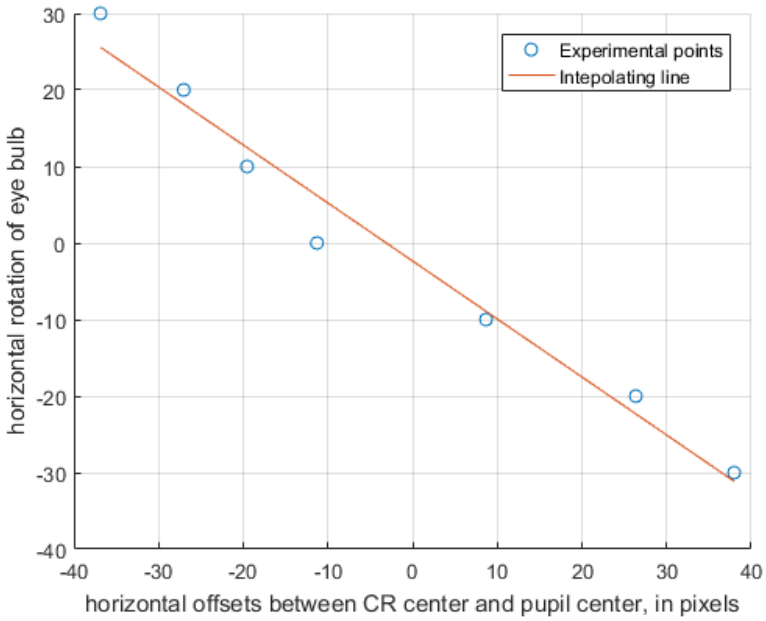

Figure 51: Results of horizontal rotation experiment.

Vertical Rotation: the regression results were:

$$y = 0.779x - 8.6909 \tag{3.2}$$

The R^2 test for linearity gave a result of $R = 99.55\%$, with p-value for significance $<< 0.05$.

.

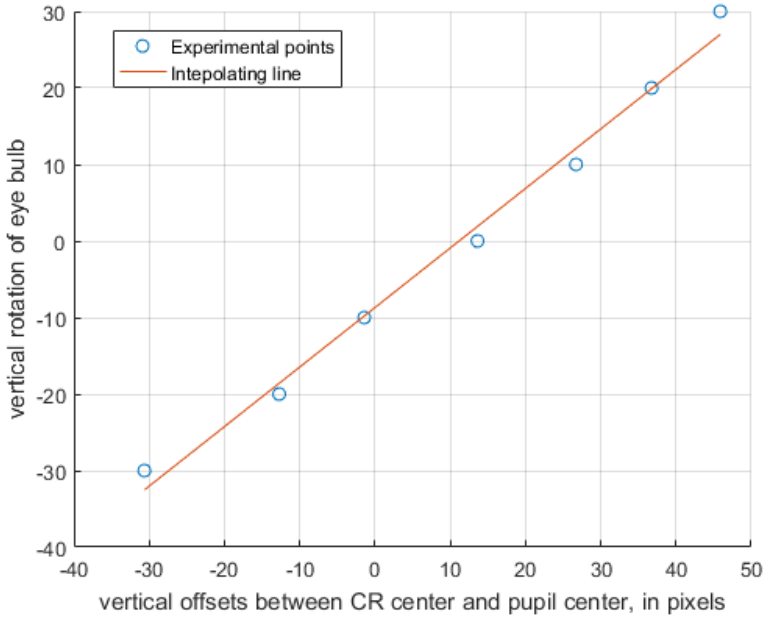

Figure 52: Results of vertical rotation experiment.

Diagonal Rotation: the regression results were:

$$y_1 = 0.6111x_1 - 6.4117 \tag{3.3}$$

$$y_2 = -0.7305x_2 - 2.6640 \tag{3.4}$$

Where

y_1 = vertical rotation of the eye,

y_2 = horizontal rotation of the eye,

x_1 = vertical component of the pupil center-CR vector,

x_2 = horizontal component of the pupil center-CR vector.

The R^2 test for linearity gave a result of $R = 98.34\%$ (p-value 0.0004) and $R = -97.46\%$ (p-value 0.001) respectively.

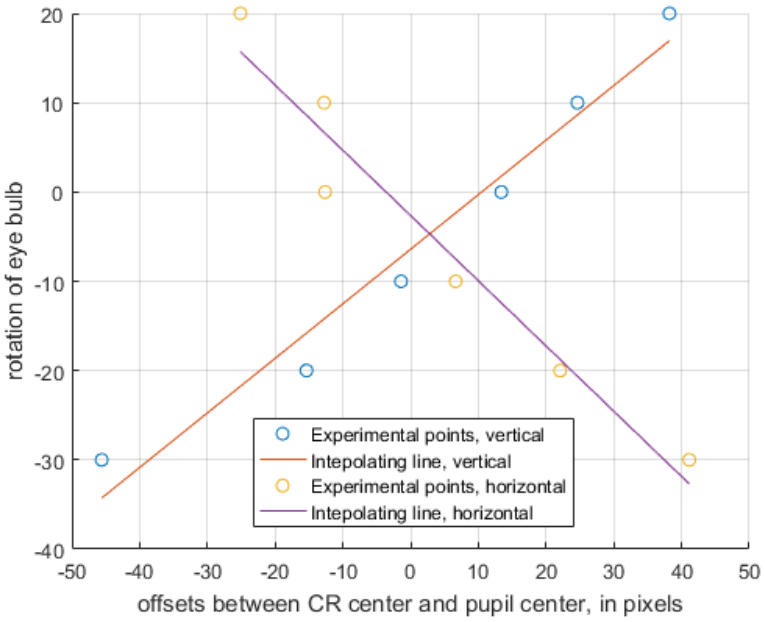

Figure 53: Results of diagonal rotation experiment.

An example of Matlab™ script handling the post-processing is shown in C.15

3.2 Definitive Experimental Procedure

Seeing the shortcomings of the simultaneous 2D rotations procedure, it was decided to analyze separately vertical and horizontal rotations. To simulate vertical rotations, given the asymmetry of the eye model, it was decided to rotate by 90° the dummy eyelids screen only. Because of this, in the post-processing steps, the pupil center-CR vector component analyzed is still the first one (i.e. the horizontal one). Consequently the slope of the regression line is negative, as in the previous experiment for horizontal rotations. The convention for rotation is the same, being rightwise rotations equivalent to upward ones and lefts wise rotations equivalent for downward ones. As the shape of the eyelids covers more on the vertical direction that in the horizontal, it was expected a narrower range of reliable results in the vertical experiment.

A previous attempt at rotating the eye model as well was tried, but the linearity of the pupil center-CR vector vs. rotation was lost for rotations of about 30°, as the curvature in that direction was much larger. Also this vertical curvature is asymmetric (more pronounced on the upper part of the model than in the lower part). Also this loss of linearity could be observed better in a single rotation experiment, rather then simultaneous 2D rotations, because the more imprecise rotations on that setup masked it.

1. Acquisition of pictures: pictures spaced 5° in the horizontal and vertical rotation are acquired, ranging ±30°. Additionally, it was also acquired a set of 10 fixation pictures at significant horizontal rotations (0°, ±5°, ±10°). Seven separate folders of pictures, one for each session, were processed separately.Since for a range of ±10° both in the vertical and horizontal setup

the iris is completely uncovered by eyelids, it was not deemed necessary also to take fixation pictures for vertical rotations.

2. Trimming, re-naming and filling of the mapping tables, see Table V.

3. Separate calibration and processing of the algorithm for the vertical and horizontal acquisition and for fixations.

4. Post-processing: for each session of acquisition, the `'Results.mat'` was loaded in Matlab™.

   Vertical and Horizontal Rotations: linear regression was calculated between the known rotations and the array of horizontal or vertical component of pupil center and CR (relevant to the rotation). Pearson correlation (R^2) coefficient was calculated, and a significance test to assess reliability of the linear hypothesis was performed. The values of the component of vector difference vs. orientation were plotted against the line defined by linear regression. The interpolation error vector (actual value of rotation minus value predicted by the interpolating line) was calculated, see Figure 55, Figure 56 and Figure 57. The value of offsets, corresponding rotations, predicted value and errors were stores in a `.csv` table.

   Fixations: mean and standard deviation (SD) of the values of the said components were calculated. The dispersion around the mean value (as Root Mean Square Error RMSE) is representative of the total noise of the system (hardware and software), see Table VI. A representative graph of such dispersion was plotted (e.g. see Figure 58). The dispersion data is saved in a `.csv` table.

Images 'Eye_00001.jpg' and 'Eye_00013.jpg' ('30deg.jpg' and 'neg30deg.jpg') of horizontal rotation needed re-trimming in order to exclude the very bright reflection from the eyelids that made tracking impossible. In some images of the vertical rotation experiment corresponding to ±20°, ±25° and ±30° ('Eye_00001', 'Eye_00002', 'Eye_00003', 'Eye_00011', 'Eye_00012' and 'Eye_00013') the pupil was covered by the eyelids (see Figure 54). The ±30° and ±25° rotations could not be processed as the pupil was completely covered, and so were excluded from the data set. The ±20° rotations could still be processed, but deemed unreliable, so a double fitting was performed, one excluding 'Eye_00003' and Eye_00011', and one including them, represented in Figure 56 and Figure 57 respectively.

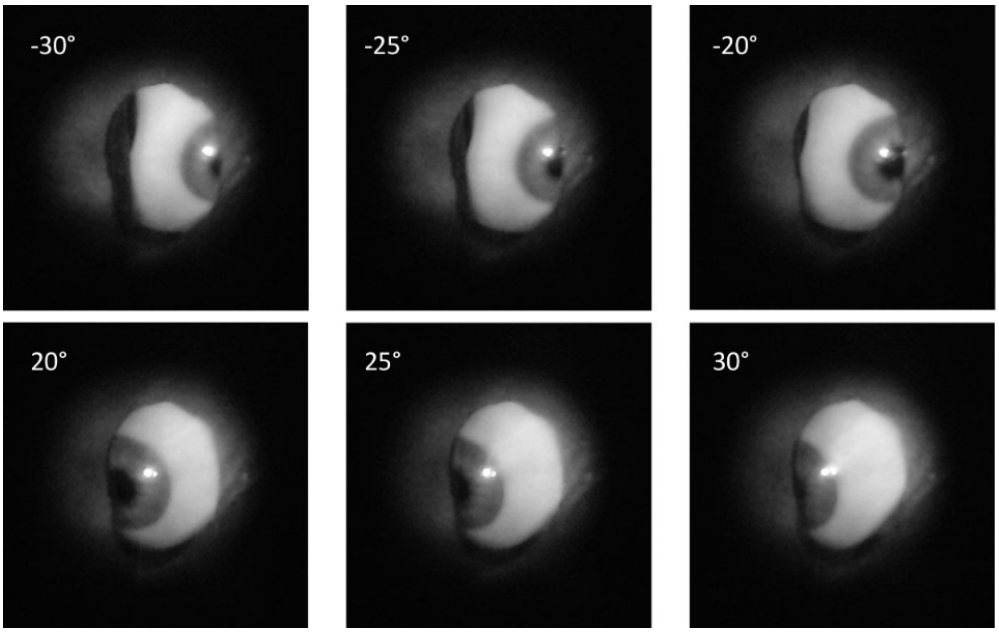

Figure 54: Images that were excluded from vertical experiments or processing.

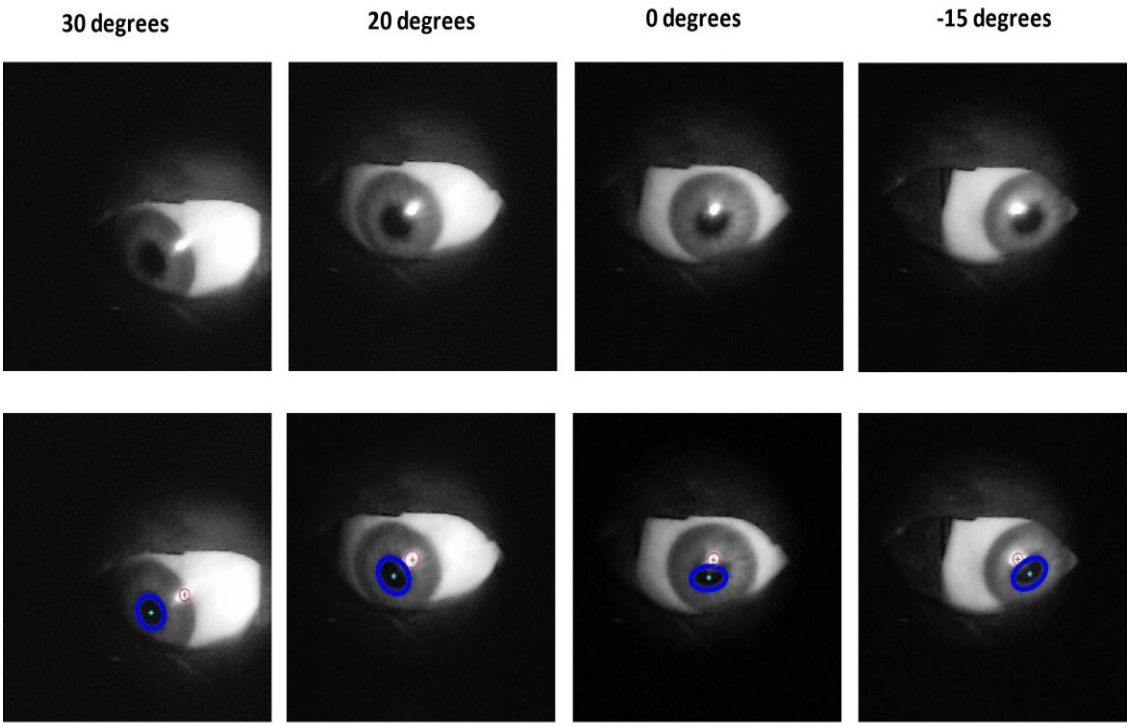

(a) Representative images from the horizontal rotation experiments (top) and the corresponding processed ones (bottom).

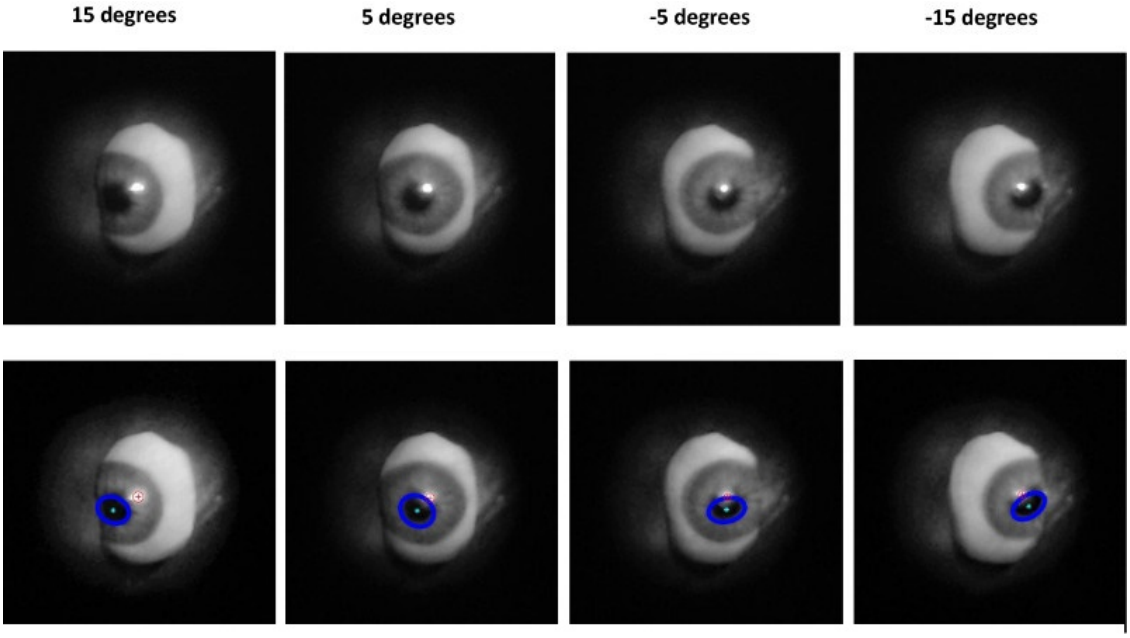

(b) Representative images from the vertical rotation experiments (top) and the corresponding processed ones (bottom).

TABLE V: MAP OF EYE FRAME NUMBER TO ROTATION (DEFINITIVE EXPERIMENT).

		HORIZONTAL ROTATION												
		-30° LEFT	**-25°**	**-20°**	**-15°**	**-10°**	**-5°**	**0°**	**5°**	**10°**	**15°**	**20°**	**25°**	**30° RIGHT**
VERTICAL ROTATION	**-30° DOWN**							neg30_0						
	-25°							neg25_0						
	-20°							neg20_0						
	-15°							neg15_0						
	-10°							neg10_0						
	-5°							neg5_0						
	0°	0_neg30	0_neg25	0_neg20	0_neg15	0_neg10	0_neg5	0_0	0_5	0_10	0_15	0_20	0_25	0_30
	10°							10_0						
	15°							15_0						
	20°							20_0						
	25°							25_0						
	30° UP							30_0						

		HORIZONTAL ROTATION												
		-30° LEFT	**-25°**	**-20°**	**-15°**	**-10°**	**-5°**	**0°**	**5°**	**10°**	**15°**	**20°**	**25°**	**30° RIGHT**
VERTICAL ROTATION	**-30° DOWN**							13						
	-25°							12						
	-20°							11						
	-15°							10						
	-10°							9						
	-5°							8						
	0°	13	12	11	10	9	8	7	6	5	4	3	2	1
	5°							6						
	10°							5						
	15°							4						
	20°							3						
	25°							2						
	30° UP							1						

Horizontal Rotation: the regression results were:

$$y = -0.6909x - 4.5604 \tag{3.5}$$

The R^2 test for linearity gave a result of $R = -99.82\%$, with p-value for significance $<< 0.05$.

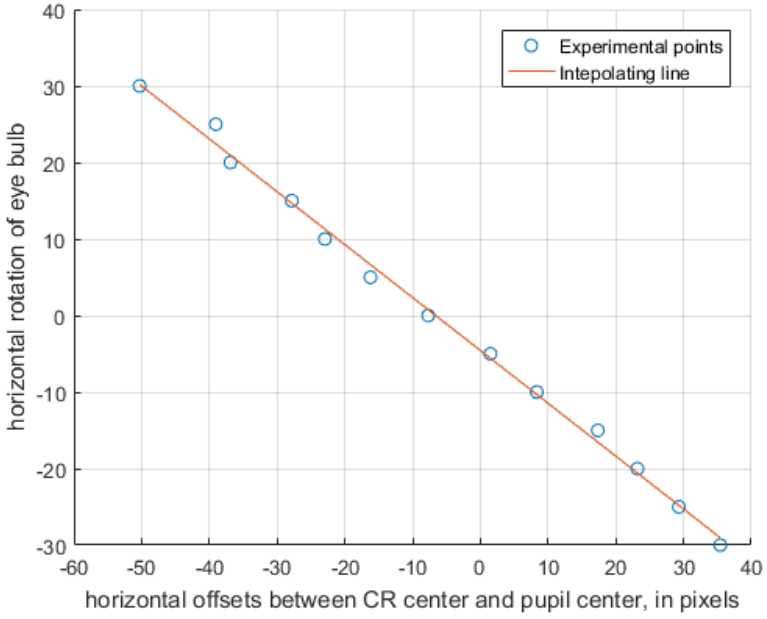

Figure 55: Results of horizontal rotation experiment.

Vertical Rotation: the regression results excluding $\pm 20^{\circ}$ pictures were:

$$y = -0.6365x - 7.2720 \tag{3.6}$$

The R^2 test for linearity gave a result of $R = -99.56\%$, with p-value for significance $<< 0.05$.

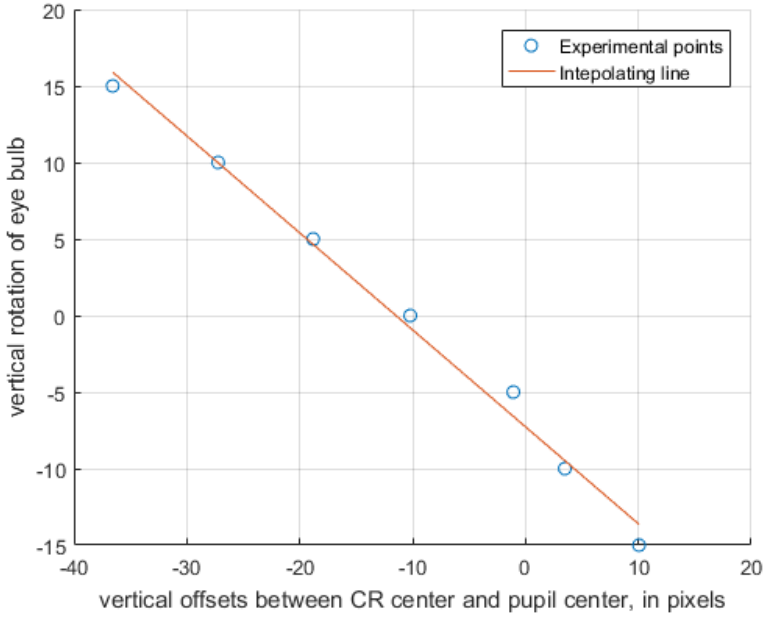

Figure 56: Results of vertical rotation experiment excluding $\pm 20^{\circ}$ pictures.

The regression results including ±20° pictures were:

$$y = -0.7003x - 8.3578 \tag{3.7}$$

The R^2 test for linearity gave a result of $R = -99.05\%$, with p-value for significance $<< 0.05$.

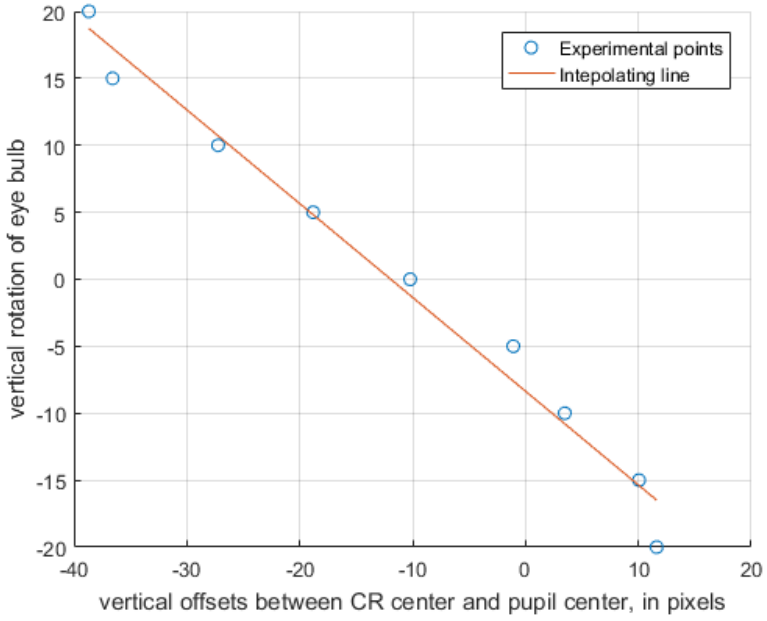

Figure 57: Results of vertical rotation experiment including ±20° pictures.

Fixations: Table VI summarizes the results of the fixation experiments.

Orientation	Mean	Standard Deviation (SD)	Root Mean Square Error (RMSE)
-10°	8.8264	0.1476	0.1400
-5°	-1.5299	0.5885	0.5583
0°	-8.2612	0.2937	0.2786
5°	-16.3478	0.4441	0.4213
10°	-23.2507	0.2040	0.1935

TABLE VI: TABLE FOR FIXATION EXPERIMENTS RESULTS (ALL VALUES ARE IN PIXELS).

An example of Matlab™ script handling the post-processing is shown in C.14. One of the graphs resulting from the processing is shown in Figure 58.

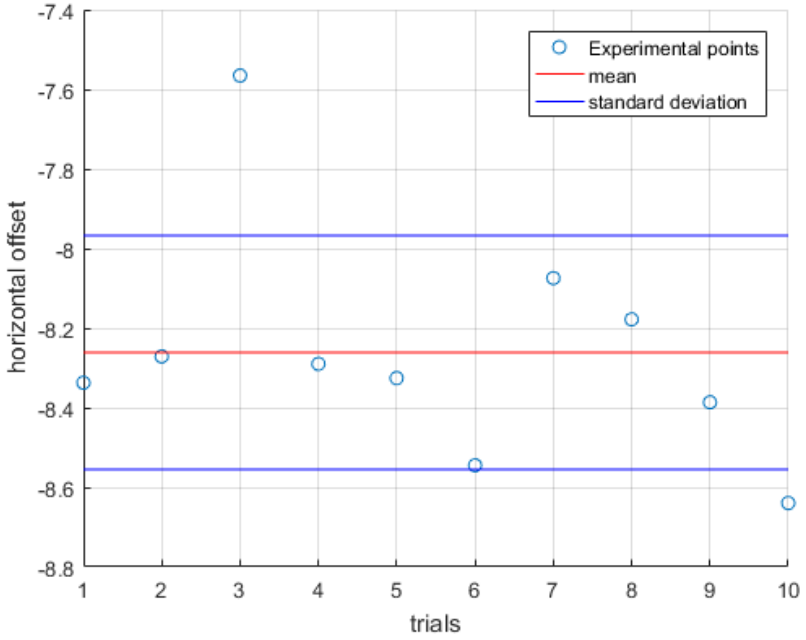

Figure 58: Dispersion of fixation experiments for 0°.

CHAPTER 4

CONCLUSIONS

4.1 Discussion on the Results

Difference between the two experiments results could be explained by:

- different rotation procedure (with the first experiment being less accurate),
- asymmetry of the eye model,
- different eyelids setup,
- coarser resolution of the first experiment.

The different slopes found in between the separate rotation experiments and the diagonal one can be attributed to the less precise control on simultaneous rotations of the 2D stage. For this reason (and the presence of the fixed eyelids) this experiment is deemed less significant than the second one. Nonetheless, the linearity of the pupil center-CR vector components vs. the rotation seems to be stable enough, as confirmed by the high determination coefficients and low p-values.

As expected in the second experiment, the reliable range for vertical tracking is reduced by the eyelids. Also, the increased R value in the fitting performed without the $\pm 20^\circ$ pictures seems to confirm that the best decision was to exclude those. Consistently with the setup, the slope value found for both vertical and horizontal rotations is similar (about -0.6/0.7 pixels per degree). The differences may be explained by the fact that the vertical experiment had less pictures to compute fitting, because at extreme rotations the eyelids covered the pupil. In fact, for rotations over 25°,

the linearity of the relation start to degrade (as it would also happen with a real eye as the CR would start to fall off the cornea), and the points become more "s-shaped" and increase the slope of the interpolation line. Conversely, rotations around 0° have a better linear alignment with a shallower slope.

Also in this case, determination coefficients are all near 100% and p-values are all near 0 (therefore much smaller than significance level).

As for the fixation experiments, they ensure a quite good noise immunity of the system, as the RMSE is of sub-pixel magnitude in all cases (and in some as low as 0.2 pixels). Consequently, the dispersion around the mean value can be considered small enough to ensure a robust measure. In any case, it is worth pointing out that this test on noise was carried out in a relatively controlled laboratory environment and that the setup was not worn by a person, therefore it does not apply to other situations.

4.2 Final Remarks

Despite the low efficiency of the light transmission along the WG and the presence of an optical system in between the eye and WG, the results are still satisfactory.

In fact, a rather simple semi-automatic image processing procedure found significant proof that the linearity of the relation between pupil center-CR vector and eye rotation is reliable. Therefore the pictures transmitted by the WG are good enough to be used for a preliminary eye-tracking, i.e. the preliminary feasibility for the use of HWG in the field of eye-tracking is proved.

This opens new perspectives for new applications, with particular regards to ODs diagnostic improvement.

Below is summarized a list of the strengths of this novel approach:

- Lightweight and compact: WG-based solutions are much smaller and lighter than traditional approaches to eye-tracking or VR applications. This also allows for potential testing in every-day conditions, not only in laboratory environment. This is potentially very useful in the perspective of continuous follow-up of patients and home-based care;
- Low cost (relatively to other VR solutions);
- The potential impact is very wide, as ODs are a widespread condition;
- Objective: normal test for BVDs and similar impairments rely heavily on the physician's judgment or on semi-quantitative scales. A wearable HWG device would be able to compute eye-related measures in quantitative units (degrees, dioptres...);
- Easily automated: this affects both time efficiency of the assessment and the need to rely on patient's collaboration. A wearable HWG device would need only to be worn and calibrated to give a reliable result in infinitely shorter time a with minimal patient compliance. The large literature of open source material to create calibration and measuring protocols can be exploited;
- Innovative: so far HWG were used as see-though displays, never for conveying pictures to a camera.

4.3 Further Developments

A number of improvements and further developments can be identified, in the more general prospective of developing a wearable prototype for comprehensive assessment of oculo-motor performances:

- Improving the HWG, firstly shifting efficiency and illumination to NIR, so to allow human testing and secondly reducing the in-coupler focal length to spectacle distance (1.2-1.4cm);
- Improving the eye-tracking eye model by creating a more realistic model with an integrated laser pointer, in order to shift from simple eye-tracking to gaze-tracking;
- Development or acquisition of an eye-model for accommodation;
- Designing a stage that allows for simultaneous vertical and horizontal rotation of the model eye, or better yet a 3D gimbal;
- Improving and automating image processing algorithm for the eye-tracking part and developing the part relative to accommodation. Possibly, creation of an open-source application;
- Development of a calibration procedure;
- Integrating camera, WG, light source into a compact prototype for both EM and accommodation measurements.

APPENDICES

Appendix A

STATISTICAL HINTS

In this Appendix are recalled the formulas used for data post-processing, as defined on Matlab™ website [38].

A.1 Mean, Standard Deviation, Root Mean Square

Given a collection of n experimental results for the variable X, i.e. $\{x_1, x_2, \ldots, x_n\}$ and being x_i the i^{th} element of this collection, then we define:

Mean: or expected value

$$E[x] = \mu_x = \frac{1}{n}\sum_{i=1}^{n} x_i \tag{A.1}$$

corresponding to `mean` command.

Standard Deviation:

$$\sigma_x = SD[x] = \sqrt{{\sigma_x}^2} \tag{A.2}$$

Where ${\sigma_x}^2$ is the *variance* defined as:

$${\sigma_x}^2 = var[x] = \frac{1}{n-1}\sum_{i=1}^{n}(x_i - \mu_x)^2 \tag{A.3}$$

corresponding to `std` and `var` command. The standard deviation is a measure of how much a distribution is dispersed around its mean value (in the case of mono-disperse distributions).

Note that this is meaningful only considering at the same time also the expected value and range of the distribution.

Root Mean Square and Root Mean Square Error:

$$RMS[x] = x_{RMS} = \sqrt{E[x_i^2]} = \sqrt{\frac{1}{n}\sum_{i=1}^{n} x_i^2} \tag{A.4}$$

corresponding to `rms` command.

$$RMSE[x] = \sqrt{E[(x - E[x])^2} = \sqrt{\frac{1}{n}\sum_{i=1}^{n}(x_i - \mu_x)^2} \tag{A.5}$$

The values of RMS and RMSE are coincident in the the case of an unbiased measure (i.e. $\mu_x = 0$). The RMSE is a value commonly used to quantify the error between observed values of a certain variable and the values predicted for the same value. In this case the predicted value of x is its mean (assumed to be representative its true value because it is the best predictor).

A.2 Linear Regression

A.2.1 Least Square Regression

In general, performing a linear regression between two sets of values means finding the coefficients of a line that best exemplifies the relation of the output (or explained or dependent) variable Y on the input (or explanatory or independent) variable X. More simply, given two sets of ob-

Appendix A (continued)

servations of the above said variables: $\{x_1, x_2, \ldots, x_n\}$ and $\{y_1, y_2, \ldots, y_m, \}$, following relation is hypothesized:

$$Y = \alpha X + \beta \tag{A.6}$$

And the regression reduces to find α and β. Of course, because of a number of reasons, the measure values will not all fall on the line predicted by the model. In the case $n = m$, in other words, it can happen that $y_i = \alpha x_i + \beta$ is not satisfied for every i.

In order to "best fit" the experimental data to the linear relation, the *least square* (LS) paradigm is most often used. In the LS approach, the optimal guesses for the regression coefficients are the ones that minimize the SSE (sum of square errors). The square prediction error e_i^2 is defined as $(y_i - \hat{y}_i)^2$, where $\hat{y}_i$ is the predicted value of the dependent variable Y for each instance of X i.e. $\hat{y}_i = \alpha x_i + \beta$ for every i. This can be seen as asking for the regression line to be as close as possible to all the experimental points as once, i.e. the distances between the points and the line must be minimized.

The regression procedure then is equivalent to finding α and β such that:

$$SSE_{min} = argmin_{\alpha,\beta} \sum_{i=1}^{n} (e_i)^2 \tag{A.7}$$

The explanation of the calculations necessary to find α and β are complex and beyond the scope of this dissertation, but they can be performed automatically by many softwares such a Matlab™, in various ways. In this specific case, the `polyfit` command was used.

Appendix A (continued)

A.2.2 The R^2 Coefficient of Determination

There are a number of figures that can be used to assess the "goodness-of-fit" of a regression. The most popular one is the R coefficient. It represents a ratio of the "explained variance" (by the prediction) to the "total variance" of the distribution.

$$R^2 = \frac{\sum_{i=1}^{n}(\hat{y}_i - \mu_y)^2}{\sum_{i=1}^{n}(y_i - \mu_y)^2} = 1 - \frac{\sum_{i=1}^{n}(e_i)^2}{\sum_{i=1}^{n}(y_i - \mu_y)^2} \tag{A.8}$$

The more R^2 tends towards one or 100%, the more the model captures the variability of the distribution. Customarily values above 90/95% are considered to be satisfactory. Note that this figure of merit makes sense only when the assumption of linearity between X and Y is solid.

In the case of simple linear regression, R^2 corresponds to the squared Pearson correlation coefficient (PCC) between the two variables X and Y:

$$\rho_{x,y} = \frac{cov(x,y)}{\sigma_x \sigma_y} \tag{A.9}$$

Where $cov(x,y)$ is the *covariance* between X and Y, that expresses the joint variability of the two variables:

$$cov(x,y) = E[(x - \mu_x)(y - \mu_y)] \tag{A.10}$$

Note that $\rho_{x,y}$ can be positive or negative: a positive correlation means that when x increases, so does y, while negative correlation means that if x increases, then y decreases.

The squared Pearson correlation coefficient can be calculated with the `corrcoef` command, that returns the value of R^2 and also the p-value for testing the significance of this correlation.

Appendix A (continued)

A.3 Hypothesis Testing

Hypothesis testing is a huge section of statistics the details of which are worth a whole separate dissertation. In this section is described only how the results from an hypothesis test run with Matlab™ should be interpreted.

In statistical field, a confirmatory hypothesis is usually a conjecture of certain relation between two data distributions, e.g. "these two distributions have same mean and variance". The hypothesis we want to verify is usually presented as *alternative hypothesis* (H_1) to the *null hypothesis* (H_0) that states that such conjecture is false. If we can reject the null hypothesis, then the conjecture can be held true, as long as new data does not prove it wrong.

The *significance level* is the probability of making the wrong decision in case it is decided to reject the null hypothesis, i.e. probability of H_0 true and H_0 rejected. Common values are 5% and 1%. The p-values are the values of the significance levels that should be chosen in order to accept the null hypothesis. If the p-values are under the specified significance level, the null hypothesis is rejected. For example, say that the chosen significance level is 5% (0.05). If the test results in a p-value of 2%, the null hypothesis can be rejected with probability 2% of having made the wrong decision (that is, H_0 was true indeed). Conversely, with a significance level of 1% the null hypothesis could not have been rejected.

There are a huge number of testing protocols, with more or less stringent hypothesis and pre-requisites and assumption on the distributions that can be used, e.g. Student t-test, Kruskal-Wallis test, z-test, Chi-square test...

In conclusion, being the null hypothesis H_0 of the `corrcoeff` command is "the two variables are linearly uncorrelated", then p-values under a certain significance level (by default 0.05) mean that

Appendix A (continued)

they null hypothesis is rejected with a high level of confidence (above 95% in this case): therefore there is no evidence to hold the variables uncorrelated.

Appendix B

LENS EQUATION

Here are given the basic principles of lens optics to provide a better understanding of the relay lens system discussed in 2.3.

When a lens is put in front of an object, the image that is created presents characteristics that depend on the lens and on the object distance from it. A lens is described primarily by its shape, that defines how light rays are deviated by it, and by its focal length (f), that describes the distance at which a parallel set of beams is collimated to a point. If a lens is convex (as in the following figures), its focal length is positive (as the light is collimated beyond the lens respect to the direction of the incident light. If it is concave, f is negative, as the beam actually diverges, so we assume f is the intersection of the extension of the beams (that is on the same same as the incoming light). The *thin lens approximation* holds when the thickness of the lens is much smaller than its diameter. In the case of the relay lenses used in the experiment, is it a quite far reaching assumption for the smaller lens, but with a bit of tinkering, a good image could be attained anyway.

As shown in Figure 1, in the case of thin lens, the relations between the distance and height of the image that is formed can be derived by the *thin lens equation*:

$$\frac{1}{f} = \frac{1}{S_1} + \frac{1}{S_2} \tag{B.1}$$

Appendix B (continued)

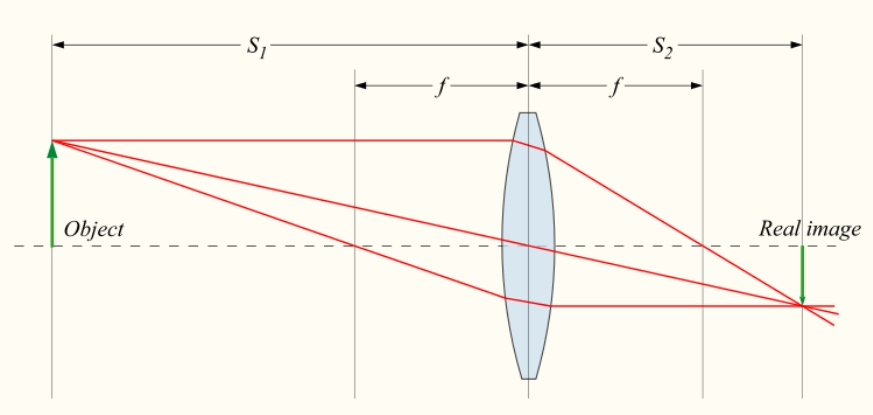

Figure 1: Thin lens equation, from [59].

Where:

f is the focal length of the lens,

S_1 is the distance of the object (o) from the lens, and

S_2 is the distance of the image (i) from the lens.

Note that by convention, if the object distance is positive having the object on the left of the lens (as in the figure), then the image distance is positive is the image is on the right side of it. If both S_1 and S_2 are positive, the image and object are on the opposite sides of the lens, an the image is said to be *real*. If S_2 were negative, the image would be on the same side of the object and it would be *virtual*. It is important to point out that only real images can be projected on sensors (such as the camera), while virtual images can be the object themselves of an imaging lens, as it happens when using a magnifying lens.

Appendix B (continued)

Consider now the object has a certain height respect to the optical axis[1], h_o. Then the height of the image (h_i) is defined as:

$$\frac{h_i}{h_o} = M \tag{B.2}$$

Where M is the *linear magnification factor*. Note that the heights can have positive or negative sign is they are above and below the optical axis respectively. It is easy to see that:

$M > 0$ means an upright image,

$M < 0$ means an inverted image,

$|M| < 1$ means a de-magnified image,

$|M| > 1$ means a magnified image.

By simple trigonometry, it is easily derived that:

$$M = -\frac{S_2}{S_1} \tag{B.3}$$

By combining two or more lenses, an object may be inverted, corrected, magnified or shrinked to the needs. Also, combining more lenses has the function to extend the length of the optical apparatus (as in periscopes). The respective distances from the lenses of the images can be found by applying the lens law repeatedly starting from the object and proceeding right (referring to the usual convention). The total magnification of the system can be found computing the product of the magnifications of each image.

---

[1]Direction of a light ray that is not deviated by the lens

Appendix B (continued)

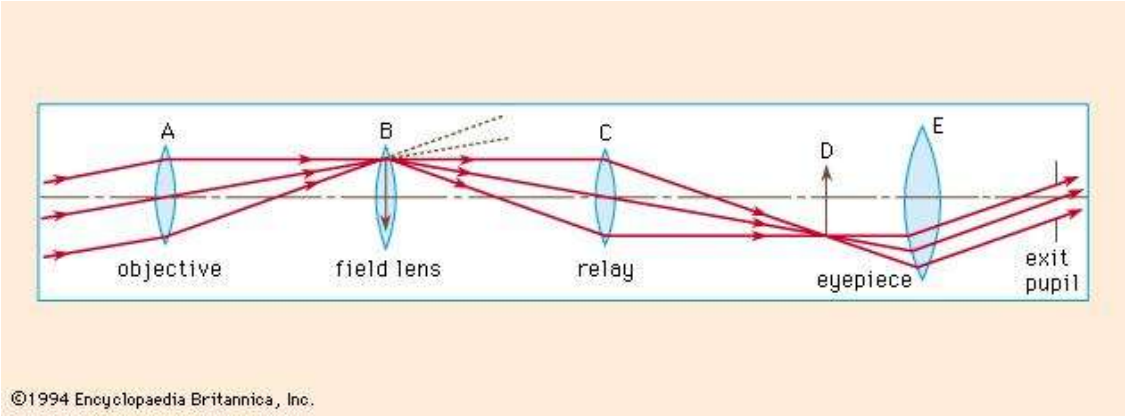

Figure 2: Relay lens system, from [30].

On `http://www.livephysics.com`, one can find a tool for calculating the image distances and magnification of two lenses systems.

In our specific application, the two lens de-magnify the image at the input and the WG is placed 40mm behind the back focal plane of the rear lens, where the (reversed) image is formed. This way, the WG can correctly focus the image as if it were the eye model.

Appendix C

CODE SNIPPETS

Here are listed the functions that were not described in detail in 2.7 for the sake of brevity. In any case, depending on you platform and Matlab™ version, it cannot be certain that copy-pasting them will work. The present appendix is given just for sake of completeness and to illustrate the procedure.

Listing C.1: Code for extracting video frames.

```
1  % Extract images from video
2
3  % This new version doesn't use shell commands nor external
4  % programs like ffmpeg, as in the oringinal version of the
5  % algorithm, so that it can be used with Matlab alone, and
6  % also should be less platform dependent.
7  % It uses snippets of code found for movie processing on
8  % Mathworks from Image Analyst, response to a question on
9  % Mathworks from Walter Roberson as well as pieces of original
10 % code. It creates the directories with the same path and name
11 % as original algorithm, so that the rest of it can be tested
12 % and broken down to need
13
```

Appendix C (continued)

```
14 % Prompt user to select movie for eye
15 [EyeFileName, EyeFolderName] = uigetfile('*.mp4','Eye movie file'
      );
16 EyeFile = strcat(EyeFolderName, EyeFileName);
17
18 % Prompt user to select movie for scene
19 [SceneFileName, SceneFolderName] = uigetfile('*.mp4','Scene movie
       file');
20 SceneFile = strcat(SceneFolderName, SceneFileName);
21
22 % Creates directorie to store frames
23 mkdir( fullfile(EyeFolderName, 'Eye') );
24 mkdir( fullfile(SceneFolderName, 'Scene') );
25
26 % Stores name
27 EyeMovieFullFileName = fullfile(EyeFile);
28 SceneMovieFullFileName = fullfile(SceneFile);
29
30 % Processes Eye movie:
31     EyeVideoObject = VideoReader(EyeMovieFullFileName);
32
```

Appendix C (continued)

```
33          % Determine how many frames there are and how many are
                    % written (it can be used to see if error
              occured)
34          EyeNumberOfFrames = EyeVideoObject.NumberOfFrames;
35          EyeNumberOfFramesWritten = 0;
36
37           % Extract out the various parts of the eye filename.
38      [folder, ~, ~] = fileparts(EyeMovieFullFileName);
39
40           % Make up a special new output subfolder for all the
41           % separate movie frames that we're going to extract and
42           % save to disk.
43      outputFolder = sprintf('%s/Eye', folder);
44
45           % Create the folder if it doesn't exist already.
46          if ~exist(outputFolder, 'dir')
47                  mkdir(outputFolder);
48      end
49      msgbox('Do NOT close the figure while algorithm is running')
50
51          % Loop through the movie, writing all frames out.
```

Appendix C (continued)

```
52      for frame = 1 : EyeNumberOfFrames
53        % Each frame will be in separate file with unique name.
54
55          % Extract the frame from the movie structure.
56        thisFrame = read(EyeVideoObject, frame);
57
58          % Construct an output image file name.
59        outputBaseFileName = sprintf('Eye_%5.5d.jpg', frame);
60        outputFullFileName = fullfile(outputFolder,
             outputBaseFileName);
61
62          % Stamp the name and frame number onto the image.
63        % At this point it's just going into the overlay,
64        % not actually getting written into the pixel values.
65        text(5, 15, outputBaseFileName, 'FontSize', 20);
66
67        % Extract the image with the text "burned into" it.
68          frameWithText = getframe(gca);
69        % frameWithText.cdata is the image with the text
70        % actually written into the pixel values.
71
```

Appendix C (continued)

```
72          % Write it out to disk.
73          imwrite(frameWithText.cdata, outputFullFileName, 'jpg');
74          progressIndication = sprintf('Wrote frame %5d of %d.',
               frame, EyeNumberOfFrames);
75          disp(progressIndication);
76          % Increment frame count (should eventually =
                        % numberOfFrames unless an error happens).
77          EyeNumberOfFramesWritten = EyeNumberOfFramesWritten + 1;
78      end
79
80      finishedMessage = sprintf('Done!  It wrote %d frames to
           folder\n"%s"', EyeNumberOfFramesWritten, outputFolder);
81      disp(finishedMessage); % Write to command window.
82      uiwait(msgbox(finishedMessage)); % Also pop up a message box.
83      close all
84
85  % Same goes for scene movie
86  SceneVideoObject = VideoReader(SceneMovieFullFileName);
87
88  % Determine how many frames there are and the written ones
89          SceneNumberOfFrames = SceneVideoObject.NumberOfFrames;
```

Appendix C (continued)

```
90          SceneNumberOfFramesWritten = 0;
91
92  % Extract out the various parts of the eye filename.
93      [folder, baseFileName, extentions] = fileparts(
            SceneMovieFullFileName);
94
95          % Make up a special new output subfolder for all the
96          % separate movie frames that we're going to extract and
                        % save to disk.
97          outputFolder = sprintf('%s/Scene', folder);
98
99          % Create the folder if it doesn't exist already.
100     if ~exist(outputFolder, 'dir')
101                 mkdir(outputFolder);
102     end
103     msgbox('Do NOT close the figure while algorithm is running')
104
105     % Loop through the movie, writing all frames out.
106     for frame = 1 : SceneNumberOfFrames
107         % Each frame will be in a separate file with unique name.
108         % Extract the frame from the movie structure.
```

Appendix C (continued)

```
109         thisFrame = read(SceneVideoObject, frame);
110
111         % Construct an output image file name.
112         outputBaseFileName = sprintf('Scene_%5.5d.jpg', frame);
113         outputFullFileName = fullfile(outputFolder,
               outputBaseFileName);
114
115            % Stamp the name and frame number onto the image.
116         % At this point it's just going into the overlay,
117         % not actually getting written into the pixel values.
118         text(5, 15, outputBaseFileName, 'FontSize', 20);
119
120            % Extract the image with the text "burned into" it.
121         frameWithText = getframe(gca);
122         % frameWithText.cdata is the image with the text
123         % actually written into the pixel values.
124
125         % Write it out to disk.
126         imwrite(frameWithText.cdata, outputFullFileName, 'jpg');
127         progressIndication = sprintf('Wrote frame %5d of %d.',
               frame, EyeNumberOfFrames);
```

Appendix C (continued)

```
128         disp(progressIndication);
129
130
131             % Increment frame count (should eventually =
132             % unless an error happens).
133         SceneNumberOfFramesWritten = SceneNumberOfFramesWritten +
                1;
134     end
135
136     finishedMessage = sprintf('Done!  It wrote %d frames to
           folder\n"%s"', SceneNumberOfFramesWritten, outputFolder);
137     disp(finishedMessage); % Write to command window.
138     uiwait(msgbox(finishedMessage)); % Also pop up a message box.
139     close all
```

Appendix C (continued)

Listing C.2: Code for identifying the frame range.

```
1  function frame = get_first_or_last_frame_num(path_name,
       file_prefix, index_len, first_or_last)
2
3  % This function get last frame number automatically
4  % NOTE about the imput: in the Eye and Scene folders the frames
5  % should be numbered as Scene_12345 and Eye_12345
6  % Input:
7  % path_name = the directory path in which we have the Eye and
8  % Scene folders where we store the frames from videos, give as
9  % string
10 % file_prefix = the prefix of file name that contains the index
11 % number
12 % ('Eye' or 'Scene')
13 % index_len = the length of frame index, (5)
14 % first_or_last = indicator;
15 %                  'first' (default) - get first frame num;
16 %                  'last' - get last frame num
17 %
18 % Output:
19 % frame = the index number of last frame, given as number
```

Appendix C (continued)

```
20
21
22 prefix_len = length(file_prefix);
23
24 if exist('first_or_last')
25
26     files1 = [];
27     files = ls(path_name);
28
29 % This is necessary because the ls command on Windows
30 % platform gives a matrix of strings, while for the strfind
31 % command needs a character vector or string (it does not matter
     % that flies1 variable makes no sense to read, if you need to
32 % read the whole name list access files).
33 % Otherwise it gives a "index exceeds matrix dimensions" error
34
35    for file = 1:size(files,1)
36         name = files(file, :);
37         files1 = [files1, name];
38     end
39
```

Appendix C (continued)

```
40      n = strfind(files1, file_prefix);
41
42      if strcmp(first_or_last, 'first')
43  % gets the 5digit number from the 1st occurrence of 'Eye' in list
44          number = files1(n(1)+prefix_len:n(1)+prefix_len+index_len
                -1);
45      elseif strcmp(first_or_last, 'last')
46  % gets the 5digit number from the last occurrence of 'Eye'
47          number = files1(n(end)+prefix_len:n(end)+prefix_len+
                index_len-1);
48      else
49          fprintf(1, 'ERROR! The input of ''first_or_last'' is
                wrong');
50          return
51      end
52
53  end
54
55  frame = uint16(str2num(number));
```

Appendix C (continued)

Listing C.3: Initialization code.

```
dir_name = uigetdir(pwd,'Select working folder, must be the same
    for algorithm and Eye folder');
mkdir(fullfile(dir_name, 'Results'))
res_name = strcat(dir_name, '/Results/');
eye_file_name = sprintf('%s/Eye/Eye_', dir_name);

first_frame = get_first_or_last_frame_num(sprintf('%s/Eye/',
    dir_name), 'Eye_', 5, 'first');
last_frame = get_first_or_last_frame_num(sprintf('%s/Eye/',
    dir_name), 'Eye_', 5, 'last');
frame_range = last_frame-first_frame+1;
CR_matrix = zeros(frame_range, 3);
Ellipse_matrix = zeros(frame_range, 5);
Diff_vector_matrix = zeros(frame_range, 2);
frame_index = first_frame;
smoothing_CR = 2;
window_w = 181;
```

Appendix C (continued)

Listing C.4: Code for importing a grayscale image.

```
function [I] = read_gray_image(file, index);
I = im2double(rgb2gray(imread(sprintf('%s%05d.jpg', file, index))
    ));
```

Listing C.5: Code for importing a colored image.

```
function [I] = read_image(file, index);
I = im2double(imread(sprintf('%s%05d.jpg', file, index)));
```

Listing C.6: Windowing code.

```
    I1 = read_gray_image(eye_file_name, frame_index);
    I1 = im2uint8(I1);
    CX = floor(size(I1,1)/2);
    CY = floor(size(I1,2)/2);
```

Appendix C (continued)

```
5       offset_x = CX-floor(window_w/2);
6       offset_y = CY-floor(window_w/2);
7       Iw1 = I1(CX-floor(window_w/2):CX+floor(window_w/2), CY-floor(
            window_w/2):CY+floor(window_w/2));
```

Listing C.7: CR mask code.

```
1  function [BW,maskedImage] = segmentImage_CR(im)
2  %segmentImage segments image using auto-generated code from
3  % imageSegmenter App
4  % [BW,MASKEDIMAGE] = segmentImage(IM) segments image IM using
5  % auto-generated code from the imageSegmenter App. The final
6  % segmentation is returned in BW and a masked image is
7  % returned in MASKEDIMAGE.
8
9  % Auto-generated by imageSegmenter app on 07-Nov-2017
10 %----------------------------------------------------
11
```

Appendix C (continued)

```
12
13 % Initialize segmentation with threshold
14 mask = im>200;
15
16 % Suppress components connected to image border
17 BW = imclearborder(mask);
18
19 % Fill holes
20 BW = imfill(BW, 'holes');
21
22 % Form masked image from input image and segmented image.
23 maskedImage = im;
24 maskedImage(~BW) = 0;
25 end
```

Appendix C (continued)

Listing C.8: Pupil mask code.

```
function [BW,maskedImage] = segmentImage_pupil(im)
%segmentImage segments image using auto-generated code from
% imageSegmenter App
%[BW,MASKEDIMAGE] = segmentImage(IM) segments image IM using
% auto-generated code from the imageSegmenter App. The final
% segmentation is returned in BW and a masked image is
% returned in MASKEDIMAGE.

% Auto-generated by imageSegmenter app on 07-Nov-2017
%----------------------------------------------------


% Initialize segmentation with threshold
mask = im>200;

% Suppress components connected to image border
BW = imclearborder(mask);

% Filter components by area
BW = bwareafilt(BW, [369 Inf]);
```

Appendix C (continued)

```
21
22 % Form masked image from input image and segmented image.
23 maskedImage = im;
24 maskedImage(~BW) = 0;
25 end
```

Listing C.9: Parameter extraction code.

```
1 % segment image to find CR => ONLY ONE REGION SHOULD BE LARGEST
2     [bw1, Imask1] = segmentImage_CR_1(Iw1);
3 %   imshow(Imask1)
4 % => uncomment look if okay otherwise fix segmentation
5
6     [labeled1,numObjects1]= bwlabel(Imask1,8);
7     props_CR = regionprops(labeled1,'Area','Centroid','
          EquivDiameter');
8     areas = [props_CR.Area];
9     max_area_index = find(areas == max(max(areas)));
```

Appendix C (continued)

```
10      CRr = props_CR(max_area_index(1)).EquivDiameter/2;
11      CRx = props_CR(max_area_index(1)).Centroid(1);
12      CRy = props_CR(max_area_index(1)).Centroid(2);
13
14  % remove CR
15      Iw1 = remove_corneal_reflection(Iw1, CRx, CRy, CRr*
            smoothing_CR);
16
17  %      imshow(I1) % => uncomment and check if it's ok otherwise
        fix smoothing
18
19  % invert image to find pupil
20      Iw2 = imcomplement(Iw1);
21      [bw2, Imask2] = segmentImage_pupil_1(Iw2);
22
23  %      imshow(Imask2) % => uncomment and look if okay otherwise
        fix segmentation
24
25      [labeled2,numObjects2] = bwlabel(Imask2,8);
```

Appendix C (continued)

```
26      props_pupil = regionprops(labeled2,'Area','Centroid','
           Eccentricity', 'MajorAxisLength', 'MinorAxisLength', '
           Orientation');
27
28      % construct the pupil ellipse vector
29      %   [a b cx cy theta]
30      %   a - the ellipse axis of x direction
31      %   b - the ellipse axis of y direction
32      %   cx - the x coordinate of ellipse center
33      %   cy - the y coordinate of ellipse center
34      %   theta - orientation of ellipse in deg respect to x axis
35      areas = [props_pupil.Area];
36      max_area_index = find(areas == max(max(areas)));
37      a = props_pupil(max_area_index(1)).MajorAxisLength;
38      b = props_pupil(max_area_index(1)).MinorAxisLength;
39      cx = props_pupil(max_area_index(1)).Centroid(1)+offset_x;
40      cy = props_pupil(max_area_index(1)).Centroid(2)+offset_y;
41      theta = props_pupil(max_area_index(1)).Orientation;
42      pupil_ellipse = [a, b, cx, cy, theta];
43      CRx = CRx+offset_x;
44      CRy = CRy+offset_y;
```

Appendix C (continued)

Listing C.10: Code for removing corneal reflection.

```
function [I] = remove_corneal_reflection(I, crx, cry, crr)
% Removes corneal reflection from input image using radial
% interpolation
% Input:
% I = input image
% [crx cry] = corneal reflection center
% crr = corneal reflection radius
% Output:
% I = output image with the corneal reflection removed
% NOTE - the original version had also and angle step size as %
    inpt, but it seems it is not used also in the original code, %
     so it was removed

if crx==0 || cry==0 || crr<=0
   return;
end

[height, width] = size(I);

```

Appendix C (continued)

```
18 if crx-crr < 1 || crx+crr > width || cry-crr < 1 || cry+crr >
       height
19     fprintf(1, 'Error! Corneal reflection is too near the image
           border\n');
20     return;
21 end
22
23 % creates vector for angles
24 theta=(0:pi/360:2*pi);
25
26 % horizontally stacks theta vector (theta is taken as row and %
       rows are stacked one onto the other crr times) => angular
27 % coodinates: for each radius value there is a theta vector of
28 % angles to consider
29 crr = ceil(crr);
30 tmat = repmat(theta',[1 crr]);
31
32 % vertically stacks 1:crr vector (1:crr vector is taken as
33 % column and column are lined one beside the other
34 % lenght(theta) times) => radial coordinates: for each theta
35 % angle there are the (1:crr) radius values to consider
```

Appendix C (continued)

```
rmat = repmat([1:crr],[length(theta) 1]);

% transforms radial coordinates into cartesian
[xmat,ymat]=pol2cart(tmat,rmat);

% reshape ymat and xmat into row vectors, the xv, yv pairs
% creates a map of all the points in the corneal reflex area
% in cartesian coordinates
xv=reshape(xmat,[1 numel(xmat)]);
yv=reshape(ymat,[1 numel(ymat)]);

% creates average gray value of all the points on the border
avgmat=ones(size(rmat))*mean(I(round(ymat(:,end)+cry)+(round(xmat
    (:,end)+crx)-1)*height));
permat=repmat(I(round(ymat(:,end)+cry)+(round(xmat(:,end)+crx)-1)
    *height),[1 crr]);
permat = double(permat);
% weight matrix
wmat=repmat((1:crr)/crr,[length(theta) 1]);
imat=-avgmat.*(wmat-1) + permat.*(wmat);
I(round(yv+cry)+(round(xv+crx-1).*height))=imat;
```

Appendix C (continued)

Listing C.11: Code for plotting CR and pupil ellipse on image.

```
handle = figure('visible', 'off');
Image = read_image(eye_file_name, frame_index);
imshow(Image);
hold on

% plot ellipse on image from regionprops
t = linspace(0,2*pi,50);
phi = deg2rad(-theta);
x = cx + (a/2)*cos(t)*cos(phi) - (b/2)*sin(t)*sin(phi);
y = cy + (a/2)*cos(t)*sin(phi) + (b/2)*sin(t)*cos(phi);
plot(x,y,'b','Linewidth',5)
scatter(cx, cy, 'c*')

% plot CR on image
th = 0:pi/50:2*pi;
xunit = CRr * cos(th) + CRx;
yunit = CRr * sin(th) + CRy;
plot(xunit, yunit, 'r');
scatter(CRx, CRy, 20, 'r+');
hold off
```

Appendix C (continued)

```
21
22      % save image
23      save_image(res_name, frame_index);
24
25      % close figure handle
26      close(figure)
27
28      % udpate matrices
29      CR_matrix(frame_index, :) = [CRx, CRy, CRr];
30      Ellipse_matrix(frame_index, :) = pupil_ellipse;
31      Diff_vector_matrix(frame_index, 1) = cx-CRx;
32      Diff_vector_matrix(frame_index, 2) = cy-CRy;
33      frame_index = frame_index + 1;
```

Appendix C (continued)

Listing C.12: Code for saving resulting color image.

```
function save_image(res_name, frame_index)
% image must be existsing already, so that one can choose if
% it will be visible or not

   F = getframe ;
   res_filename = strcat(res_name, sprintf('Eye_res_%5.5d.jpg',
      frame_index));
   imwrite(F.cdata, res_filename)
 return
```

Listing C.13: Code for saving extracted data.

```
results_data_name = sprintf('%s/Results.mat', res_name);
save(results_data_name, 'first_frame', 'last_frame', 'CR_matrix',
    'Ellipse_matrix', 'Diff_vector_matrix')
```

Appendix C (continued)

Listing C.14: Results processing code for fixations.

```
% Results processing
file = 'C:\Users\chawanmayur\Documents\MATLAB_1
\fixation_results.xls';
x_offsets = Diff_vector_matrix(:, 1);
trials = (1:10)';

% de-trending the data and SD and RMSE computation
(RMSE is take respect to
% the mean value)
mu = mean(x_offsets);
SD = std(x_offsets);
x_detrend = x_offsets - mu;
% SD =
%
%     0.2937
RMS = sqrt(mean((x_offsets - mu).^2));
% RMS =
%
%     0.2786

```

Appendix C (continued)

```

% plotting the results
figure('visible', 'on')
scatter(trials, x_offsets)
xlabel 'trials'
ylabel 'horizontal offset'
grid on
hold on
XL = xlim();
plot( XL, [mu, mu], 'r')
plot( XL, [mu+SD, mu+SD], 'b')
plot( XL, [mu-SD, mu-SD], 'b')
legend('Experimental points', 'mean', 'standard deviation')

% visualizing fitting errors
T = table(trials, x_offsets, x_detrend,'VariableNames',{'Trial','
    Offset','Deviation_from_Mean'});
writetable(T, 'Table.csv')

res = {'horizontal offsets', -8.3373    -8.2712    -7.5653
    -8.2899    -8.3257 ...
```

Appendix C (continued)

```
    -8.5448    -8.0744    -8.1779    -8.3863    -8.6396;
    'trials',    1     2     3     4     5     6     7     8
       9    10};
xlswrite(file, res)
```

Listing C.15: Results processing code for vertical rotation.

```
% Results processing
file = 'C:\Users\chawanmayur\Documents\MATLAB_1\Backup\
   vertical_results.xls'
y_offsets = Diff_vector_matrix(:, 2)';
angles = [30:-10:-30];

% fitting linear model to data
[line, err] = polyfit(y_offsets, angles, 1);

% line =
%
```

Appendix C (continued)

```
%    0.7779   -8.6909

% err =
%
%          R: [2x2 double]
%         df: 5
%      normr: 5.0345

interpolated = polyval(line, y_offsets);

% plotting the results
figure('visible', 'on')
scatter(y_offsets, angles)
xlabel 'vertical offsets between CR center and pupil center, in
    pixels'
ylabel 'vertical rotation of eye bulb'
grid on
hold on
plot(y_offsets, interpolated)
legend('Experimental points', 'Intepolating line')

```

Appendix C (continued)

```
% visualizing fitting errors
T = table(y_offsets',angles',interpolated',(angles-interpolated)
    ','VariableNames',{'y_offsets','Angles','Fitted_values','Error
    '});
writetable(T, 'Table.csv')

res = {'vertical offsets', 45.8888   36.7634   26.7172   13.6224
      -1.4198  -12.7326  -30.6321;...
    'vertical rotation angles',   -30   -20   -10     0    10
        20    30};
xlswrite(file, res)


% evaluating coefficient of determination R
[R, p] = corrcoef(y_offsets, angles);
% R =
%
%     1.0000    0.9955
%     0.9955    1.0000
%
%
```

Appendix C (continued)

```
48 % p =
49 %
50 %      1.0000     0.0000
51 %      0.0000     1.0000
```

Appendix D

PERMISSIONS TO REPRINT MATERIAL

In this appendix are listed the copies of the permissions used to reprint figures and tables from published material.

If the material was under Creative Commons license or similar agreement, the hyperlink to the web page of the licence is provided in the Cited Literature section, as in the case of [30, 59] etc.

SPRINGER NATURE LICENSE TERMS AND CONDITIONS

Aug 19, 2018

This Agreement between UIC -- Beatrice Pazzucconi ("You") and Springer Nature ("Springer Nature") consists of your license details and the terms and conditions provided by Springer Nature and Copyright Clearance Center.

License Number	4412401282209
License date	Aug 19, 2018
Licensed Content Publisher	Springer Nature
Licensed Content Publication	Springer eBook
Licensed Content Title	Head-Mounted System Software Development
Licensed Content Author	Andrew Duchowski
Licensed Content Date	Jan 1, 2007
Type of Use	Thesis/Dissertation
Requestor type	academic/university or research institute
Format	print and electronic
Portion	figures/tables/illustrations
Number of figures/tables /illustrations	1
Will you be translating?	no
Circulation/distribution	<501
Author of this Springer Nature content	no
Title	Preliminary feasibility of a holographic based eye tracker
Instructor name	n/a
Institution name	University of Illinois at Chicago
Expected presentation date	Mar 2019
Portions	figure 7.1
Requestor Location	UIC 851 S Morgan St, SEO 218 CHICAGO, IL 60607 United States Attn: USBJ
Billing Type	Invoice
Billing Address	UIC 851 S Morgan St, SEO 218 CHICAGO, IL 60607 United States

	Attn: USBJ
Total	0.00 USD

Terms and Conditions

Springer Nature Terms and Conditions for RightsLink Permissions

Springer Nature Customer Service Centre GmbH (the Licensor) hereby grants you a non-exclusive, world-wide licence to reproduce the material and for the purpose and requirements specified in the attached copy of your order form, and for no other use, subject to the conditions below:

1. The Licensor warrants that it has, to the best of its knowledge, the rights to license reuse of this material. However, you should ensure that the material you are requesting is original to the Licensor and does not carry the copyright of another entity (as credited in the published version).

   If the credit line on any part of the material you have requested indicates that it was reprinted or adapted with permission from another source, then you should also seek permission from that source to reuse the material.

2. Where **print only** permission has been granted for a fee, separate permission must be obtained for any additional electronic re-use.

3. Permission granted **free of charge** for material in print is also usually granted for any electronic version of that work, provided that the material is incidental to your work as a whole and that the electronic version is essentially equivalent to, or substitutes for, the print version.

4. A licence for 'post on a website' is valid for 12 months from the licence date. This licence does not cover use of full text articles on websites.

5. Where **'reuse in a dissertation/thesis'** has been selected the following terms apply: Print rights of the final author's accepted manuscript (for clarity, NOT the published version) for up to 100 copies, electronic rights for use only on a personal website or institutional repository as defined by the Sherpa guideline (www.sherpa.ac.uk/romeo/).

6. Permission granted for books and journals is granted for the lifetime of the first edition and does not apply to second and subsequent editions (except where the first edition permission was granted free of charge or for signatories to the STM Permissions Guidelines http://www.stm-assoc.org/copyright-legal-affairs/permissions/permissions-guidelines/), and does not apply for editions in other languages unless additional translation rights have been granted separately in the licence.

7. Rights for additional components such as custom editions and derivatives require additional permission and may be subject to an additional fee. Please apply to Journalpermissions@springernature.com/bookpermissions@springernature.com for these rights.

8. The Licensor's permission must be acknowledged next to the licensed material in print. In electronic form, this acknowledgement must be visible at the same time as the figures/tables/illustrations or abstract, and must be hyperlinked to the journal/book's homepage. Our required acknowledgement format is in the Appendix below.

9. Use of the material for incidental promotional use, minor editing privileges (this does not include cropping, adapting, omitting material or any other changes that affect the meaning, intention or moral rights of the author) and copies for the disabled are permitted under this licence.

10. Minor adaptations of single figures (changes of format, colour and style) do not require the Licensor's approval. However, the adaptation should be credited as shown in Appendix

below.

Appendix — Acknowledgements:

For Journal Content:
Reprinted by permission from [**the Licensor**]: [**Journal Publisher** (e.g. Nature/Springer/Palgrave)] [**JOURNAL NAME**] [**REFERENCE CITATION** (Article name, Author(s) Name), [**COPYRIGHT**] (year of publication)

For **Advance Online Publication papers:**
Reprinted by permission from [**the Licensor**]: [**Journal Publisher** (e.g. Nature/Springer/Palgrave)] [**JOURNAL NAME**] [**REFERENCE CITATION** (Article name, Author(s) Name), [**COPYRIGHT**] (year of publication), advance online publication, day month year (doi: 10.1038/sj.[JOURNAL ACRONYM].)

For Adaptations/Translations:
Adapted/Translated by permission from [**the Licensor**]: [**Journal Publisher** (e.g. Nature/Springer/Palgrave)] [**JOURNAL NAME**] [**REFERENCE CITATION** (Article name, Author(s) Name), [**COPYRIGHT**] (year of publication)

Note: For any republication from the British Journal of Cancer, the following credit line style applies:

Reprinted/adapted/translated by permission from [**the Licensor**]: on behalf of Cancer Research UK: : [**Journal Publisher** (e.g. Nature/Springer/Palgrave)] [**JOURNAL NAME**] [**REFERENCE CITATION** (Article name, Author(s) Name), [**COPYRIGHT]** (year of publication)

For **Advance Online Publication** papers:
Reprinted by permission from The [**the Licensor**]: on behalf of Cancer Research UK: [**Journal Publisher** (e.g. Nature/Springer/Palgrave)] [**JOURNAL NAME**] [**REFERENCE CITATION** (Article name, Author(s) Name), [**COPYRIGHT**] (year of publication), advance online publication, day month year (doi: 10.1038/sj.[JOURNAL ACRONYM])

For Book content:
Reprinted/adapted by permission from [**the Licensor**]: [**Book Publisher** (e.g. Palgrave Macmillan, Springer etc) [**Book Title**] by [**Book author**(s)] [**COPYRIGHT**] (year of publication)

Other Conditions:

Version 1.1

SPRINGER NATURE LICENSE TERMS AND CONDITIONS

Aug 19, 2018

This Agreement between UIC -- Beatrice Pazzucconi ("You") and Springer Nature ("Springer Nature") consists of your license details and the terms and conditions provided by Springer Nature and Copyright Clearance Center.

License Number	4412400905838
License date	Aug 19, 2018
Licensed Content Publisher	Springer Nature
Licensed Content Publication	Springer eBook
Licensed Content Title	Eye Tracking Techniques
Licensed Content Author	Andrew Duchowski
Licensed Content Date	Jan 1, 2007
Type of Use	Thesis/Dissertation
Requestor type	academic/university or research institute
Format	print and electronic
Portion	figures/tables/illustrations
Number of figures/tables /illustrations	3
Will you be translating?	no
Circulation/distribution	<501
Author of this Springer Nature content	no
Title	Preliminary feasibility of a holographic based eye tracker
Instructor name	n/a
Institution name	n/a
Expected presentation date	Mar 2019
Portions	figure 5.3, 5.4, 5.8
Requestor Location	UIC 851 S Morgan St, SEO 218 CHICAGO, IL 60607 United States Attn: USBJ
Billing Type	Invoice
Billing Address	UIC 851 S Morgan St, SEO 218 CHICAGO, IL 60607 United States

	Attn: USBJ
Total	0.00 USD

Terms and Conditions

Springer Nature Terms and Conditions for RightsLink Permissions

Springer Nature Customer Service Centre GmbH (the Licensor) hereby grants you a non-exclusive, world-wide licence to reproduce the material and for the purpose and requirements specified in the attached copy of your order form, and for no other use, subject to the conditions below:

1. The Licensor warrants that it has, to the best of its knowledge, the rights to license reuse of this material. However, you should ensure that the material you are requesting is original to the Licensor and does not carry the copyright of another entity (as credited in the published version).

   If the credit line on any part of the material you have requested indicates that it was reprinted or adapted with permission from another source, then you should also seek permission from that source to reuse the material.

2. Where **print only** permission has been granted for a fee, separate permission must be obtained for any additional electronic re-use.

3. Permission granted **free of charge** for material in print is also usually granted for any electronic version of that work, provided that the material is incidental to your work as a whole and that the electronic version is essentially equivalent to, or substitutes for, the print version.

4. A licence for 'post on a website' is valid for 12 months from the licence date. This licence does not cover use of full text articles on websites.

5. Where **'reuse in a dissertation/thesis'** has been selected the following terms apply: Print rights of the final author's accepted manuscript (for clarity, NOT the published version) for up to 100 copies, electronic rights for use only on a personal website or institutional repository as defined by the Sherpa guideline (www.sherpa.ac.uk/romeo/).

6. Permission granted for books and journals is granted for the lifetime of the first edition and does not apply to second and subsequent editions (except where the first edition permission was granted free of charge or for signatories to the STM Permissions Guidelines http://www.stm-assoc.org/copyright-legal-affairs/permissions/permissions-guidelines/), and does not apply for editions in other languages unless additional translation rights have been granted separately in the licence.

7. Rights for additional components such as custom editions and derivatives require additional permission and may be subject to an additional fee. Please apply to Journalpermissions@springernature.com/bookpermissions@springernature.com for these rights.

8. The Licensor's permission must be acknowledged next to the licensed material in print. In electronic form, this acknowledgement must be visible at the same time as the figures/tables/illustrations or abstract, and must be hyperlinked to the journal/book's homepage. Our required acknowledgement format is in the Appendix below.

9. Use of the material for incidental promotional use, minor editing privileges (this does not include cropping, adapting, omitting material or any other changes that affect the meaning, intention or moral rights of the author) and copies for the disabled are permitted under this licence.

10. Minor adaptations of single figures (changes of format, colour and style) do not require the Licensor's approval. However, the adaptation should be credited as shown in Appendix

below.

Appendix — Acknowledgements:

For Journal Content:
Reprinted by permission from [**the Licensor**]: [**Journal Publisher** (e.g. Nature/Springer/Palgrave)] [**JOURNAL NAME**] [**REFERENCE CITATION** (Article name, Author(s) Name), [**COPYRIGHT**] (year of publication)

For **Advance Online Publication papers:**
Reprinted by permission from [**the Licensor**]: [**Journal Publisher** (e.g. Nature/Springer/Palgrave)] [**JOURNAL NAME**] [**REFERENCE CITATION** (Article name, Author(s) Name), [**COPYRIGHT**] (year of publication), advance online publication, day month year (doi: 10.1038/sj.[JOURNAL ACRONYM].)

For Adaptations/Translations:
Adapted/Translated by permission from [**the Licensor**]: [**Journal Publisher** (e.g. Nature/Springer/Palgrave)] [**JOURNAL NAME**] [**REFERENCE CITATION** (Article name, Author(s) Name), [**COPYRIGHT**] (year of publication)

Note: For any republication from the British Journal of Cancer, the following credit line style applies:

Reprinted/adapted/translated by permission from [**the Licensor**]: on behalf of Cancer Research UK: : [**Journal Publisher** (e.g. Nature/Springer/Palgrave)] [**JOURNAL NAME**] [**REFERENCE CITATION** (Article name, Author(s) Name), [**COPYRIGHT]** (year of publication)

For **Advance Online Publication** papers:
Reprinted by permission from The [**the Licensor**]: on behalf of Cancer Research UK: [**Journal Publisher** (e.g. Nature/Springer/Palgrave)] [**JOURNAL NAME**] [**REFERENCE CITATION** (Article name, Author(s) Name), [**COPYRIGHT**] (year of publication), advance online publication, day month year (doi: 10.1038/sj.[JOURNAL ACRONYM])

For Book content:
Reprinted/adapted by permission from [**the Licensor**]: [**Book Publisher** (e.g. Palgrave Macmillan, Springer etc) [**Book Title**] by [**Book author**(s)] [**COPYRIGHT**] (year of publication)

Other Conditions:

Version 1.1

SPRINGER NATURE LICENSE TERMS AND CONDITIONS

Aug 18, 2018

This Agreement between UIC -- Beatrice Pazzucconi ("You") and Springer Nature ("Springer Nature") consists of your license details and the terms and conditions provided by Springer Nature and Copyright Clearance Center.

License Number	4411990464827
License date	Aug 18, 2018
Licensed Content Publisher	Springer Nature
Licensed Content Publication	Behavior Research Methods
Licensed Content Title	Survey of eye movement recording methods
Licensed Content Author	Laurence R. Young, David Sheena
Licensed Content Date	Jan 1, 1975
Licensed Content Volume	7
Licensed Content Issue	5
Type of Use	Thesis/Dissertation
Requestor type	academic/university or research institute
Format	print and electronic
Portion	figures/tables/illustrations
Number of figures/tables /illustrations	3
Will you be translating?	no
Circulation/distribution	<501
Author of this Springer Nature content	no
Title	Preliminary feasibility of a holographic based eye tracker
Instructor name	n/a
Institution name	n/a
Expected presentation date	Mar 2019
Portions	figure 6, 22, 43, 44a
Requestor Location	UIC 851 S Morgan St, SEO 218 CHICAGO, IL 60607 United States Attn: USBJ
Billing Type	Invoice
Billing Address	UIC 851 S Morgan St, SEO 218

CHICAGO, IL 60607
United States
Attn: USBJ

Total 0.00 USD

Terms and Conditions

Springer Nature Terms and Conditions for RightsLink Permissions

Springer Nature Customer Service Centre GmbH (the Licensor) hereby grants you a non-exclusive, world-wide licence to reproduce the material and for the purpose and requirements specified in the attached copy of your order form, and for no other use, subject to the conditions below:

1. The Licensor warrants that it has, to the best of its knowledge, the rights to license reuse of this material. However, you should ensure that the material you are requesting is original to the Licensor and does not carry the copyright of another entity (as credited in the published version).

   If the credit line on any part of the material you have requested indicates that it was reprinted or adapted with permission from another source, then you should also seek permission from that source to reuse the material.

2. Where **print only** permission has been granted for a fee, separate permission must be obtained for any additional electronic re-use.

3. Permission granted **free of charge** for material in print is also usually granted for any electronic version of that work, provided that the material is incidental to your work as a whole and that the electronic version is essentially equivalent to, or substitutes for, the print version.

4. A licence for 'post on a website' is valid for 12 months from the licence date. This licence does not cover use of full text articles on websites.

5. Where **'reuse in a dissertation/thesis'** has been selected the following terms apply: Print rights of the final author's accepted manuscript (for clarity, NOT the published version) for up to 100 copies, electronic rights for use only on a personal website or institutional repository as defined by the Sherpa guideline (www.sherpa.ac.uk/romeo/).

6. Permission granted for books and journals is granted for the lifetime of the first edition and does not apply to second and subsequent editions (except where the first edition permission was granted free of charge or for signatories to the STM Permissions Guidelines http://www.stm-assoc.org/copyright-legal-affairs/permissions/permissions-guidelines/), and does not apply for editions in other languages unless additional translation rights have been granted separately in the licence.

7. Rights for additional components such as custom editions and derivatives require additional permission and may be subject to an additional fee. Please apply to Journalpermissions@springernature.com/bookpermissions@springernature.com for these rights.

8. The Licensor's permission must be acknowledged next to the licensed material in print. In electronic form, this acknowledgement must be visible at the same time as the figures/tables/illustrations or abstract, and must be hyperlinked to the journal/book's homepage. Our required acknowledgement format is in the Appendix below.

9. Use of the material for incidental promotional use, minor editing privileges (this does not include cropping, adapting, omitting material or any other changes that affect the meaning, intention or moral rights of the author) and copies for the disabled are permitted under this licence.

10. Minor adaptations of single figures (changes of format, colour and style) do not require the Licensor's approval. However, the adaptation should be credited as shown in Appendix below.

Appendix — Acknowledgements:

For Journal Content:
Reprinted by permission from [**the Licensor**]: [**Journal Publisher** (e.g. Nature/Springer/Palgrave)] [**JOURNAL NAME**] [**REFERENCE CITATION** (Article name, Author(s) Name), [**COPYRIGHT**] (year of publication)

For **Advance Online Publication papers:**
Reprinted by permission from [**the Licensor**]: [**Journal Publisher** (e.g. Nature/Springer/Palgrave)] [**JOURNAL NAME**] [**REFERENCE CITATION** (Article name, Author(s) Name), [**COPYRIGHT**] (year of publication), advance online publication, day month year (doi: 10.1038/sj.[JOURNAL ACRONYM].)

For Adaptations/Translations:
Adapted/Translated by permission from [**the Licensor**]: [**Journal Publisher** (e.g. Nature/Springer/Palgrave)] [**JOURNAL NAME**] [**REFERENCE CITATION** (Article name, Author(s) Name), [**COPYRIGHT**] (year of publication)

Note: For any republication from the British Journal of Cancer, the following credit line style applies:

Reprinted/adapted/translated by permission from [**the Licensor**]: on behalf of Cancer Research UK: : [**Journal Publisher** (e.g. Nature/Springer/Palgrave)] [**JOURNAL NAME**] [**REFERENCE CITATION** (Article name, Author(s) Name), [**COPYRIGHT]** (year of publication)

For **Advance Online Publication** papers:
Reprinted by permission from The [**the Licensor**]: on behalf of Cancer Research UK: [**Journal Publisher** (e.g. Nature/Springer/Palgrave)] [**JOURNAL NAME**] [**REFERENCE CITATION** (Article name, Author(s) Name), [**COPYRIGHT**] (year of publication), advance online publication, day month year (doi: 10.1038/sj.[JOURNAL ACRONYM])

For Book content:
Reprinted/adapted by permission from [**the Licensor**]: [**Book Publisher** (e.g. Palgrave Macmillan, Springer etc) [**Book Title**] by [**Book author**(s)] [**COPYRIGHT**] (year of publication)

Other Conditions:

Version 1.1

Questions? customercare@copyright.com or +1-855-239-3415 (toll free in the US) or +1-978-646-2777.

Title:	Eye Tracking and Head Movement Detection: A State-of-Art Survey
Author:	Amer Al-Rahayfeh
Publication:	IEEE Journal of Translational Engineering in Health and Medicine
Publisher:	IEEE
Date:	2013

Logged in as:
Beatrice Pazzucconi
UIC
Account #:
3001264029

Thesis / Dissertation Reuse

The IEEE does not require individuals working on a thesis to obtain a formal reuse license, however, you may print out this statement to be used as a permission grant:

Requirements to be followed when using any portion (e.g., figure, graph, table, or textual material) of an IEEE copyrighted paper in a thesis:

1) In the case of textual material (e.g., using short quotes or referring to the work within these papers) users must give full credit to the original source (author, paper, publication) followed by the IEEE copyright line © 2011 IEEE.
2) In the case of illustrations or tabular material, we require that the copyright line © [Year of original publication] IEEE appear prominently with each reprinted figure and/or table.
3) If a substantial portion of the original paper is to be used, and if you are not the senior author, also obtain the senior author's approval.

Requirements to be followed when using an entire IEEE copyrighted paper in a thesis:

1) The following IEEE copyright/ credit notice should be placed prominently in the references: © [year of original publication] IEEE. Reprinted, with permission, from [author names, paper title, IEEE publication title, and month/year of publication]
2) Only the accepted version of an IEEE copyrighted paper can be used when posting the paper or your thesis on-line.
3) In placing the thesis on the author's university website, please display the following message in a prominent place on the website: In reference to IEEE copyrighted material which is used with permission in this thesis, the IEEE does not endorse any of [university/educational entity's name goes here]'s products or services. Internal or personal use of this material is permitted. If interested in reprinting/republishing IEEE copyrighted material for advertising or promotional purposes or for creating new collective works for resale or redistribution, please go to http://www.ieee.org/publications_standards/publications/rights/rights_link.html to learn how to obtain a License from RightsLink.

If applicable, University Microfilms and/or ProQuest Library, or the Archives of Canada may supply single copies of the dissertation.

SPRINGER NATURE LICENSE TERMS AND CONDITIONS

Aug 20, 2018

This Agreement between UIC -- Beatrice Pazzucconi ("You") and Springer Nature ("Springer Nature") consists of your license details and the terms and conditions provided by Springer Nature and Copyright Clearance Center.

License Number	4413160120160
License date	Aug 20, 2018
Licensed Content Publisher	Springer Nature
Licensed Content Publication	Springer eBook
Licensed Content Title	Robust Eye Movement Recognition Using EOG Signal for Human-Computer Interface
Licensed Content Author	Siriwadee Aungsakun, Angkoon Phinyomark, Pornchai Phukpattaranont et al
Licensed Content Date	Jan 1, 2011
Type of Use	Thesis/Dissertation
Requestor type	academic/university or research institute
Format	print and electronic
Portion	figures/tables/illustrations
Number of figures/tables /illustrations	1
Will you be translating?	no
Circulation/distribution	<501
Author of this Springer Nature content	no
Title	Preliminary feasibility of a holographic based eye tracker
Instructor name	n/a
Institution name	University of Illinois at Chicago
Expected presentation date	Mar 2019
Portions	1
Requestor Location	UIC 851 S Morgan St, SEO 218 CHICAGO, IL 60607 United States Attn: USBJ
Billing Type	Invoice
Billing Address	UIC 851 S Morgan St, SEO 218

CHICAGO, IL 60607
United States
Attn: USBJ

Total 0.00 USD

Terms and Conditions

Springer Nature Terms and Conditions for RightsLink Permissions

Springer Nature Customer Service Centre GmbH (the Licensor) hereby grants you a non-exclusive, world-wide licence to reproduce the material and for the purpose and requirements specified in the attached copy of your order form, and for no other use, subject to the conditions below:

1. The Licensor warrants that it has, to the best of its knowledge, the rights to license reuse of this material. However, you should ensure that the material you are requesting is original to the Licensor and does not carry the copyright of another entity (as credited in the published version).

   If the credit line on any part of the material you have requested indicates that it was reprinted or adapted with permission from another source, then you should also seek permission from that source to reuse the material.

2. Where **print only** permission has been granted for a fee, separate permission must be obtained for any additional electronic re-use.

3. Permission granted **free of charge** for material in print is also usually granted for any electronic version of that work, provided that the material is incidental to your work as a whole and that the electronic version is essentially equivalent to, or substitutes for, the print version.

4. A licence for 'post on a website' is valid for 12 months from the licence date. This licence does not cover use of full text articles on websites.

5. Where **'reuse in a dissertation/thesis'** has been selected the following terms apply: Print rights of the final author's accepted manuscript (for clarity, NOT the published version) for up to 100 copies, electronic rights for use only on a personal website or institutional repository as defined by the Sherpa guideline (www.sherpa.ac.uk/romeo/).

6. Permission granted for books and journals is granted for the lifetime of the first edition and does not apply to second and subsequent editions (except where the first edition permission was granted free of charge or for signatories to the STM Permissions Guidelines http://www.stm-assoc.org/copyright-legal-affairs/permissions/permissions-guidelines/), and does not apply for editions in other languages unless additional translation rights have been granted separately in the licence.

7. Rights for additional components such as custom editions and derivatives require additional permission and may be subject to an additional fee. Please apply to Journalpermissions@springernature.com/bookpermissions@springernature.com for these rights.

8. The Licensor's permission must be acknowledged next to the licensed material in print. In electronic form, this acknowledgement must be visible at the same time as the figures/tables/illustrations or abstract, and must be hyperlinked to the journal/book's homepage. Our required acknowledgement format is in the Appendix below.

9. Use of the material for incidental promotional use, minor editing privileges (this does not include cropping, adapting, omitting material or any other changes that affect the meaning, intention or moral rights of the author) and copies for the disabled are permitted under this licence.

10. Minor adaptations of single figures (changes of format, colour and style) do not require the Licensor's approval. However, the adaptation should be credited as shown in Appendix below.

Appendix — Acknowledgements:

For Journal Content:
Reprinted by permission from [**the Licensor**]: [**Journal Publisher** (e.g. Nature/Springer/Palgrave)] [**JOURNAL NAME**] [**REFERENCE CITATION** (Article name, Author(s) Name), [**COPYRIGHT**] (year of publication)

For **Advance Online Publication papers:**
Reprinted by permission from [**the Licensor**]: [**Journal Publisher** (e.g. Nature/Springer/Palgrave)] [**JOURNAL NAME**] [**REFERENCE CITATION** (Article name, Author(s) Name), [**COPYRIGHT**] (year of publication), advance online publication, day month year (doi: 10.1038/sj.[JOURNAL ACRONYM].)

For Adaptations/Translations:
Adapted/Translated by permission from [**the Licensor**]: [**Journal Publisher** (e.g. Nature/Springer/Palgrave)] [**JOURNAL NAME**] [**REFERENCE CITATION** (Article name, Author(s) Name), [**COPYRIGHT**] (year of publication)

Note: For any republication from the British Journal of Cancer, the following credit line style applies:

Reprinted/adapted/translated by permission from [**the Licensor**]: on behalf of Cancer Research UK: : [**Journal Publisher** (e.g. Nature/Springer/Palgrave)] [**JOURNAL NAME**] [**REFERENCE CITATION** (Article name, Author(s) Name), [**COPYRIGHT]** (year of publication)

For **Advance Online Publication** papers:
Reprinted by permission from The [**the Licensor**]: on behalf of Cancer Research UK: [**Journal Publisher** (e.g. Nature/Springer/Palgrave)] [**JOURNAL NAME**] [**REFERENCE CITATION** (Article name, Author(s) Name), [**COPYRIGHT**] (year of publication), advance online publication, day month year (doi: 10.1038/sj.[JOURNAL ACRONYM])

For Book content:
Reprinted/adapted by permission from [**the Licensor**]: [**Book Publisher** (e.g. Palgrave Macmillan, Springer etc) [**Book Title**] by [**Book author**(s)] [**COPYRIGHT**] (year of publication)

Other Conditions:

Version 1.1

SPRINGER NATURE LICENSE TERMS AND CONDITIONS

Aug 22, 2018

This Agreement between UIC -- Beatrice Pazzucconi ("You") and Springer Nature ("Springer Nature") consists of your license details and the terms and conditions provided by Springer Nature and Copyright Clearance Center.

License Number	4414281042146
License date	Aug 22, 2018
Licensed Content Publisher	Springer Nature
Licensed Content Publication	Machine Vision and Applications
Licensed Content Title	Pupil detection for head-mounted eye tracking in the wild: an evaluation of the state of the art
Licensed Content Author	Wolfgang Fuhl, Marc Tonsen, Andreas Bulling et al
Licensed Content Date	Jan 1, 2016
Licensed Content Volume	27
Licensed Content Issue	8
Type of Use	Thesis/Dissertation
Requestor type	academic/university or research institute
Format	print and electronic
Portion	figures/tables/illustrations
Number of figures/tables /illustrations	1
Will you be translating?	no
Circulation/distribution	<501
Author of this Springer Nature content	no
Title	Preliminary feasibility of a holographic based eye tracker
Instructor name	n/a
Institution name	University of Illinois at Chicago
Expected presentation date	Mar 2019
Portions	figure 5
Requestor Location	UIC 851 S Morgan St, SEO 218 CHICAGO, IL 60607 United States Attn: USBJ
Billing Type	Invoice

Billing Address	UIC 851 S Morgan St, SEO 218 CHICAGO, IL 60607 United States Attn: USBJ
Total	0.00 USD

Terms and Conditions

Springer Nature Terms and Conditions for RightsLink Permissions

Springer Nature Customer Service Centre GmbH (the Licensor) hereby grants you a non-exclusive, world-wide licence to reproduce the material and for the purpose and requirements specified in the attached copy of your order form, and for no other use, subject to the conditions below:

1. The Licensor warrants that it has, to the best of its knowledge, the rights to license reuse of this material. However, you should ensure that the material you are requesting is original to the Licensor and does not carry the copyright of another entity (as credited in the published version).

   If the credit line on any part of the material you have requested indicates that it was reprinted or adapted with permission from another source, then you should also seek permission from that source to reuse the material.

2. Where **print only** permission has been granted for a fee, separate permission must be obtained for any additional electronic re-use.

3. Permission granted **free of charge** for material in print is also usually granted for any electronic version of that work, provided that the material is incidental to your work as a whole and that the electronic version is essentially equivalent to, or substitutes for, the print version.

4. A licence for 'post on a website' is valid for 12 months from the licence date. This licence does not cover use of full text articles on websites.

5. Where **'reuse in a dissertation/thesis'** has been selected the following terms apply: Print rights of the final author's accepted manuscript (for clarity, NOT the published version) for up to 100 copies, electronic rights for use only on a personal website or institutional repository as defined by the Sherpa guideline (www.sherpa.ac.uk/romeo/).

6. Permission granted for books and journals is granted for the lifetime of the first edition and does not apply to second and subsequent editions (except where the first edition permission was granted free of charge or for signatories to the STM Permissions Guidelines http://www.stm-assoc.org/copyright-legal-affairs/permissions/permissions-guidelines/), and does not apply for editions in other languages unless additional translation rights have been granted separately in the licence.

7. Rights for additional components such as custom editions and derivatives require additional permission and may be subject to an additional fee. Please apply to Journalpermissions@springernature.com/bookpermissions@springernature.com for these rights.

8. The Licensor's permission must be acknowledged next to the licensed material in print. In electronic form, this acknowledgement must be visible at the same time as the figures/tables/illustrations or abstract, and must be hyperlinked to the journal/book's homepage. Our required acknowledgement format is in the Appendix below.

9. Use of the material for incidental promotional use, minor editing privileges (this does not

include cropping, adapting, omitting material or any other changes that affect the meaning, intention or moral rights of the author) and copies for the disabled are permitted under this licence.

10. Minor adaptations of single figures (changes of format, colour and style) do not require the Licensor's approval. However, the adaptation should be credited as shown in Appendix below.

Appendix — Acknowledgements:

For Journal Content:
Reprinted by permission from [**the Licensor**]: [**Journal Publisher** (e.g. Nature/Springer/Palgrave)] [**JOURNAL NAME**] [**REFERENCE CITATION** (Article name, Author(s) Name), [**COPYRIGHT**] (year of publication)

For **Advance Online Publication papers:**
Reprinted by permission from [**the Licensor**]: [**Journal Publisher** (e.g. Nature/Springer/Palgrave)] [**JOURNAL NAME**] [**REFERENCE CITATION** (Article name, Author(s) Name), [**COPYRIGHT**] (year of publication), advance online publication, day month year (doi: 10.1038/sj.[JOURNAL ACRONYM].)

For Adaptations/Translations:
Adapted/Translated by permission from [**the Licensor**]: [**Journal Publisher** (e.g. Nature/Springer/Palgrave)] [**JOURNAL NAME**] [**REFERENCE CITATION** (Article name, Author(s) Name), [**COPYRIGHT**] (year of publication)

Note: For any republication from the British Journal of Cancer, the following credit line style applies:

Reprinted/adapted/translated by permission from [**the Licensor**]: on behalf of Cancer Research UK: : [**Journal Publisher** (e.g. Nature/Springer/Palgrave)] [**JOURNAL NAME**] [**REFERENCE CITATION** (Article name, Author(s) Name), [**COPYRIGHT]** (year of publication)

For **Advance Online Publication** papers:
Reprinted by permission from The [**the Licensor**]: on behalf of Cancer Research UK: [**Journal Publisher** (e.g. Nature/Springer/Palgrave)] [**JOURNAL NAME**] [**REFERENCE CITATION** (Article name, Author(s) Name), [**COPYRIGHT**] (year of publication), advance online publication, day month year (doi: 10.1038/sj.[JOURNAL ACRONYM])

For Book content:
Reprinted/adapted by permission from [**the Licensor**]: [**Book Publisher** (e.g. Palgrave Macmillan, Springer etc) [**Book Title**] by [**Book author**(s)] [**COPYRIGHT**] (year of publication)

Other Conditions:

Version 1.1

Questions? customercare@copyright.com or +1-855-239-3415 (toll free in the US) or +1-978-646-2777.

BMJ PUBLISHING GROUP LTD. LICENSE TERMS AND CONDITIONS

Aug 25, 2018

This Agreement between UIC -- Beatrice Pazzucconi ("You") and BMJ Publishing Group Ltd. ("BMJ Publishing Group Ltd.") consists of your license details and the terms and conditions provided by BMJ Publishing Group Ltd. and Copyright Clearance Center.

License Number	4415960756559
License date	Aug 25, 2018
Licensed Content Publisher	BMJ Publishing Group Ltd.
Licensed Content Publication	British Journal of Ophthalmology
Licensed Content Title	Screening for convergence insufficiency using the CISS is not indicated in young adults
Licensed Content Author	Anna M Horwood,Sonia Toor,Patricia M Riddell
Licensed Content Date	May 1, 2014
Licensed Content Volume	98
Licensed Content Issue	5
Type of Use	Dissertation/Thesis
Requestor type	Individual
Format	Print and electronic
Portion	Figure/table/extract
Number of figure/table /extracts	1
Descriptionof figure/table /extracts	figure 1
Will you be translating?	No
Circulation/distribution	10
Title of your thesis / dissertation	Preliminary feasibility of a holographic based eye tracker
Expected completion date	Mar 2019
Estimated size(pages)	90
Requestor Location	UIC 851 S Morgan St, SEO 218 CHICAGO, IL 60607 United States Attn: USBJ
Publisher Tax ID	GB674738491
Billing Type	Invoice
Billing Address	UIC 851 S Morgan St, SEO 218

CHICAGO, IL 60607
United States
Attn: USBJ

Total 0.00 USD

Terms and Conditions

BMJ Group Terms and Conditions for Permissions

When you submit your orderyou are subject to the terms and conditions set out below. You will also haveagreed to the Copyright Clearance Center's ("CCC") terms and conditionsregarding billing and payment https://s100.copyright.com/App/PaymentTermsAndConditions.jsp. CCC are acting as the BMJ Publishing Group Limited's ("BMJ Group's") agent.

Subject to the terms set outherein, the BMJ Group hereby grants to you (the Licensee) a non-exclusive,non-transferable licence to re-use material as detailed in your request forthis/those purpose(s) only and in accordance with the following conditions:

1) **Scope of Licence:** Useof the Licensed Material(s) is restricted to the ways specified by you duringthe order process and any additional use(s) outside of those specified in thatrequest, require a further grant of permission.

2) **Acknowledgement:** Inall cases, due acknowledgement to the original publication with permission fromthe BMJ Group should be stated adjacent to the reproduced Licensed Material.The format of such acknowledgement should read as follows:

"Reproduced from [publicationtitle, author(s), volume number, page numbers, copyright notice year] withpermission from BMJ Publishing Group Ltd."

3) **Third Party Material**:BMJ Group acknowledges to the best of its knowledge, it has the rights to licenceyour reuse of the Licensed Material, subject always to the caveat thatimages/diagrams, tables and other illustrative material included within, whichhave a separate copyright notice, are presumed as excluded from the licence. Therefore,you should ensure that the Licensed Material you are requesting is original toBMJ Group and does not carry the copyright of another entity (as credited inthe published version). If the credit line on any part of the material you haverequested in any way indicates that it was reprinted or adapted by BMJ Groupwith permission from another source, then you should seek permission from thatsource directly to re-use the Licensed Material, as this is outside of thelicence granted herein.

4) **Altering/ModifyingMaterial:** The text of any material for which a licence is granted may notbe altered in any way without the prior express permission of the BMJ Group. Subject to Clause 3 above however, single figure adaptations do not require BMJGroup's approval; however, the adaptation should be credited as follows:

"Adapted by permission fromBMJ Publishing Group Limited. [publication title, author, volume number, pagenumbers, copyright notice year]

5) **Reservation of Rights:**The BMJ Group reserves all rights not specifically granted in the combinationof (i) the licence details provided by you and accepted in the course of thislicensing transaction, (ii) these terms and conditions and (iii) CCC's Billing and Payment Terms and Conditions.

6) **Timing of Use:** Firstuse of the Licensed Material must take place within 12 months of the grant ofpermission.

7). **Creation of Contractand Termination:** Once you have submitted an order via Rightslink and thisis received by CCC, and subject to you completing accurate details of yourproposed use, this is when a binding contract is in effect and our acceptanceoccurs. As you are ordering rights from a periodical, to the fullest extentpermitted by law, you will have no right to cancel the contract from this pointother than for BMJ Group's material breach or fraudulent misrepresentation oras otherwise permitted under a statutory right. Payment must be made inaccordance with CCC's Billing and

Payment Terms and conditions. In the eventthat you breach any material condition of these terms and condition or any of CCC's Billing and Payment Terms and Conditions, the license is automatically terminated uponwritten notice from the BMJ Group or CCC or as otherwise provided for in CCC's Billing and Payment Terms and Conditions, where these apply.. Continued use of materials wherea licence has been terminated, as well as any use of the Licensed Materialsbeyond the scope of an unrevoked licence, may constitute intellectual propertyrights infringement and BMJ Group reserves the right to take any and all actionto protect its intellectual property rights in the Licensed Materials.

8. **Warranties:** BMJGroup makes no express or implied representations or warranties with respect tothe Licensed Material and to the fullest extent permitted by law this isprovided on an "as is" basis. For the avoidance of doubt BMJ Group does notwarrant that the Licensed Material is accurate or fit for any particularpurpose.

9. **Limitation ofLiability:** To the fullest extent permitted by law, the BMJ Group disclaimsall liability for any indirect, consequential or incidental damages (includingwithout limitation, damages for loss of profits, information or interruption)arising out of the use or inability to use the Licensed Material or theinability to obtain additional rights to use the Licensed Material. To thefullest extent permitted by law, the maximum aggregate liability of the BMJGroup for any claims, costs, proceedings and demands for direct losses causedby BMJ Group's breaches of its obligations herein shall be limited to twice theamount paid by you to CCC for the licence granted herein.

10. **Indemnity:** You hereby indemnify and holdharmless the BMJ Group and their respective officers, directors, employees andagents, from and against any and all claims, costs, proceeding or demands arisingout of your unauthorised use of the Licensed Material.

11. **No Transfer of License:** This licence ispersonal to you, and may not be assigned or transferred by you without priorwritten consent from the BMJ Group or its authorised agent(s). BMJ Groupmay assign or transfer any of its rights and obligations under this Agreement,upon written notice to you.

12. **No Amendment Except inWriting:** This licence may not be amended except in a writing signed by bothparties (or, in the case of BMJ Group, by CCC on the BMJ Group's behalf).

13. **Objection to Contraryterms:** BMJ Group hereby objects to any terms contained in any purchaseorder, acknowledgment, check endorsement or other writing prepared by you,which terms are inconsistent with these terms and conditions or CCC's Billing and Payment Terms and Conditions. These terms and conditions, together with CCC's Billing and Payment Terms and Conditions (which to the extent they are consistent areincorporated herein), comprise the entire agreement between you and BMJ Group (and CCC) and the Licensee concerning this licensing transaction. In the event ofany conflict between your obligations established by these terms and conditionsand those established by CCC's Billing and Payment Terms and Conditions, theseterms and conditions shall control.

14. **Revocation:** BMJGroup or CCC may, within 30 days of issuance of this licence, deny thepermissions described in this licence at their sole discretion, for any reasonor no reason, with a full refund payable to you should you have not been ableto exercise your rights in full. Notice of such denial will be made using thecontact information provided by you. Failure to receive such notice from BMJGroup or CCC will not, to the fullest extent permitted by law alter orinvalidate the denial. For the fullest extent permitted by law in no event willBMJ Group or CCC be responsible or liable for any costs, expenses or damageincurred by you as a result of a denial of your permission request, other thana refund of the amount(s) paid by you to BMJ Group and/or CCC for denied permissions.

15. **Restrictions to thelicense**:

15.1 Promotion: BMJ Group will not give permission to reproduce infull or in part any

Licensed Material for use in the promotion of thefollowing:

a) non-medical products thatare harmful or potentially harmful to health: alcohol, baby milks and/or, sunbeds

b) medical products that donot have a product license granted by the Medicines and Healthcare productsRegulatory Agency (MHRA) or its international equivalents. Marketing of theproduct may start only after data sheets have been released to members of themedical profession and must conform to the marketing authorization contained inthe product license.

16. **Translation**: This permission is granted for non-exclusive worldEnglish language rights only unless explicitly stated in your licence. Iftranslation rights are granted, a professional translator should be employedand the content should be reproduced word for word preserving the integrity ofthe content.

17. **General:**Neither party shall be liable for failure, default or delay in performingits obligations under this Licence, caused by a Force Majeure event which shallinclude any act of God, war, or threatened war, act or threatened act ofterrorism, riot, strike, lockout, individual action, fire, flood, drought,tempest or other event beyond the reasonable control of either party.

17.1 Inthe event that any provision of this Agreement is held to be invalid, theremainder of the provisions shall continue in full force and effect.

17.2 Thereshall be no right whatsoever for any third party to enforce the terms andconditions of this Agreement. The Parties hereby expressly wish to exclude theoperation of the Contracts (Rights of Third Parties) Act 1999 and any otherlegislation which has this effect and is binding on this agreement.

17.3 Tothe fullest extent permitted by law, this Licence will be governed by the lawsof England and shall be governed and construed in accordance with the laws of England. Any action arising out of or relating to this agreement shall be brought in courtssituated in England save where it is necessary for BMJ Group for enforcement tobring proceedings to bring an action in an alternative jurisdiction.

Thesis / Dissertation Reuse

The IEEE does not require individuals working on a thesis to obtain a formal reuse license, however, you may print out this statement to be used as a permission grant:

Requirements to be followed when using any portion (e.g., figure, graph, table, or textual material) of an IEEE copyrighted paper in a thesis:

1) In the case of textual material (e.g., using short quotes or referring to the work within these papers) users must give full credit to the original source (author, paper, publication) followed by the IEEE copyright line © 2011 IEEE.
2) In the case of illustrations or tabular material, we require that the copyright line © [Year of original publication] IEEE appear prominently with each reprinted figure and/or table.
3) If a substantial portion of the original paper is to be used, and if you are not the senior author, also obtain the senior author's approval.

Requirements to be followed when using an entire IEEE copyrighted paper in a thesis:

1) The following IEEE copyright/ credit notice should be placed prominently in the references: © [year of original publication] IEEE. Reprinted, with permission, from [author names, paper title, IEEE publication title, and month/year of publication]
2) Only the accepted version of an IEEE copyrighted paper can be used when posting the paper or your thesis on-line.
3) In placing the thesis on the author's university website, please display the following message in a prominent place on the website: In reference to IEEE copyrighted material which is used with permission in this thesis, the IEEE does not endorse any of [university/educational entity's name goes here]'s products or services. Internal or personal use of this material is permitted. If interested in reprinting/republishing IEEE copyrighted material for advertising or promotional purposes or for creating new collective works for resale or redistribution, please go to http://www.ieee.org/publications_standards/publications/rights/rights_link.html to learn how to obtain a License from RightsLink.

If applicable, University Microfilms and/or ProQuest Library, or the Archives of Canada may supply single copies of the dissertation.

CITED LITERATURE

1. Advanced vision therapy center: Oculomotor dysfunction. Available at `https://www.advancedvisiontherapycenter.com/about/blog/e_930/Signs_of_a_Vision_Problem/2016/7/Oculomotor_Dysfunction.html` online, accessed Aug 25 2018.

2. RP photonics encyclopedia: Waveguides. Available at `https://www.rp-photonics.com/waveguides.html` online, accessed Aug 23 2018.

3. Trappe family eyecare: Binocular disorders. Available at `https://trappeeyecare.com/vision-and-learning-center/binocular-vision-disorders/` online, accessed Aug 25 2018.

4. Al-Rahayfeh, A. and Faezipour, M.: Eye tracking and head movement detection: A state-of-art survey. IEEE J Transl Eng Health Med, 1:2100212 –2100212, 2013.

5. Andreu, J., Solnais, C., and Sriskandarajah, K.: EALab (Eye Activity Lab): a MATLAB Toolbox for Variable Extraction, Multivariate Analysis and Classification of Eye-Movement Data. Neuroinformatics, 14, 09 2015.

6. Argenta, C., Murphy, A., Hinton, J., Cook, J., Sherrill, T., and Snarski, S.: Graphical user interface concepts for tactical augmented reality. Proc SPIE Int Soc Opt Eng, 76880I, 2010.

7. Bahill, A. T. and D. Adler, a. L. S.: Most naturally occurring human saccades have magnitudes of 15 degrees or less. Invest ophthalmol, 14:468–9, 07 1975.

8. Berger, C., Winkels, M., Lischke, A., and Hoeppner, J.: GazeAlyze: a MATLAB toolbox for the analysis of eye movement data. Behav Res Methods, 44:404–19, 2012.

9. Boardman, J. P. and Fletcher-Watson, S.: What can eye-tracking tell us? Arch Dis Child, 2017.

10. Borsting, E., Mitchell, G., Kulp, M., Scheiman, M., Amster, D., Cotter, S., Coulter, R., et al.: Improvement in academic behaviors after successful treatment of convergence insufficiency. Optom Vis Sci, 89:12–8, 11 2011.

CITED LITERATURE (continued)

11. Borsting, E., Rouse, M. W., Deland, P. N., Hovett, S., Kimura, D., Park, M., and Stephens, B.: Association of symptoms and convergence and accommodative insufficiency in school-age children. Optometry, 74:25–34, 01 2003.

12. Buzzelli, A. R.: Stereopsis, accommodative and vergence facility: do they relate to dyslexia? Optom Vis Sci, 68:842–846, 1991.

13. Cameron, A.: The application of holographic optical waveguide technology to q-sight family of helmet-mounted displays. Proc SPIE Int Soc Opt Eng, 73260H, 2009.

14. Djeraba, C.: State of art of eye tracking. Technical Report of LIFL, 7, 2005.

15. Duchowski, A. T.: Eye tracking methodology. Springer, 2 edition, 2007.

16. Eames, T. H. E.: Low fusion convergence as a factor in reading disability. Am J Ophthalmol, 17:709–710, 1934.

17. Erdenebat, M.-U., Lim, Y.-T., Kwon, K.-C., Darkhanbaatar, N., and Kim, N.: Waveguide-type head-mounted display system for AR application. In State of the Art Virtual Reality and Augmented Reality Knowhow, ed. N. Mohamudally, chapter 4. Rijeka, IntechOpen, Available under Creative Commons licence available at `https://creativecommons.org/licenses/by/3.0/`, online, accessed Aug 23 2018, 2018.

18. Falck-Ytter, T., Bölte, S., and Gredebäck, G.: Eye tracking in early autism research. J. Neurodev. Disord., 5(1):28, 09 2013.

19. Fuhl, W., Tonsen, M., Bulling, A., and Kasneci, E.: Pupil detection for head-mounted eye tracking in the wild: an evaluation of the state of the art. Mach Vis Appl, 27(8):1275–1288, 11 2016.

20. Giel, K. E., Friederich, H.-C., Teufel, M., Hautzinger, M., Enck, P., and Zipfel, S.: Attentional processing of food pictures in individuals with anorexia nervosaan eye-tracking study. Biol Psychiatry, 69(7):661 – 667, 2011. Reduced Behavioral Flexibility in Addiction.

21. Grayson, C.: Upload: Holographic waveguides: What you need to know to understand the smartglasses market. Available at `https://uploadvr.com/waveguides-smartglasses/` online, accessed Aug 23 2018.

22. Gredebäck, G., Johnson, S., and Hofsten, C.: Eye tracking in infancy research. Dev Psychol, 35:1–19, 01 2010.

CITED LITERATURE (continued)

23. Guestrin, E. D. and Eizenman, M.: General theory of remote gaze estimation using the pupil center and corneal reflections. IEEE T Bio-Med Eng, 53(6):1124–1133, 2006.

24. Haggerty, H., Richardson, S., Hrisos, S., Strong, N. P., and Clarke, M. P.: The Newcastle Control Score: a new method of grading the severity of intermittent distance exotropia. Br J Ophthalmol, 88(2):233235, 02 2004.

25. Hatt, S. R., Liebermann, L., Leske, D. A., Mohney, B. G., and Holmes, J. M.: Improved assessment of control in intermittent exotropia using multiple measures. Am J Ophthalmol, 152(5):872876, 11 2011.

26. Hiroshi, M., Katsuyuki, A., Ikuo, M., Satoshi, N., Takuji, Y., Mieko, K., Kazuma, A., and Masataka, O.: 8.4: Distinguished paper: A full color eyewear display using holographic planar waveguides. SID Symposium Digest of Technical Papers, 39(1):89–92, 2005.

27. Holmqvist, K., Nyström, M., Andersson, R., Dewhurst, R., Jarodzka, H., and van de Weijer, J.: Eye Tracking: A Comprehensive Guide To Methods And Measures. Oxford University Press, 01 2011.

28. Horwood, A. M., Toor, S., and Riddell, P. M.: Screening for convergence insufficiency using the ciss is not indicated in young adults. Br J Ophthalmol, 98(5):679–683, 2014.

29. Itti, L.: New eye-tracking techniques may revolutionize mental health screening. Neuron, 88(3):442 – 444, 2015.

30. Kingslake, R. and Thompson, B. J.: Optics. Available at `https://www.britannica.com/science/optics#ref420083`, online, accessed Aug 29 2018 and reproduced under the terms of use for students in dissertations, available at `http://corporate.britannica.com/termsofuse.html`.

31. Laby, D. M., Rosenbaum, A. L., Kirschen, D. G., Davidson, J. L., Rosenbaum, L. J., Strasser, C., and Mellman, M. F.: The visual function of professional baseball players. Am J Ophthalmol, 122(4):476–85, 1996.

32. Lara, F., Cacho, P., García, A., and Megías, R.: General binocular disorders: prevalence in a clinic population. Ophthalmic Physiol Opt, 21(1):70–74, 2002.

33. Li, D., Babcock, J. S., and Parkhurst, D. J.: openEyes: a low-cost head-mounted eye-tracking solution. In ETRA, 2006.

CITED LITERATURE (continued)

34. Li, D. and Parkhurst, D. J.: Open-source software for real-time visible-spectrum eye tracking. In The 2nd Conference on Communication by Gaze In teraction COGAIN 2006: Gazing into the Future, 2006.

35. Li, D. and Parkhurst, D. J.: Starburst : A robust algorithm for video-based eye tracking. 2012.

36. Li, D., Winfield, D., and Parkhurst, D. J.: Starburst: A hybrid algorithm for video-based eye tracking combining feature-based and model-based approaches. 2005 IEEE Computer Society Conference on Computer Vision and Pattern Recognition (CVPR'05) - Workshops, pages 79–79, 2005.

37. Liu, C., Pazzucconi, B., Liu, J., Liu, L., and Yao, X.: A holographic waveguide based eye tracker. Proc SPIE Int Soc Opt Eng, 10474, 02 2018.

38. MathWorks™: Documentation. Available at `https://it.mathworks.com/help/`, online, accessed Sep 6 2018.

39. Mirza, K. and Sarayeddine, K.: Optinvent: Description of various see-through wearable display techniques using waveguides. Available at `http://www.optinvent.com/waveguide-ar-displays/` online, accessed Aug 23 2018.

40. Niesłuchowska, M.: Work with visual display units and its effect on the eye. Klin Oczna, 109:1–3, 2007.

41. Nilsson-Benfatto, M., Öqvist-Seimyr, G., Ygge, J., Pansell, T., Rydberg, A. C., and Jacobson, C.: Screening for dyslexia using eye tracking during reading. PloS one, 2016.

42. Quaid, P. and Simpson, T.: Association between reading speed, cycloplegic refractive error, and oculomotor function in reading disabled children versus controls. Graefes Arch Clin Exp Ophthalmol, 251(1):169–187, 2013.

43. Rosch, J. L. and Vogel-Walcutt, J.: A review of eye-tracking applications as tools for training. Cognition, Technology & Work, 15, 08 2012.

44. Rouse, M. W., Borsting, E., Hyman, L., Hussein, M., Cotter, S. A., M, M. F., Scheiman, M., M, M. G., and DeLand, P. N.: Frequency of convergence insufficiency among fifth and sixth graders. The Convergence Insufficiency and Reading Study (CIRS) group. Optom Vis Sci, 76(9):643–9, 09 1999.

45. Rucker, J.: Oculomotor disorders. Semin Neurol, 27:244–56, 08 2007.

CITED LITERATURE (continued)

46. S, Aungsakun, S., A. Phinyomark, a. P. P., and Limsakul, C.: Robust eye movement recognition using eog signal for human-computer interface. Softw Eng Comput Sys, pages 714–723, 2011.

47. Samadani, U., Ritlop, R., Reyes, M., Nehrbass, E., Li, M., Lamm, E., Pekarsky-Schneider, J., et al.: Eye tracking detects disconjugate eye movements associated with structural traumatic brain injury and concussion. J Neourotrauma, 2015.

48. Scheiman, M., Gallaway, M., Coulter, R., Reinstein, F., Ciner, E., Herzberg, C., and Parisi, M.: Prevalence of vision and ocular disease conditions in a clinical pediatric population. J Am Optom Assoc, 67:193–202, 1996.

49. Scheiman, M., Mitchell, G. L., Cotter, S., Cooper, J., Kulp, M., Rous, M., et al.: A randomized clinical trial of treatments for symptomatic convergence insufficiency in children. Arch Ophthalmol, 126(10):13361349, 10 2008.

50. Scheiman, M. and Wick, B.: Clinical Management of Binocular Vision: Heterophoric, Accommodative, and Eye Movement Disorders. Lippincott Williams & Wilkins, 2013.

51. Spataro, R., Ciriacono, M., Manno, C., and LaBella, V.: The eye-tracking computer device for communication in amyotrophic lateral sclerosis. Acta Neurol Scand, 130(1):40–45, 2013.

52. Svanera, M.: Studio di tecniche per linseguimento della posizione e dei movimenti oculari. Bachelor thesis, Università degli Studi di Brescia, 2011.

53. SYNOPSIS FROM DIGILENS INC.WHITE PAPER, J. .: Switchable Bragg Gratings (SBG) based waveguides used by DigiLens Inc. vs. Surface Relief Gratings (SRG) licensed by Nokia used by other companies in augmented and virtual reality displays. Technical report, Digilens. Inc, 01 2015.

54. Thiagarajan, P., Ciuffreda, K., and Ludlam, D.: Vergence dysfunction in mild traumatic brain injury (mTBI): a review. Ophthalmic Physiol Opt, 31(5):456–468, 2011.

55. Wikipedia: Available at `https://commons.wikimedia.org/wiki/File:Diagram_of_four_Purkinje_images.svg`, under Creative Commons licence available at `https://creativecommons.org/licenses/by-sa/4.0/deed.en`, online, accessed Aug 21 2018.

56. Wikipedia: Beam splitter. Available at `https://en.wikipedia.org/wiki/Beam_splitter`, under Creative Commons licence available at `https://creativecommons.org/publicdomain/zero/1.0/deed.en`, online, accessed Aug 31 2018.

CITED LITERATURE (continued)

57. Wikipedia: Binocular vision. Available at https://en.wikipedia.org/wiki/Binocular_vision#Disorders online, accessed Aug 25 2018.

58. Wikipedia: Holography. Available at https://en.wikipedia.org/wiki/Holography online, accessed Aug 23 2018.

59. Wikipedia: Lens (optics). Available at https://en.wikipedia.org/wiki/Lens_(optics), under GNU free documentation licence available at https://commons.wikimedia.org/wiki/Commons:GNU_Free_Documentation_License,_version_1.2, online, accessd Aug 30 2018.

60. Wikipedia: Optical head-mounted display. Available at https://en.wikipedia.org/wiki/Optical_head-mounted_display online, accessed Aug 23 2018.

61. Wikipedia: Waveguide (optics). Available at https://en.wikipedia.org/wiki/Waveguide_(optics) online, accessed Aug 23 2018.

62. Yan, Z., Li, W., Zhou, Y., Kang, M., and Zheng, Z.: Virtual display design using waveguide hologram in conical mounting configuration. Optical Engineering, 50:50 – 50 – 9, 2011.

63. Young, L. R. and Sheena, D.: Survey of eye movement recording methods. Behav Res Methods Instrum Comput, 7:397–429, 09 1975.

64. Zhang, N., Liu, J., Han, J., Li, X., Yang, F., Wang, X., Hu, B., and Wang, Y.: Improved holographic waveguide display system. Appl Opt, 54, 04 2015.

65. Zhengmin, W., Juan, L., and Yongtian, W.: 64.1: High efficiency waveguide display system with achromatic volume hologram and a prism in-coupler. SID Symposium Digest of Technical Papers, 44(1):888–890, 2103.

VITA

NAME	Beatrice Pazzucconi
EDUCATION	
	Master of Science in Bioengineering, University of Illinois at Chicago, USA, Fall 2017
	Bachelor Degree in Biomedical engineering, Politecnico di Milano, Italy, September 2016
LANGUAGE SKILLS	
Italian	Native speaker
English	Full working proficiency
	TOEFL iBT (Reading 30, Listening 30, Speaking 24, Writing 25) in 2012
	ACT plus writing (composite score 30, English 28, Mathematics 31, Reading 34, Science 28, combined English/Writing 26) in 2012
	IELTS Academic (9 Listening, 9 Reading, 6.5 Writing, 7.5 Speaking, 8 overall), level C1 in 2016
	A.Y. 2017/18 One Semester of study abroad in Chicago, Illinois
	A.Y. 2016/17 and 2017/2018. Lessons and exams attended almost exclusively in English
SCHOLARSHIPS	
A.Y. from 2013/2014 to 2017/2018	Italian scholarship for high academic proficiency (from Politecnico di Milano)
A.Y. 2018/2019	Italian scholarship for developing thesis abroad (from Politecnico di Milano)
PUBLICATIONS	
	Changgeng Liu, Beatrice Pazzucconi, Juan Liu, Lei Liu, and Xincheng Yao: A holographic waveguide based eye tracking device, ARVO 2018 conference abstract, published April 2018. The abstract was also selected with other 4 abstracts to be part of an on-site press conference highlighting the latest advancements in vision science on May 1st 2018

VITA (continued)

	Beatrice Pazzucconi: Optical Tweezers in Biomedical Applications, UIC Bioengineering Student Journal (UBSJ), Spring 2018, Vol. IX, No. 1 (Graduate volume)
	Changgeng Liu, Beatrice Pazzucconi, Juan Liu, Lei Liu, and Xincheng Yao: A holographic waveguide based eye tracking device, SPIE proceedings paper, published Feb. 2018.
TECHNICAL SKILLS	
Basic level	knowledge of Linux Ubuntu OS, OrCAD™ software, R for statistics, Weka, C and Python programming languages, Microsoft Excel™ and LibreOffice spreadsheets, operation of optical systems (lenses, LEDs...) and 3D printers
Average level	knowledge of Microsoft Windows™ OS, Microsoft Word™, LibreOffice and Apache OpenOffice™ text editors, soldering skills
Advanced level	SolidWorks® CAD software, MathWorks MATLAB®, WYSIWYG editor environment LaTeX
WORK EXPERIENCE AND PROJECTS	
March 2016 - Sep 2016	Design and Realisation of a Table Top Robotic Game for Motor Impaired Children for Bachelor Thesis at Politecnico di Milano (with Fabio Paini and Damiano Quadraro)
	Use of prototyping boards; design (with OrCAD™), soldering and assembly of electronic circuits; design (with SolidWorks®) assembly of wooden, plastic and metal parts for the game structure; testing and problem shooting in the game use with children.
Sep 2017 - Dec 2017	Simple Mu-waves Event-Related De- synchronization Detection for Binary Input-BCI as project for the course of Neural Engineering II - Neural Coding (with Martina Berni and Greta Pastore)
	Use OpenBCI® Cyton Board and headset for EEG acquisition; use of MATLAB® to process the data.
March 2017-present	Master Thesis at Polimi on optical measure on cystic fibrosis *sputum* samples